Toward a new theory of the fractional quantum Hall effect

Sergey A. Mikhailov

Angaben zur Veröffentlichung / Publication details:

Mikhailov, Sergey A. 2024. "Toward a new theory of the fractional quantum Hall effect." *Nanomaterials* 14 (3): 297. https://doi.org/10.3390/nano14030297.

nanomaterials

MDPI

Article

Toward a New Theory of the Fractional Quantum Hall Effect

Sergey A. Mikhailov

Institute of Physics, University of Augsburg, D-86135 Augsburg, Germany;
sergey.mikhailov@physik.uni-augsburg.de

Abstract: The fractional quantum Hall effect was experimentally discovered in 1982. It was observed that the Hall conductivity σ_{yx} of a two-dimensional electron system is quantized, $\sigma_{yx} = e^2/3h$, in the vicinity of the Landau level filling factor $\nu = 1/3$. In 1983, Laughlin proposed a trial many-body wave function, which he claimed described a "new state of matter"—a homogeneous incompressible liquid with fractionally charged quasiparticles. Here, I develop an exact diagonalization theory that allows one to calculate the energy and other physical properties of the ground and excited states of a system of N two-dimensional Coulomb interacting electrons in a strong magnetic field. I analyze the energies, electron densities, and other physical properties of the systems with $N \leq 7$ electrons continuously as a function of magnetic field in the range $1/4 \lesssim \nu < 1$. The results show that both the ground and excited states of the system resemble a sliding Wigner crystal whose parameters are influenced by the magnetic field. Energy gaps in the many-particle spectra appear and disappear as the magnetic field changes. I also calculate the physical properties of the $\nu = 1/3$ Laughlin state for $N \leq 8$ and compare the results with the exact ones. This comparison, as well as an analysis of some other statements published in the literature, show that the Laughlin state and its fractionally charged excitations do not describe the physical reality, neither at small N nor in the thermodynamic limit. The results obtained shed new light on the nature of the ground and excited states in the fractional quantum Hall effect.

Keywords: fractional quantum Hall effect; exact diagonalization; two-dimensional electron gas; electron–electron interaction

Citation: Mikhailov, S.A. Toward a New Theory of the Fractional Quantum Hall Effect. *Nanomaterials* **2024**, *14*, 297. https://doi.org/10.3390/nano14030297

Academic Editor: Orion Ciftja

Received: 22 December 2023
Revised: 20 January 2024
Accepted: 22 January 2024
Published: 31 January 2024

1. Introduction

1.1. Historical Background

The quantum Hall effect was discovered by Klaus von Klitzing in 1980 [1]. He studied the longitudinal (R_{xx}) and Hall ($R_H = R_{xy}$) resistances of a degenerate two-dimensional (2D) electron gas (EG) in the inversion layer of a Si-MOSFET (metal-oxide semiconductor field effect transistor). The sample was placed in a strong perpendicular magnetic field $B \approx 18$ T and cooled down to $T \approx 1.5$ K. The resistances R_{xx} and R_{xy} were measured as a function of the gate voltage V_g, applied between the metallic gate and the 2DEG, which changed the density n_s of the 2D electrons and the Landau level filling factor

$$\nu = \pi n_s \lambda^2; \tag{1}$$

here

$$\lambda \equiv \sqrt{2} l_B = \sqrt{\frac{2\hbar c}{|e|B}} = \sqrt{\frac{2\hbar}{m^\star \omega_c}}, \tag{2}$$

l_B is the magnetic length, $\omega_c = |e|B/m^\star c$ is the cyclotron frequency, and $m^\star$ is the effective mass of electrons. He found that, when ν is close to integer values $\nu \approx i$, $i = 1, 2, 3, \ldots$, the diagonal resistance R_{xx} becomes negligibly small, while the Hall resistance takes on, with a very high accuracy, quantized values, corresponding to the Hall conductivity

$$\sigma_{yx} = \frac{e^2}{h}\nu = \frac{e^2}{h}i, \;\; i = 1, 2, 3, \ldots \tag{3}$$

The origin of this fascinating physical phenomenon, which was called the *integer quantum Hall effect*, was quickly understood [1] in terms of the single-particle picture. The Landau quantization of electron motion leads to the appearance of energy gaps in the electron spectrum when $\nu \approx i$; the classical formula for the Hall conductivity $\sigma_{yx} = n_s ec/B$, together with the relation (1), immediately gives the quantized values (3). The stabilization of σ_{yx} at the levels (3) and the vanishing of σ_{xx} in finite intervals around $\nu = i$ was explained by the influence of disorder, see, e.g., Ref. [2].

The time of mysteries came a little later. In 1982, Tsui, Stormer, and Gossard published a paper [3] where the same transport coefficients (R_{xx} and R_{xy}) were measured in another material system, GaAs/AlGaAs heterojunction. The main difference between the new experiment and the one performed by von Klitzing was that the mobility of 2D electrons was higher ($\mu \sim 10^5$ cm^2/Vs) and the temperature was lower (T down to ~0.48 K). In the experiment [3], the density of the electrons was fixed while the magnetic field varied from zero up to ~22 T. Like in Ref. [1], the already familiar integer quantization of R_{xy} was observed around $\nu = 1, 2, 3, \ldots$, but—very surprisingly—a very similar plateau was found around $\nu \approx 1/3$, where the measured R_H corresponded to the Hall conductivity

$$\sigma_{yx} = \frac{e^2}{h}\nu, \;\; \nu = \frac{1}{3}. \tag{4}$$

Subsequent experimental studies showed that such a *fractional* quantization of σ_{yx} and the corresponding suppression of σ_{xx} is the case around many fractions of the form $\nu = p/q$ where p and q are integers and q is odd, as well as around some fractions with an even denominator, see, e.g., Ref. [4].

If $\nu < 1$, all electrons occupy the highly degenerate lowest Landau level, and there are no energy gaps in the single-particle electron spectrum. Therefore, the mysterious feature at $\nu = 1/3$ could only be explained within a many-body approach, taking into account electron–electron interactions. As known, when considered as classical point particles, Coulomb-interacting electrons form the Wigner crystal [5], and Tsui et al. [3] put forward a hypothesis that the observed 1/3 feature in the Hall conductivity is related to the formation of the Wigner crystal (or a charge density wave) with a triangular symmetry. However, in 1983, Laughlin [6] proposed the following trial wave function for the ground state of the N-particle system at $\nu = 1/m$:

$$\Psi_{\mathrm{LS}}^{(m)}(\boldsymbol{r}_1, \boldsymbol{r}_2, \ldots, \boldsymbol{r}_N) \propto \left(\prod_{1 \le j < k \le N} (z_j - z_k)^m \right) \exp\left(-\frac{1}{2} \sum_{j=1}^{N} |z_j|^2 \right), \tag{5}$$

where LS means the "Laughlin state", m is the odd integer, $\boldsymbol{r}_j = (x_j, y_j)$, and $z_j = (x_j - iy_j)/\lambda$ are the normalized complex coordinates of 2D electrons. The function $\Psi_{\mathrm{LS}}^{(m)}$ is an eigenfunction of the total angular momentum operator with the eigenvalue $\mathcal{L} = mN(N-1)/2$ (in units of $\hbar$). If $m = 1$, it coincides with the wave function of the so-called maximum density droplet (MDD) state proposed earlier in Ref. [7] for the ground state of the system at $\nu = 1$. The MDD state is characterized by a uniform electron density at $r \lesssim R = \sqrt{N/\pi n_s}$, see Section 5 for further details.

For $m = 3$ and 5, the energy of the states (5) in the thermodynamic limit was evaluated in Ref. [6], and it was found that it is lower than the energy of the charge density wave calculated in Refs. [8,9] using the Hartree–Fock [8] and second-order perturbation theory [9]. The projections of $\Psi_{\mathrm{LS}}^{(m=3)}$ and $\Psi_{\mathrm{LS}}^{(m=5)}$ onto the numerically calculated exact ground states for three and four particles were also calculated and found to be close to 1. Apart from the function (5), Laughlin also "generated" many-body wave functions for the elementary excitations of the system and stated that they describe quasiparticles with fractional charge e/m. Finally, he concluded that the wave function (5) describes the ground

state of the system at $\nu = 1/m$ and is "an incompressible quantum fluid with fractionally charged excitations" [6]. A few critical comments on the wave function (5) followed [10], and several more attempts to find an alternative ground state of the fractional quantum Hall effect (FQHE) system [11,12] have been made, but finally, the LS (5) was accepted by the community [13] as the closest approximation to the ground-state wave function at $\nu = 1/m$ (with $m = 3$ and 5). Laughlin's ideas have been developed in a very large number of subsequent publications, see, e.g., Refs. [14–25] and the review articles [26–30]. In order to explain the fractions $\nu = p/q$ different from $1/3$, various theoretical approaches have been proposed, for example, hierarchical schemes [15] or the composite fermions theory [17]. According to the currently accepted version of the FQHE theory, based on the theory [6], a 2D electron system placed in a strong magnetic field undergoes a sequence of phase transitions at various fractional values of ν into highly idealized dissipationless states [27]. Reports on the experimental observations of fractionally charged quasiparticles were published in Refs. [31–33].

1.2. Brief Overview of Results of This Work

In this paper, I develop an exact diagonalization theory that enables the calculation of the energy and other physical properties of the ground and excited states of N two-dimensional Coulomb interacting electrons placed in a strong magnetic field. It is assumed that all electrons are spin-polarized and occupy only the lowest Landau-level states. It is also assumed that the electrons are in the field of a neutralizing positively charged background, which has the shape of a disk of radius $R = \sqrt{N/\pi n_s}$ and a constant surface density n_s. I present the exact results for the ground and excited states of the systems of $N \leq 7$ electrons, both for $\nu = 1/3$ and for arbitrary ν varying from $\nu = 1$ to $\nu \simeq 1/4$ in dependence of the magnetic field B. The results show that electron–electron and background–electron interactions lift the degeneracy of the Landau levels and lead to the appearance of energy gaps in the many-body spectra of the FQHE system. As the magnetic field B changes, the width of the energy gaps oscillates, remaining on the order of e^2/l_B in finite intervals of the magnetic field and disappearing at separate B-points. The oscillations of the gap width are caused by the interplay of the Coulomb repulsive forces and the compressive action of the B field. Both the ground and excited states of the FQHE system have a shape reminiscent of a Wigner crystal (or a Wigner molecule) in the sense that the electron density maxima are in the same places where one would expect to find Coulomb interacting point charges. All these results shed new light on the true nature of the ground and excited states of the 2D electron systems in strong magnetic fields and lead to a better understanding of the FQHE effect.

A large part of this paper is devoted to a detailed analysis of the currently accepted theory of this phenomenon. I investigate the physical properties of the state (5) for $N \leq 8$, as well as of its "fractionally charged" excitations, and show that they have no relation to the true ground and excited states of the FQHE system. The results obtained in this work force the conclusion that the Laughlin liquid with its fractionally charged excitations does not exist.

It should be noted that, although the currently accepted FQHE theory claims that the Laughlin function well describes the properties of the system in the thermodynamic limit, no precise evidence for such statements has been presented. Moreover, it is obvious that such evidence cannot exist since, in order to obtain it, it would be necessary to solve the many-body Schrödinger equation for a very large number ($N \ggg 1$) of strongly interacting particles. On the other hand, some exact results have been obtained in the literature for systems with a small number of particles, see, e.g., the exact diagonalization calculations of Ref. [18] (for $\nu = 1/3$ and $N \leq 9$) and of Ref. [19] (for $\nu = 1/3$ and $N \leq 12$). Although the results of these *exact* calculations have been found in clear contradiction with the *variational* theory of Ref. [6], the Laughlin theory was not questioned. In Ref. [18], the discrepancies were ignored, while in Ref. [19], a complicated and questionable interpretation in terms of an edge reconstruction of the LS into a "chiral striped phase" was put

forward. I discuss these and some other statements of the currently accepted FQHE theory in Sections 6.7 and 8 below.

The rest of the paper is organized as follows. In Section 2, I formulate the problem and discuss all the technical issues needed for the remaining part of the paper; in particular, the many-particle matrix elements of the Hamiltonian and other physical quantities are calculated there. In Section 3, the classical solution of the problem, the Wigner crystal, is briefly discussed. In Section 4, the results of the exact solution of the problem for $\nu = 1/3$ and up to $N = 7$ particles are presented. Then, I switch to a discussion of the LS. In Section 5, I overview the physical properties of the MDD state ($\nu = 1$) which are used in the subsequent discussion of the FQHE problem. In Section 6, the energy and other physical properties of the trial state (5) for $m = 1/\nu = 3$ and $N \leq 8$ are calculated and compared with the exact results from Section 4.

After the complete analysis of the case $\nu = 1/3$, I present in Section 7 the results of the exact solution of the problem for $\nu \leq 1$. In Section 8, a number of statements of the currently accepted FQHE theory are analyzed and discussed, and finally, in Section 9, all the results of this work are summarized and conclusions are formulated. Mathematical details are given in the Appendices A–C.

2. Theory

2.1. Single-Particle Problem

Let us consider a single 2D electron moving in the plane $z = 0$ in the presence of a uniform external magnetic field $\boldsymbol{B} = (0, 0, B)$. Its quantum-mechanical motion is described by the single-particle Schrödinger equation

$$\frac{1}{2m^\star}\left(\hat{\boldsymbol{p}} + \frac{|e|}{2c}\boldsymbol{B}\times\boldsymbol{r}\right)^2\phi(\boldsymbol{r}) = \epsilon\phi(\boldsymbol{r}). \tag{6}$$

Its solution,

$$\epsilon \equiv \epsilon_{n,l} = \hbar\omega_c\left(n + \frac{l + |l| + 1}{2}\right),\ \ 0 \leq n < \infty,\ \ -\infty < l < +\infty, \tag{7}$$

$$\phi(\mathbf{r}) \equiv \phi_{n,l}(\boldsymbol{r}) = \frac{e^{il\theta}}{\sqrt{\pi}\lambda}\left(\frac{n!}{(n+|l|)!}\right)^{1/2}\exp\left(-\frac{r^2}{2\lambda^2}\right)\left(\frac{r}{\lambda}\right)^{|l|}L_n^{|l|}\left(\frac{r^2}{\lambda^2}\right), \tag{8}$$

is characterized by the radial quantum number n and the azimuthal (angular momentum) quantum number l [34–36]. The functions (8) represent a complete basis set in a 2D space.

The states with $n = 0$ and non-positive l, $l \leq 0$, belong to the lowest Landau level. The corresponding energy is equal to $\hbar\omega_c/2$ and the corresponding wave functions are

$$|L\rangle \equiv \psi_L(\boldsymbol{r}) \equiv \phi_{n=0,l\leq 0}(\boldsymbol{r}) = \frac{1}{\lambda\sqrt{\pi L!}}\left(\frac{r}{\lambda}e^{-i\theta}\right)^L\exp\left(-\frac{r^2}{2\lambda^2}\right) = \frac{z^L e^{-|z|^2/2}}{\lambda\sqrt{\pi L!}}, \tag{9}$$

where $L = -l = 0, 1, 2, \ldots$, and $z = (x - iy)/\lambda$. The states (9) are normalized, $\langle L|L'\rangle = \delta_{LL'}$, and represent a complete subset of functions in two dimensions belonging to the lowest Landau level with $\epsilon_{0,l} = \hbar\omega_c/2$. The matrix elements of the exponential function $e^{i\boldsymbol{q}\cdot\boldsymbol{r}}$ between the single-particle states (9) are

$$\langle L|e^{i\boldsymbol{q}\cdot\boldsymbol{r}}|L'\rangle = i^{|L-L'|}e^{i(L-L')\alpha}\sqrt{\frac{(\min\{L,L'\})!}{(\max\{L,L'\})!}}\left(\frac{q\lambda}{2}\right)^{|L-L'|}\exp\left(-\frac{(q\lambda)^2}{4}\right)L_{\min\{L,L'\}}^{|L-L'|}\left(\frac{(q\lambda)^2}{4}\right), \tag{10}$$

where α is the polar angle of the vector $\boldsymbol{q}$, $\boldsymbol{q} = q(\cos\alpha, \sin\alpha)$, and $L_n^l(x)$ are the Laguerre polynomials.

2.2. Positive Background

N electrons repel each other by Coulomb forces; therefore, a compensating positive background is required to keep them together and to ensure the system electroneutrality. I will use two physically reasonable models of the positive background density. The first model, also used, for example, in Refs. [6,23–25], assumes that the positive background has the shape of a disk with a uniform charge density n_s and a radius $R = \sqrt{N/\pi n_s}$,

$$n_b^{\rm st}(\boldsymbol{r}) = n_s\Theta(R - r) = n_s\Theta(\sqrt{N} - x). \tag{11}$$

Here, $x = r/a_0$, $\Theta(x)$ is the Heaviside step function, and the length a_0 is defined as

$$\pi n_s a_0^2 = 1. \tag{12}$$

In the second model, the density profile is smoothed near the disk edge at the length $\sim a_0$,

$$n_b^{\rm sm}(\boldsymbol{r}) = n_s e^{-x^2}\sum_{k=0}^{N-1}\frac{(x^2)^k}{k!} = n_s\frac{\Gamma(N, x^2)}{\Gamma(N)} = n_s Q(N, x^2), \tag{13}$$

where $\Gamma(N)$ is the Euler Gamma function, $\Gamma(N, z)$ is the incomplete Gamma function, and

$$Q(N, x) = \frac{\Gamma(N, x)}{\Gamma(N)} \tag{14}$$

is the regularized incomplete Gamma function. The smooth density profile (13) actually gives a more adequate description of the real density distribution, since in real systems, the edge is always smeared over a certain length, for example, over the distance between the 2D gas and the donor layer in GaAs/AlGaAs heterostructures or over the average distance between electrons a_0. The length a_0, defined in (12), will be used as the length unit throughout the paper. In contrast to other possible options for choosing the length unit (e.g., l_B or λ, like in many publications), a_0 does not depend on B, which is more convenient for the system behavior analysis at varying magnetic fields, see Section 7.

Both density profiles, namely (11) and (13), satisfy the condition

$$\int n_b(\boldsymbol{r})d\boldsymbol{r} = N \tag{15}$$

and are shown in Figure 1 for $N = 100$. The Fourier transforms of the density profiles (11) and (13) are determined by the formulas

$$n_{\boldsymbol{q}}^{b,\rm st} \equiv \int d\boldsymbol{r} n_b(\boldsymbol{r})e^{i\boldsymbol{q}\cdot\boldsymbol{r}} = N\frac{J_1(qR)}{qR/2} = 2N\frac{J_1(qa_0\sqrt{N})}{qa_0\sqrt{N}}, \tag{16}$$

and

$$n_{\boldsymbol{q}}^{b,\rm sm} = \exp\left(-\frac{(qa_0)^2}{4}\right)L_{N-1}^1\left(\frac{(qa_0)^2}{4}\right), \tag{17}$$

respectively, where J_1 is the Bessel function, and L_n^k are the Laguerre polynomials.

The potential well created by the positively charged background disk with the density (11) or (13) is described by the formula

$$V_b(\boldsymbol{r}) = \frac{e^2}{a_0}U_N\left(\frac{r}{a_0}\right), \tag{18}$$

where

$$U_N^{\rm st}(x) = -\frac{4}{\pi}\begin{cases}\sqrt{N}\mathrm{E}\left(\frac{x^2}{N}\right), & x^2 \le N\\ x\mathrm{E}\left(\frac{N}{x^2}\right) - \frac{x^2-N}{x}\mathrm{K}\left(\frac{N}{x^2}\right), & x^2 \ge N\end{cases}, \tag{19}$$

for the step-like density profile (11), and

$$U_N^{\mathrm{sm}}(x) = -\sum_{m=0}^{N-1} \binom{N}{m+1} \frac{(-1)^m}{m!} \Gamma\left(m+\frac{1}{2}\right) {}_1F_1\left(m+\frac{1}{2}, 1; -x^2\right) \tag{20}$$

for the smooth density profile (13). Here, the functions $\mathrm{K}(m)$ and $\mathrm{E}(m)$, defined as

$$\mathrm{K}(m) = \int_0^{\pi/2} \frac{d\theta}{\sqrt{1-m\sin^2\theta}}, \quad \mathrm{E}(m) = \int_0^{\pi/2} d\theta \sqrt{1-m\sin^2\theta}, \tag{21}$$

are the complete elliptic integrals of the first and second kinds, respectively, $\binom{n}{m}$ are the binomial coefficients, $\Gamma(x)$ is the Gamma function, and ${}_1F_1(a,b;z)$ is the degenerate (confluent) hypergeometric function, Equation (A14). Figure 2 shows the functions (19) and (20) for $N = 7$. In the case of the step-like density profile, the potential well is slightly deeper, while in the case of the smooth density profile, it is slightly wider. The depths of both potential wells grow with N as $\sqrt{N}$, $U_N^{\mathrm{sm}}(0) = -2\Gamma(N+1/2)/\Gamma(N) \approx U_N^{\mathrm{st}}(0) = -2\sqrt{N}$. In real, macroscopically large samples ($N \sim 10^{11}$–10^{12}), this depth is of the keV scale.

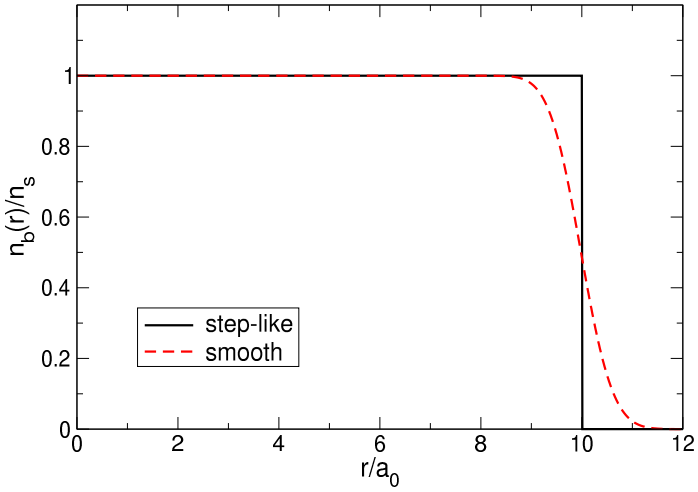

Figure 1. The positive background density $n_b(r)$ for $N = 100$ in the step-like and smooth density profile models.

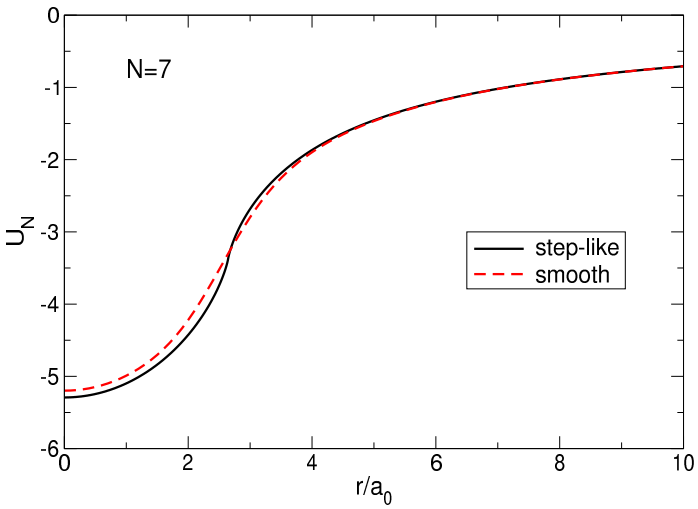

Figure 2. The potential energies (19) and (20) of the positive background with the density profiles (11) and (13) for $N = 7$.

2.3. Many-Body Hamiltonian

The Hamiltonian of N interacting 2D electrons, placed in the magnetic field $\boldsymbol{B} = (0, 0, B)$ and in the attractive potential (18) of the positively charged background with the density (11) or (13), has the form

$$\hat{\mathcal{H}} = \hat{K} + \hat{V}_C = \frac{1}{2m}\sum_{j=1}^{N}\left(\hat{\boldsymbol{p}}_j + \frac{|e|}{2c}\boldsymbol{B}\times\boldsymbol{r}_j\right)^2 + \hat{V}_C. \tag{22}$$

Here, $\hat{K}$ is the total kinetic energy operator and the Coulomb interaction energy $\hat{V}_C = \hat{V}_{bb} + \hat{V}_{eb} + \hat{V}_{ee}$ consists of the sum of background–background, background–electron, and electron–electron interaction energies

$$\hat{V}_C = \frac{e^2}{2}\int\frac{n_b(\boldsymbol{r})n_b(\boldsymbol{r}')d\boldsymbol{r}d\boldsymbol{r}'}{|\boldsymbol{r}-\boldsymbol{r}'|} - e^2\int n_b(\boldsymbol{r})d\boldsymbol{r}\sum_{j=1}^{N}\frac{1}{|\boldsymbol{r}-\boldsymbol{r}_j|} + \frac{e^2}{2}\sum_{j\neq k=1}^{N}\frac{1}{|\boldsymbol{r}_j-\boldsymbol{r}_k|}. \tag{23}$$

In order to calculate the energy $\hat{V}_C$, it is convenient to rewrite (23) in terms of the Fourier transforms of the electron and background charge densities. This gives

$$\hat{V}_C = \frac{e^2}{2\pi}\int\frac{d\boldsymbol{q}}{q}\left(\frac{1}{2}\left(n_{\boldsymbol{q}}^b\right)^2 - n_{\boldsymbol{q}}^b\sum_{j=1}^{N}e^{-i\boldsymbol{q}\cdot\boldsymbol{r}_j} + \frac{1}{2}\sum_{j\neq k=1}^{N}e^{i\boldsymbol{q}\cdot\boldsymbol{r}_j}e^{-i\boldsymbol{q}\cdot\boldsymbol{r}_k}\right), \tag{24}$$

where $n_{\boldsymbol{q}}^b$ are given by Equations (16) and (17) for the step-like and smooth density profiles, respectively. The Hamiltonian (22) commutes with the total angular momentum operator

$$\hat{\mathcal{L}}_z = \sum_{j=1}^{N}(\boldsymbol{r}_j\times\hat{\boldsymbol{p}}_j)_z. \tag{25}$$

The total angular momentum quantum number $\mathcal{L} \equiv \mathcal{L}_z$ can be used to classify the many-body basis wave functions.

2.4. Basis Many-Body Wave Functions

Let us consider N spin-polarized electrons at the lowest Landau level. Each of the particles can occupy one of the states (9). If the j-th particle is in the single-particle state $|L_j\rangle = \psi_{L_j}(\boldsymbol{r})$, the corresponding many-body wave function can be written as a Slater determinant

$$|L_1, L_2, \ldots, L_N\rangle = \frac{1}{\sqrt{N!}}\begin{vmatrix} \psi_{L_1}(\boldsymbol{r}_1) & \psi_{L_1}(\boldsymbol{r}_2) & \ldots & \psi_{L_1}(\boldsymbol{r}_N) \\ \psi_{L_2}(\boldsymbol{r}_1) & \psi_{L_2}(\boldsymbol{r}_2) & \ldots & \psi_{L_2}(\boldsymbol{r}_N) \\ \ldots & \ldots & \ldots & \ldots \\ \psi_{L_N}(\boldsymbol{r}_1) & \psi_{L_N}(\boldsymbol{r}_2) & \ldots & \psi_{L_N}(\boldsymbol{r}_N) \end{vmatrix}. \tag{26}$$

The functions (26) are orthogonal and normalized,

$$\langle L_1', L_2', \ldots, L_N'|L_1, L_2, \ldots, L_N\rangle = \delta_{L_1'L_1}\delta_{L_2'L_2}\ldots\delta_{L_N'L_N}. \tag{27}$$

They are eigenfunctions of the kinetic energy operator

$$\hat{K}|L_1, L_2, \ldots, L_N\rangle = N\frac{\hbar\omega_c}{2}|L_1, L_2, \ldots, L_N\rangle, \tag{28}$$

and of the total angular momentum operator $\hat{\mathcal{L}}$

$$\hat{\mathcal{L}}_z|L_1, L_2, \ldots, L_N\rangle = \left(\sum_{i=1}^{N}L_i\right)|L_1, L_2, \ldots, L_N\rangle, \tag{29}$$

where the latter is measured in units of $\hbar$. The many-body wave functions (26) represent the orthonormal basis set of functions belonging to the lowest Landau level.

If N electrons occupy the single-particle states with the lowest possible angular momenta L from $L = 0$ up to $L = N - 1$, one obtains the many-body MDD configuration $\Psi_{\rm mdd} = |0, 1, 2, \ldots, N-1\rangle$, Ref. [7]. This MDD configuration has the lowest possible total angular momentum

$$\mathcal{L} = \mathcal{L}_{\rm min} = \sum_{L=0}^{N-1} L = \frac{N(N-1)}{2}. \tag{30}$$

If $\mathcal{L} > \mathcal{L}_{\rm min}$, there exist, in general, more than one many-body electronic configurations corresponding to the given N and $\mathcal{L}$. For example, Tables 1 and 2 show possible many-body configurations for $N = 2$ and $N = 3$ and several $\mathcal{L}$'s. The number $N_{mbs}(N, \mathcal{L})$ of many-body configurations grows with $\mathcal{L}$ for a given N.

Table 1. Possible many-body configurations in a system of $N = 2$ electrons. $N_{mbs}(N, \mathcal{L})$ is the total number of all many-particle configurations with a given N and $\mathcal{L}$.

$\mathcal{L}$	Configurations	N_{mbs}
1	$\|0,1\rangle$	1
2	$\|0,2\rangle$	1
3	$\|0,3\rangle$ $\|1,2\rangle$	2
4	$\|0,4\rangle$ $\|1,3\rangle$	2
5	$\|0,5\rangle$ $\|1,4\rangle$ $\|2,3\rangle$	3
6	$\|0,6\rangle$ $\|1,5\rangle$ $\|2,4\rangle$	3
7	$\|0,7\rangle$ $\|1,6\rangle$ $\|2,5\rangle$ $\|3,4\rangle$	4

Table 2. Possible many-body configurations in a system of $N = 3$ particles. $N_{mbs}(N, \mathcal{L})$ is the total number of all many-particle configurations with given N and $\mathcal{L}$.

$\mathcal{L}$	Configurations	N_{mbs}
3	$\|0,1,2\rangle$	1
4	$\|0,1,3\rangle$	1
5	$\|0,1,4\rangle$ $\|0,2,3\rangle$	2
6	$\|0,1,5\rangle$ $\|0,2,4\rangle$ $\|1,2,3\rangle$	3
7	$\|0,1,6\rangle$ $\|0,2,5\rangle$ $\|0,3,4\rangle$ $\|1,2,4\rangle$	4
8	$\|0,1,7\rangle$ $\|0,2,6\rangle$ $\|0,3,5\rangle$ $\|1,2,5\rangle$ $\|1,3,4\rangle$	5
9	$\|0,1,8\rangle$ $\|0,2,7\rangle$ $\|0,3,6\rangle$ $\|0,4,5\rangle$ $\|1,2,6\rangle$ $\|1,3,5\rangle$ $\|2,3,4\rangle$	7
10	$\|0,1,9\rangle$ $\|0,2,8\rangle$ $\|0,3,7\rangle$ $\|0,4,6\rangle$ $\|1,2,7\rangle$ $\|1,3,6\rangle$ $\|1,4,5\rangle$ $\|2,3,5\rangle$	8
11	$\|0,1,10\rangle$ $\|0,2,9\rangle$ $\|0,3,8\rangle$ $\|0,4,7\rangle$ $\|0,5,6\rangle$ $\|1,2,8\rangle$ $\|1,3,7\rangle$ $\|1,4,6\rangle$ $\|2,3,6\rangle$ $\|2,4,5\rangle$	10
12	$\|0,1,11\rangle$ $\|0,2,10\rangle$ $\|0,3,9\rangle$ $\|0,4,8\rangle$ $\|0,5,7\rangle$ $\|1,2,9\rangle$ $\|1,3,8\rangle$ $\|1,4,7\rangle$ $\|1,5,6\rangle$ $\|2,3,7\rangle$ $\|2,4,6\rangle$ $\|3,4,5\rangle$	12

2.5. Many-Body Matrix Elements

To calculate the various physical properties of an N-electron system, one needs the matrix elements of one-particle or two-particle operators

$$\langle L_1', L_2', \ldots, L_N'| \sum_{j=1}^{N} \hat{F}_1(\boldsymbol{r}_j) |L_1, L_2, \ldots, L_N\rangle, \tag{31}$$

$$\langle L_1', L_2', \ldots, L_N'| \sum_{j=1}^{N} \sum_{k=1, k\neq j}^{N} \hat{F}_2(\boldsymbol{r}_j, \boldsymbol{r}_k) |L_1, L_2, \ldots, L_N\rangle, \tag{32}$$

with many-body states (26). In this paper, only the matrix elements (31) and (32) between the many-body states $\langle L_1', L_2', \ldots, L_N'|$ and $|L_1, L_2, \ldots, L_N\rangle$ that belong to the same total angular momentum $\mathcal{L}$ will be needed, i.e., $\sum_{j=1}^{N} L_j = \sum_{j=1}^{N} L_j' = \mathcal{L}$. This means that, if the bra and ket configurations are different, they differ by two or more single-particle states.

For example, the configurations $\langle 0,1,8|$ and $|0,2,7\rangle$, $\langle 0,3,6|$ and $|1,3,5\rangle$ differ by two single-particle states, while the configurations $\langle 0,1,8|$ and $|2,3,4\rangle$ differ by three single-particle states, as can be seen in Table 2. The matrix elements between the bra and ket configurations which differ by only one single-particle state, e.g., between the configurations $\langle 0,1,8|$ and $|0,1,9\rangle$, will not be considered since they correspond to different values of the total angular momentum $\mathcal{L}$.

Now, I calculate the matrix elements of several one-particle and two-particle operators of the type (31) and (32). For brevity, the short notations $|s\rangle \equiv |\Psi_s\rangle \equiv |L_1^{(s)}, L_2^{(s)}, \ldots, L_N^{(s)}\rangle$ for the functions (26) will be used.

2.5.1. Electron Density

The operator of the electron density has the form

$$\hat{n}_e(\boldsymbol{r}) = \sum_{j=1}^{N} \delta(\boldsymbol{r} - \boldsymbol{r}_j). \tag{33}$$

The off-diagonal matrix elements of (33) are evidently zero. Then, one obtains

$$\langle \Psi_s | \hat{n}_e(\boldsymbol{r}) | \Psi_{s'} \rangle = \delta_{ss'} \sum_{j=1}^{N} \langle L_j^{(s)} | \delta(\boldsymbol{r} - \boldsymbol{r}_j) | L_j^{(s)} \rangle = \delta_{ss'} \sum_{j=1}^{N} |\psi_{L_j^{(s)}}(\boldsymbol{r})|^2, \tag{34}$$

where $\psi_{L_j^{(s)}}(\boldsymbol{r})$ is the single-particle wave function (9) of the j-th particle in the s-th many-body configuration.

2.5.2. Fourier Transform of the Electron Density

The Fourier transform of the density operator (33) is

$$\hat{n}_{\boldsymbol{q}}^{e} = \int d\boldsymbol{r} \hat{n}_e(\boldsymbol{r}) e^{i\boldsymbol{q}\cdot\boldsymbol{r}} = \sum_{j=1}^{N} e^{i\boldsymbol{q}\cdot\boldsymbol{r}_j}. \tag{35}$$

Using Equation (10), I obtain

$$\langle \Psi_s | \hat{n}_{\boldsymbol{q}}^{e} | \Psi_{s'} \rangle = \delta_{ss'} \sum_{j=1}^{N} \langle L_j^{(s)} | e^{i\boldsymbol{q}\cdot\boldsymbol{r}_j} | L_j^{(s)} \rangle = \delta_{ss'} \exp\left(-\frac{(q\lambda)^2}{4}\right) \sum_{j=1}^{N} L_{L_j^{(s)}}^{0}\left(\frac{(q\lambda)^2}{4}\right). \tag{36}$$

2.5.3. Background–Background Interaction Energy

The background–background interaction energy V_{bb} is given by the first term in Equation (24). Since V_{bb} does not depend on the coordinates of electrons, the matrix $\langle \Psi_s | \hat{V}_{bb} | \Psi_{s'} \rangle$ is diagonal and all the matrix elements are the same. For the step-like (11) and smooth (13) density profiles, they are given by the following formulas

$$\langle \Psi_s | \hat{V}_{bb}^{\mathrm{st}} | \Psi_{s'} \rangle = \delta_{ss'} \frac{e^2}{a_0} \frac{8}{3\pi} N^{3/2}, \tag{37}$$

$$\langle \Psi_s | \hat{V}_{bb}^{\mathrm{sm}} | \Psi_{s'} \rangle = \delta_{ss'} \frac{e^2}{a_0} \sqrt{\frac{\pi}{8}} \mathcal{J}(N-1, N-1, 1, 1, 0; 1, 1), \tag{38}$$

where the integrals $\mathcal{J}(n_1, n_2, l_1, l_2, k; \alpha, \beta)$ are defined and calculated in Appendix A, see Equations (A1) and (A2).

2.5.4. Background–Electron Interaction Energy

The background–electron interaction energy is given by the second term in Equation (24). Its many-body matrix elements are

$$\langle \Psi_s | \hat{V}_{be} | \Psi_{s'} \rangle = -\frac{e^2}{2\pi} \int \frac{d\boldsymbol{q}}{q} n^b_{\boldsymbol{q}} \langle \Psi_s | \left(\hat{n}^e_{\boldsymbol{q}} \right)^\star | \Psi_{s'} \rangle. \tag{39}$$

Substituting the Fourier transforms of the background and electron densities from Equations (16), (17) and (36) into (39), I obtain the following results. In the case of the step-like density profile calculations give (for details see Appendix B.1)

$$\langle \Psi_s | \hat{V}^{\rm st}_{be} | \Psi_{s'} \rangle = -\delta_{ss'} \frac{e^2}{a_0} N \sqrt{\beta} \sum_{j=1}^{N} \sum_{m=0}^{L_j^{(s)}} \begin{pmatrix} L_j^{(s)} \\ m \end{pmatrix} \frac{(-1)^m}{m!} \Gamma\left(m + \frac{1}{2} \right) {}_1F_1\left(m + \frac{1}{2}, 2; -N\beta \right), \tag{40}$$

where

$$\beta = \frac{a_0^2}{\lambda^2} = \frac{1}{\nu} \tag{41}$$

is the inverse Landau level filling factor. In the case of the smooth density profile, the results are expressed it terms of the integral $\mathcal{J}$ (Appendix A)

$$\langle \Psi_s | \hat{V}^{\rm sm}_{be} | \Psi_{s'} \rangle = -\delta_{ss'} \frac{e^2}{a_0} \sqrt{\frac{\pi\beta}{2}} \sum_{j=1}^{N} \mathcal{J}(L_j^{(s)}, N-1, 0, 1, 0; 1, \beta). \tag{42}$$

The matrix elements (40) and (42) depend on the magnetic field B.

2.5.5. Electron–Electron Interaction Energy

The electron–electron interaction energy is given by the third term in Equation (24). Calculating its many-body matrix elements, I obtain the following result

$$\langle \Psi_s | \hat{V}_{ee} | \Psi_{s'} \rangle = \delta_{ss'} \left(V^H_{ss} - V^F_{ss} \right) + (1 - \delta_{ss'}) V^{\rm off}_{ss'}, \tag{43}$$

where the diagonal matrix elements are given by the difference of Hartree and Fock contributions,

$$V^H_{ss} = \frac{e^2}{2a_0} \int_0^\infty dq a_0 \sum_{i=1}^{N} \langle L_i^{(s)} | e^{i\boldsymbol{q}\cdot\boldsymbol{r}} | L_i^{(s)} \rangle \sum_{j=1}^{N} \langle L_j^{(s)} | e^{-i\boldsymbol{q}\cdot\boldsymbol{r}} | L_j^{(s)} \rangle, \tag{44}$$

$$V^F_{ss} = \frac{e^2}{2a_0} \int_0^\infty dq a_0 \sum_{i=1}^{N} \sum_{j=1}^{N} \left| \langle L_i^{(s)} | e^{i\boldsymbol{q}\cdot\boldsymbol{r}} | L_j^{(s)} \rangle \right|^2. \tag{45}$$

Substituting here the matrix elements of the exponential functions from Equation (10), I obtain

$$V^H_{ss} = \frac{e^2}{a_0} \sqrt{\frac{\pi\beta}{8}} \sum_{j=1}^{N} \sum_{k=1}^{N} \mathcal{K}(L_j^{(s)}, L_k^{(s)}, 0), \tag{46}$$

$$V^F_{ss} = \frac{e^2}{a_0} \sqrt{\frac{\pi\beta}{8}} \sum_{j=1}^{N} \sum_{k=1}^{N} \mathcal{K}(L_{\rm min}, L_{\rm min}, \delta L), \tag{47}$$

where the integrals $\mathcal{K}$ are related to the integrals $\mathcal{J}$ defined above, see Appendix A, and in the last formula

$$L_{\rm min} = \min\{L_j^{(s)}, L_k^{(s)}\}, \;\; L_{\rm max} = \max\{L_j^{(s)}, L_k^{(s)}\}, \;\; \delta L = |L_j^{(s)} - L_k^{(s)}| = L_{\rm max} - L_{\rm min}. \tag{48}$$

The formulation of the results for the off-diagonal matrix elements ($s \neq s'$) requires a slightly longer discussion. First, since $s \neq s'$, the sets of numbers L_j^s and $L_j^{s'}$, $j = 1, 2, \ldots, N$, differ from each other. In general, these sets may differ by one, two or more numbers. The case when they differ by only one number is excluded, as explained above. If they differ by more than two numbers, the corresponding matrix elements equal zero,

$$\langle \Psi_s | \hat{V}_{ee} | \Psi_{s'} \rangle = 0, \text{ if the sets } L_j^s \text{ and } L_j^{s'} \text{ differ by more than two numbers.} \quad (49)$$

Thus, the matrix elements $\langle \Psi_s | \hat{V}_{ee} | \Psi_{s'} \rangle$ are nonzero if and only if the states $|s\rangle$ and $|s'\rangle$ differ from each other by the single-particle states of exactly two particles. For example, for three particles, with the total angular momentum $\mathcal{L} = 9$, Table 2, the matrix elements

$$\langle 0,2,7 | \hat{V}_{ee} | 0,4,5 \rangle \text{ and } \langle 0,1,8 | \hat{V}_{ee} | 1,2,6 \rangle \quad (50)$$

are finite (only two numbers in the bra and ket configurations are different), but the matrix element

$$\langle 0,2,7 | \hat{V}_{ee} | 1,3,5 \rangle \quad (51)$$

is zero (all three numbers are different).

Let the configurations

$$|s\rangle = |\ldots, \underbrace{L_1^s}_{p_1^s}, \ldots, \underbrace{L_2^s}_{p_2^s}, \ldots\rangle \text{ and } |s'\rangle = |\ldots, \underbrace{L_1^{s'}}_{p_1^{s'}}, \ldots, \underbrace{L_2^{s'}}_{p_1^{s'}}, \ldots\rangle \quad (52)$$

differ from each other by the L-states of exactly two particles. I designate them as L_1^s, L_2^s and $L_1^{s'}$, $L_2^{s'}$, and their serial numbers in the sets $|s\rangle$ and $|s'\rangle$ as p_1^s, p_2^s, $p_1^{s'}$, $p_2^{s'}$; all other states in (52), designated by dots, are identical. For example, for the first of the matrix elements in (50), $\langle 0,2,7 | \hat{V}_{ee} | 0,4,5 \rangle$, these numbers are $L_1^s = 2$, $L_2^s = 7$, $p_1^s = 2$, $p_2^s = 3$, and $L_1^{s'} = 4$, $L_2^{s'} = 5$, $p_1^{s'} = 2$, $p_2^{s'} = 3$. For the second matrix element in (50), $\langle 0,1,8 | \hat{V}_{ee} | 1,2,6 \rangle$, they are $L_1^s = 0$, $L_2^s = 8$, $p_1^s = 1$, $p_2^s = 3$, and $L_1^{s'} = 2$, $L_2^{s'} = 6$, $p_1^{s'} = 2$, $p_2^{s'} = 3$.

Now one can formulate the results for the off-diagonal matrix elements of the electron–electron interaction energy. Calculations show that for $s \neq s'$

$$\begin{aligned} V_{ss'}^{\text{off}} &= \frac{e^2}{a_0}\sqrt{\frac{\pi\beta}{2}}(-1)^{p_1^s + p_2^s + p_1^{s'} + p_2^{s'}} \\ &\times \left[\mathcal{K}\Big(\min\{L_1^s, L_1^{s'}\}, \min\{L_2^s, L_2^{s'}\}, |L_1^s - L_1^{s'}|\Big) - \mathcal{K}\Big(\min\{L_1^s, L_2^{s'}\}, \min\{L_2^s, L_1^{s'}\}, |L_1^s - L_2^{s'}|\Big)\right], \end{aligned} \quad (53)$$

where the integrals $\mathcal{K}$ are defined in Equation (A3).

Equations (43), (46), (47), and (53) give the matrix elements of the electron–electron interaction between the basis many-body configurations (26). Note that the magnetic field enters these formulas only via the common prefactor $\sqrt{\beta}$, which means that, for all values of B, the *ee*-interaction matrix needs to be calculated only once.

2.5.6. Pair Correlation Function

The operator of the pair correlation function is defined as

$$\hat{P}(\boldsymbol{r}, \boldsymbol{r}') = \sum_{j=1}^{N} \sum_{k=1, k\neq j}^{N} \delta(\boldsymbol{r} - \boldsymbol{r}_j)\delta(\boldsymbol{r}' - \boldsymbol{r}_k). \quad (54)$$

Its diagonal and off-diagonal matrix elements are determined by the following formulas,

$$\langle \Psi_s | \hat{P}(\boldsymbol{r}, \boldsymbol{r}') | \Psi_s \rangle = \sum_{j=1}^{N} \sum_{k=1}^{N} \left(|\psi_{L_j^{(s)}}(\boldsymbol{r})|^2 |\psi_{L_k^{(s)}}(\boldsymbol{r}')|^2 - \psi^\star_{L_j^{(s)}}(\boldsymbol{r}) \psi_{L_k^{(s)}}(\boldsymbol{r}) \psi_{L_j^{(s)}}(\boldsymbol{r}') \psi^\star_{L_k^{(s)}}(\boldsymbol{r}') \right), \quad (55)$$

$$\langle \Psi_s | \hat{P}(\boldsymbol{r}, \boldsymbol{r}') | \Psi_{s'} \rangle = (-1)^{p_1^s + p_2^s + p_1^{s'} + p_2^{s'}} \left(\psi^{\star}_{L_1^s}(\boldsymbol{r}) \psi^{\star}_{L_2^s}(\boldsymbol{r}') \det \begin{vmatrix} \psi_{L_1^{s'}}(\boldsymbol{r}) & \psi_{L_2^{s'}}(\boldsymbol{r}) \\ \psi_{L_1^{s'}}(\boldsymbol{r}') & \psi_{L_2^{s'}}(\boldsymbol{r}') \end{vmatrix} + (\boldsymbol{r} \leftrightarrow \boldsymbol{r}') \right), \quad s \neq s', \tag{56}$$

where the numbers L_1^s, L_2^s, $L_1^{s'}$, $L_2^{s'}$, as well as p_1^s, p_2^s, $p_1^{s'}$, $p_2^{s'}$ have the same meaning as in the previous Section.

2.6. General Solution of the Many-Body Schrödinger Problem

Let us consider the N-particle Schrödinger equation

$$\hat{\mathcal{H}} \Psi(\boldsymbol{r}_1, \boldsymbol{r}_2, \ldots, \boldsymbol{r}_N) = E \Psi(\boldsymbol{r}_1, \boldsymbol{r}_2, \ldots, \boldsymbol{r}_N). \tag{57}$$

In order to solve it for a given total angular momentum $\mathcal{L}$, the function Ψ should be searched in the form of a linear combination of all $N_{mbs}(N, \mathcal{L})$ many-body configurations corresponding to given values of N and $\mathcal{L}$,

$$|\Psi\rangle = \sum_{s'=1}^{N_{mbs}} A_{s'} |\Psi_{s'}\rangle. \tag{58}$$

In this formula, A_s are unknown numbers. Substituting (58) into (57) and multiplying the resulting equation by $\langle \Psi_s |$, one reduces the Schrödinger problem to the matrix equation

$$\sum_{s'=1}^{N_{mbs}} \langle \Psi_s | \hat{\mathcal{H}} | \Psi_{s'} \rangle A_{s'} = E A_s. \tag{59}$$

The size of the Hamiltonian matrix $\mathcal{H}_{ss'} \equiv \langle \Psi_s | \hat{\mathcal{H}} | \Psi_{s'} \rangle$ here is $N_{mbs} \times N_{mbs}$. Solving the eigenvalue problem (59), one can find N_{mbs} solutions for given N and $\mathcal{L}$: the energies $E_{N,\mathcal{L},k}$ and the sets of numbers $A_s^{N,\mathcal{L},k}$, $k = 1, \ldots, N_{mbs}$, which give the corresponding many-body wave functions according to the expansion (58). After the numbers $A_s^{N,\mathcal{L},k}$ are found, one can also calculate all the physical properties of the ground or excited many-body states, for example, the electron density and the pair correlation function, using the corresponding matrix elements found in Section 2.5.

All matrix elements of the Hamiltonian $\mathcal{H}_{ss'}$ are calculated analytically, see Section 2.5. As a result, the energies and the wave functions of the N-electron system can be calculated, in principle, with a very high accuracy for any $\nu \leq 1$ and any $\mathcal{L}$ and N. In practice, the computation time becomes too large if N or $\mathcal{L}$ are much greater than one, but the ground state physics of an FQHE system can be well understood even if the number of particles is less than or on the order of ten. The results for $N = 7$ are especially valuable, because seven spin-polarized electrons form a highly symmetric piece of a macroscopic Wigner crystal, as can be seen in Figure 3g.

In Section 4, I present the results of the theory for $2 \leq N \leq 7$ and the Landau level filling factor $\nu = 1/3$. Before doing so, however, it is useful to discuss the purely classical solution of the problem.

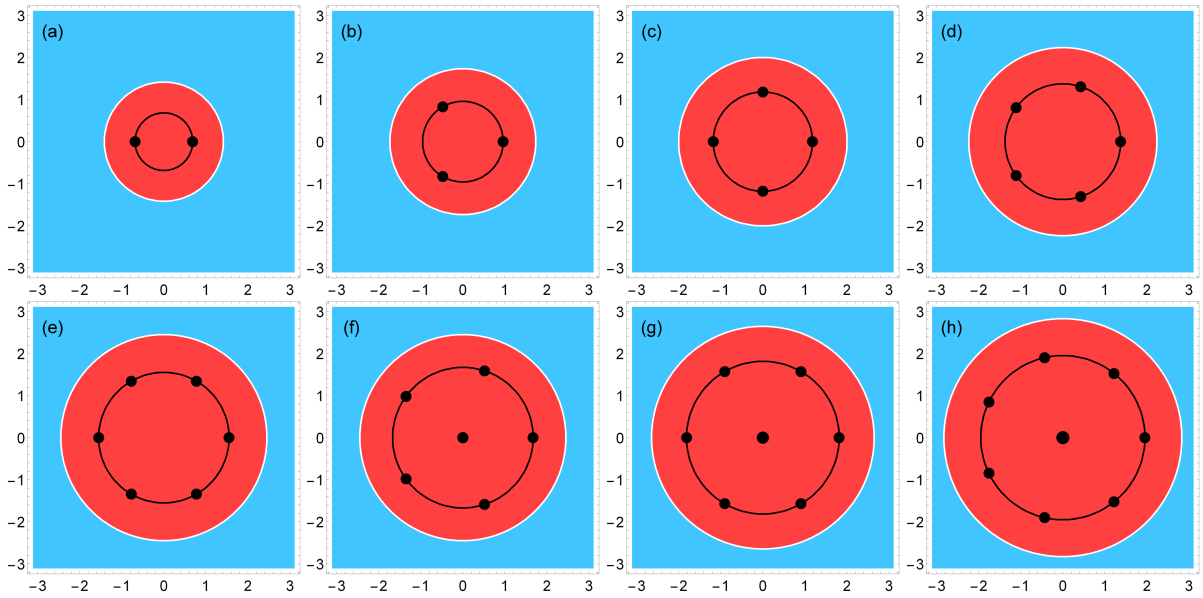

Figure 3. Configurations of the Wigner crystal molecules with $N = 2, \ldots, 8$ in the field of the positively charged background with the step-like density (11). The white circle shows the boundary of the positively charged disk; the length unit is a_0. For $N \leq 5$, the single-shell configurations (**a**–**d**) have a lower energy. For $N \geq 7$, the two-shell configurations (**g**,**h**) have a lower energy. For $N = 6$, the energies of the single-shell (**e**) and the two-shell (**f**) configurations are very close.

3. Wigner Crystal

The physics of the considered system is determined by the interplay of attractive forces acting on the electrons by the positively charged background, and the inter-electron Coulomb forces repelling them from each other. If N (≤ 8) classical point charges are placed in the attractive potential of the positive background, they may form two types of Wigner molecules (at small N), Figure 3: with a single shell, when all N particles are located on a ring of a finite radius R_s, Figure 3a–e, and with two shells, when one particle is at the center of the positively charged disk, and $N-1$ particles are located on a ring around the center, Figure 3f–h. I denote these two configurations as $(0, N)$ and $(1, N-1)$, respectively. To understand which of the two possibilities is actually the case, one should calculate the total energy of the Wigner molecules in both situations.

The potential energy of the positively charged background disk is described by Equations (18) and (19) for the step-like density profile and by Equations (18) and (20) for the smooth density profile. Both potential energies are shown in Figure 2. In the single-shell configuration $(0, N)$, the (dimensionless) complex coordinates of electrons can be written as

$$Z_j = R_s e^{i2\pi(j-1)/N}, \quad j = 1, 2, \ldots, N, \tag{60}$$

with R_s being the shell radius. Then, the total energy of the system is

$$E_{(0,N)}(R_s) = \sum_{j=1}^{N} U_N(|Z_j|) + \sum_{j=1}^{N-1} \sum_{k=j+1}^{N} \frac{1}{|Z_j - Z_k|} = N U_N(R_s) + \frac{1}{R_s} S_N, \tag{61}$$

where $U_N(R)$ are given either by (19) or by (20), and

$$S_N = \sum_{j=1}^{N-1} \sum_{k=j+1}^{N} \frac{1}{|1 - e^{i2\pi(k-j)/N}|}. \tag{62}$$

In the two-shell Wigner molecule $(1, N-1)$, the particle coordinates are

$$Z_j = R_s e^{i2\pi(j-1)/(N-1)}, \quad j = 1, 2, \ldots, N-1, \quad Z_N = 0 \tag{63}$$

and the total energy has the form

$$E_{(1,N-1)}(R_s) = (N-1)U_N(R_s) + U_N(0) + \frac{1}{R_s}\Big(S_{N-1} + (N-1)\Big). \tag{64}$$

Minimizing the energies (61) and (64) with respect to R_s, one can find the radii of the shells $R_s(N)$, for both types of molecules and both types of the density profiles, and their total energies. The results of such calculations are shown in Tables 3 and 4 for the step-like and smooth density profiles. One sees that, for both density profiles, the energy of the $(0, N)$ configuration is smaller than that of the $(1, N-1)$ configuration if $N \leq 5$. The opposite inequality, $E_{(0,N)} > E_{(1,N-1)}$, is valid at $N = 7$ and 8. If $N = 6$, the energies of both configurations are very close to each other: in the case of the step-like density profile (11), the two-shell configuration has a slightly lower energy, with a difference of 0.051%. In the case of the smooth density profile (13), the one-shell configuration has a slightly lower energy, with a difference of 0.871%. Thus, the classical solution of the problem has a rotational symmetry C_n of order n, where

$$n = n^{\mathrm{st}}(N) = \begin{cases} N & \text{if } N \leq 5 \\ N-1 & \text{if } 6 \leq N \leq 8 \end{cases} \tag{65}$$

in the case of the step-like density profile, and

$$n = n^{\mathrm{sm}}(N) = \begin{cases} N & \text{if } N \leq 6 \\ N-1 & \text{if } 7 \leq N \leq 8 \end{cases} \tag{66}$$

in the case of the smooth density profile. At $N = 6$, the C_6 and C_5 configurations have very close energies, so that both of them can be realized in a real system, depending, for example, on the tiny details of the confinement potential. With a further increase in the number of particles ($N \gtrsim 10$), one should expect that configurations with $n = n^{\mathrm{st}}(N) = n^{\mathrm{sm}}(N) = 6$, will have the lowest energy, like in the macroscopic Wigner crystal.

Table 3. Parameters of the Wigner molecules in one-shell $(0, N)$ and two-shell $(1, N-1)$ configurations for the step-like density profile (11) and $2 \leq N \leq 8$. R is the radius of the positively charged background disk, and $R_s(N)$ are the radii of the shells obtained by the minimization of the energies (61) and (64). $E_{(0,N)}/N$ and $E_{(1,N-1)}/N$ are the Wigner molecule energies per particle for two configurations. The lengths are in units a_0, and the energies are in units e^2/a_0.

N	R	Configuration	$R_s(N)$	$E_{(0,N)}/N$	Configuration	$R_s(N)$	$E_{(1,N-1)}/N$
2	1.41421	(0, 2)	0.684302	−2.289449			
3	1.73205	(0, 3)	0.956542	−2.578969	(1, 2)	1.196868	−2.460699
4	2.00000	(0, 4)	1.178838	−2.813969	(1, 3)	1.361107	−2.745380
5	2.23607	(0, 5)	1.373422	−3.012388	(1, 4)	1.518623	−2.983587
6	2.44949	(0, 6)	1.549288	−3.184857	(1, 5)	1.669034	−3.186483
7	2.64575	(0, 7)	1.711287	−3.337907	(1, 6)	1.812600	−3.362913
8	2.82843	(0, 8)	1.862429	−3.475824	(1, 7)	1.949843	−3.519063

Table 4. The same as in Table 3 but for the smooth density profile (13).

N	R	Configuration	$R_s(N)$	$E_{(0,N)}/N$	Configuration	$R_s(N)$	$E_{(1,N-1)}/N$
2	1.41421	(0, 2)	0.621826	−2.067436			
3	1.73205	(0, 3)	0.888015	−2.379006	(1, 2)	1.127002	−2.250789
4	2.00000	(0, 4)	1.107700	−2.630306	(1, 3)	1.282076	−2.553625
5	2.23607	(0, 5)	1.301195	−2.841207	(1, 4)	1.437241	−2.782655
6	2.44949	(0, 6)	1.476787	−3.023620	(1, 5)	1.587616	−3.020984
7	2.64575	(0, 7)	1.638979	−3.184841	(1, 6)	1.732047	−3.206801
8	2.82843	(0, 8)	1.790593	−3.329631	(1, 7)	1.870522	−3.370707

The N-dependencies of the Wigner molecule energies for both configurations are shown in Figure 4. In general, the energy of the system with the step-like density is lower than that of the system with the smooth density by 9.7%–1.2% depending on N. This is due to the fact that, in the case of a step-like density, the potential well is deeper and narrower than in the case of a smooth density, as shown in Figure 2. The spatial distribution of the positive background density and the positions of the charged point particles in the Wigner molecules are additionally illustrated in Figure 3.

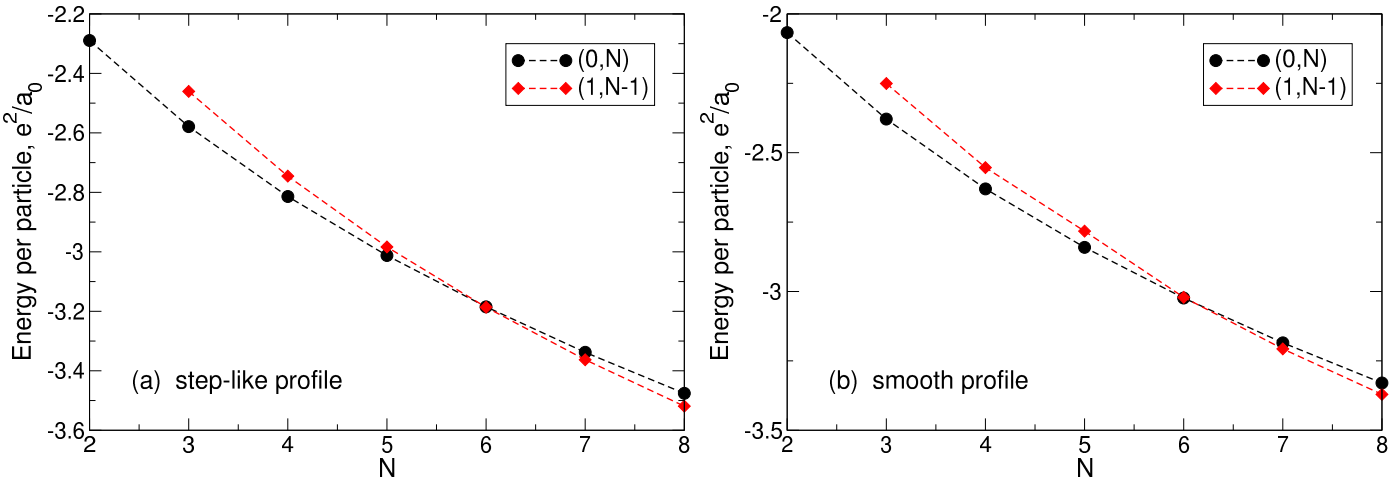

Figure 4. The energy per particle of the Wigner crystal molecules in the N-electron systems with the $(0, N)$ and $(1, N-1)$ configurations for (**a**) the step-like and (**b**) smooth density profiles.

Thus, if $N \leq 8$, electrons, considered as classical point particles, form single- or double-shell Wigner molecules shown in Figure 3. It should therefore be expected that in the quantum-mechanical solution one will have, instead of point particles, broadened (e.g., Gaussian type) wave functions near each point, these wave functions will overlap, and their positions will be averaged over the angular coordinate. The electron density should therefore have the shape of a ring of radius $R_s(N)$ (Tables 3 and 4), with an additional density maximum at $r = 0$ if $N \gtrsim 6$. The exact quantum-mechanical solution obtained in Sections 4 and 7 confirms these expectations. The features related to the symmetries of the Wigner molecules (65) and (66), including the ambiguity of the order of the symmetry axis at $N = 6$, also manifest themselves in the quantum mechanical solution, as will be seen in Section 7.1.5.

4. Exact Solution at $\nu = 1/3$

Now, I present the results of the exact quantum-mechanical solution of the FQHE problem for $N \leq 7$. Since a detailed comparison of this solution with the LS will have to be made, special attention will first be given, in this Section, to the case $\nu = 1/3$. The positive background density is assumed to be step-like, Equation (11), in this Section.

4.1. Ground State Energy and Wave Function

Laughlin assumed [6] that the total angular momentum in the ground state at $\nu = 1/3$ equals $\mathcal{L} = 3\mathcal{L}_{\min} = 3N(N-1)/2$. I have calculated a few lowest energy levels $E_s^{3\mathcal{L}_{\min}}$, $s = 1, 2, 3, \ldots$, for $\nu = 1/3$ and $\mathcal{L} = 3\mathcal{L}_{\min} = 3N(N-1)/2$, in the system with $N = 2, 3, \ldots, 7$ electrons. The results are shown in Table 5. The third and fourth columns there give the energy of the lowest ($s = 1$) and the next ($s = 2$) energy levels; the second column gives the value of the corresponding total angular momentum $\mathcal{L} = 3\mathcal{L}_{\min}$.

In addition, I calculated the energies of the states with a few neighboring angular momenta. I have found that, for the total angular momentum $\mathcal{L} = 3\mathcal{L}_{\min} - \delta\mathcal{L}$, the lowest energy level $E_1^{3\mathcal{L}_{\min}-\delta\mathcal{L}}$ lies between $E_1^{3\mathcal{L}_{\min}}$ and $E_2^{3\mathcal{L}_{\min}}$,

$$E_1^{3\mathcal{L}_{\min}} < E_1^{3\mathcal{L}_{\min}-\delta\mathcal{L}} < E_2^{3\mathcal{L}_{\min}}. \tag{67}$$

The value of $\delta\mathcal{L}$ here coincides with the order of the rotational symmetry axis (65),

$$\delta\mathcal{L} = n^{\mathrm{st}}(N). \tag{68}$$

Thus, while the ground state of the system is the lowest energy state with the angular momentum $\mathcal{L} = 3\mathcal{L}_{\min}$, the first excited state of the system is the lowest energy state with $\mathcal{L} = 3\mathcal{L}_{\min} - \delta\mathcal{L}$,

$$E_{\mathrm{GS}} = E_1^{3\mathcal{L}_{\min}}, \;\; E_{1\mathrm{st}} = E_1^{3\mathcal{L}_{\min}-\delta\mathcal{L}}. \tag{69}$$

This result is valid for the step-like density profile.

The fifth and sixth columns of Table 5 show the angular momentum $3\mathcal{L}_{\min} - \delta\mathcal{L}$ and the energy $E_1^{3\mathcal{L}_{\min}-\delta\mathcal{L}}$. The energy difference $E_{1\mathrm{st}} - E_{\mathrm{GS}}$ between the first excited and the ground state is shown in the seventh column in Table 5. This difference is always smaller than $0.1e^2/a_0$ and mainly decreases as N grows. The case of $N = 6$ particles is an exception related to the rearrangement of the shell structure from $(0, N)$ into $(1, N-1)$ at $N = 6$, see Figures 3e,f.

Table 5. Exact and Laughlin energies, as well as relevant angular momenta, of the lowest-energy states for the different numbers of particles N. Second column: The total angular momentum $3\mathcal{L}_{\min}$ corresponding to the true ground and Laughlin states. Third and fourth columns: The exact energies of the two lowest levels of the states with $\mathcal{L} = 3\mathcal{L}_{\min}$. Fifth and sixth columns: The total angular momentum $3\mathcal{L}_{\min} - \delta\mathcal{L}$ and the lowest energy $E_1^{3\mathcal{L}_{\min}-\delta\mathcal{L}}$ corresponding to the true first excited state; here $\delta\mathcal{L} = n^{\mathrm{st}}(N)$, Equation (65). Seventh column: The energy difference $E_{1\mathrm{st}} - E_{\mathrm{GS}}$ between the true first excited and the true ground state, as shown in Equation (69). Eighth column: The exactly calculated energy of the Laughlin state. Ninth column: The energy difference $E_{\mathrm{LS}} - E_{\mathrm{GS}}$ between the LS and the true ground state. All energies are in units e^2/a_0. The step-like background density profile is assumed.

N	$3\mathcal{L}_{\min}$	$E_1^{3\mathcal{L}_{\min}}$	$E_2^{3\mathcal{L}_{\min}}$	$3\mathcal{L}_{\min} - \delta\mathcal{L}$	$E_1^{3\mathcal{L}_{\min}-\delta\mathcal{L}}$	$E_{1\mathrm{st}} - E_{\mathrm{GS}}$	E_{LS}	$E_{\mathrm{LS}} - E_{\mathrm{GS}}$
2	3	−1.872042	−1.447705	1	−1.773044	0.098998	−1.871568	0.000474
3	9	−2.852911	−2.479623	6	−2.811722	0.041189	−2.840219	0.012692
4	18	−3.837655	−3.534888	14	−3.813058	0.024597	−3.809984	0.027671
5	30	−4.810806	−4.610344	25	−4.786288	0.024518	−4.779627	0.031179
6	45	−5.783597	−5.645735	40	−5.745154	0.038443	−5.754097	0.029500
7	63	−6.775065	−6.626187	57	−6.767761	0.007304	−6.732099	0.042965

Figure 5 shows the energies (per particle) of the ground and the first excited states, Equation (69), as a function of the electron number N (black circles and red squares, respectively).

The expansion coefficients A_s^{GS} of the ground state many-body wave functions $|\Psi_{\mathrm{GS}}\rangle$ over the basis states $|\Psi_s\rangle$, see Equation (58), are shown in Tables 6 and 7 for two and three particles. The largest contribution to the ground-state wave function for $N = 2$ and 3 is given by the states $|1, 2\rangle$ and $|2, 3, 4\rangle$, respectively. The vectors A_s^{GS} for $N \geq 4$ particles can be found in Ref. [37], see also Appendix C.

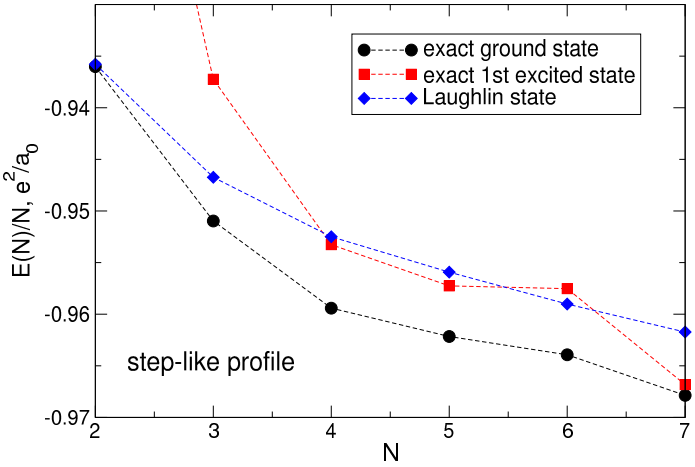

Figure 5. The energy per particle of the exact ground (black circles) and the first excited (red squares) states, Equation (69), as well as of the Laughlin state (5), at $\nu = 1/3$, as a function of the number of particles N. The energies are in units e^2/a_0.

Table 6. The expansion coefficients A_s^{GS} for the exact ground state of $N = 2$ particles.

s	State	A_s^{GS}
1	$\|0,3\rangle$	-0.47078
2	$\|1,2\rangle$	0.88225

Table 7. The expansion coefficients A_s^{GS} for the exact ground state of $N = 3$ particles.

s	State	A_s^{GS}
1	$\|0,1,8\rangle$	0.01613
2	$\|0,2,7\rangle$	-0.03971
3	$\|0,3,6\rangle$	-0.08983
4	$\|0,4,5\rangle$	0.32071
5	$\|1,2,6\rangle$	0.29234
6	$\|1,3,5\rangle$	-0.44922
7	$\|2,3,4\rangle$	0.77458

4.2. Density of Electrons in the Ground State

The density of the electrons in the exact ground states in systems with different N can be calculated using the matrix elements (34) and the expansion coefficients of the exact ground state wave function A_s^{GS},

$$n_e^{\mathrm{GS}}(r) = \sum_{s=1}^{N_{mbs}} \left(A_s^{\mathrm{GS}}\right)^2 \sum_{j=1}^{N} |\psi_{L_j^{(s)}}(\boldsymbol{r})|^2. \tag{70}$$

The results of the calculations are shown in Figure 6a for $N = 2, \ldots, 7$. The electron density calculated by quantum mechanics is in complete agreement with the expectations arising from the classical considerations in Section 3. When N grows from 2 to 4, the density curves have maxima at the points which are very close to the radii of the classical Wigner molecules for these N, and the densities in the disk center $n_e(r = 0)$ decrease, since as N increases, the electrons repel stronger from the disk center. Starting from $N = 5$, the probability of finding one electron in the disk center starts to grow. At $N = 5$, the density at $r = 0$ increases, and the maximum of the curve shifts slightly beyond the position of the classical Wigner molecule shell, since this central electron pushes the other electrons towards the edge of the disk. At $N = 6$, a local maximum at $r = 0$ appears. At $N = 7$, a giant maximum arises in the disk center, with the value of $n_e(r = 0)$, larger than the n_e-maximum at a finite $r \simeq R_s$.

Figure 6b shows the density of electrons in the exact ground state ($\mathcal{L} = 63$) and in the first excited state ($\mathcal{L} = 57$) for seven particles. It can be seen that the distribution of electrons in the first excited state also resembles a Wigner molecule, but with somewhat different parameters: in the excited state, the probability of finding an electron in the disk center is higher than in the ground state, and the radius of the outer shell of the electron ring is slightly smaller. Physical reasons for such a behavior of the densities of the ground and the first excited states will be clarified in Section 7.

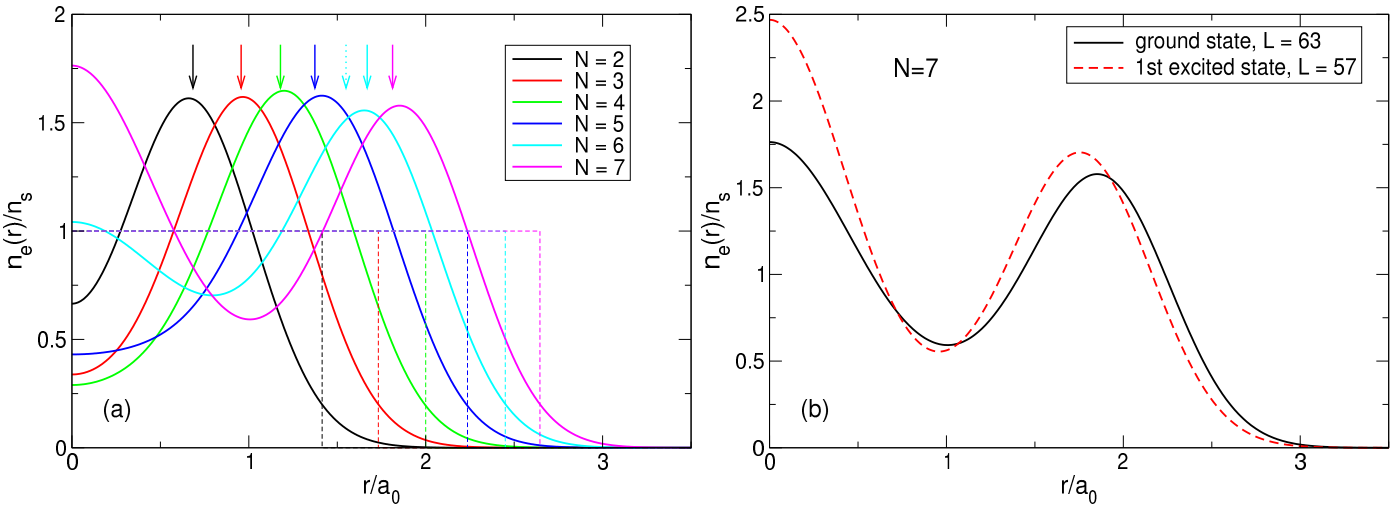

Figure 6. (**a**) The density of electrons in the exact ground state (thick solid curves), together with the density of the positive background (thin dashed curves) for $N = 2 \ldots 7$ for the step-like background density profile (11). Arrows above the curves show the radii of the outer shells $R_s(N)$ of the Wigner molecules, see Table 3; for $N = 6$, the shell radii of both $(0, N)$ (dashed arrow) and $(1, N-1)$ (solid arrow) configurations are shown. (**b**) The density of electrons in the exact ground state ($\mathcal{L} = 63$) and the first excited state ($\mathcal{L} = 57$) for $N = 7$.

The exact quantum-mechanical solution thus clearly shows that the ground state of a few (up to $N = 7$) two-dimensional electrons at the Landau level filling factor $\nu = 1/3$ has the form resembling a floating (or sliding) Wigner crystal molecule [38–42]. This agrees with the intuitive understanding of the physics of Coulomb-interacting particles.

4.3. Pair Correlation Function in the Ground State

The pair correlation function in the ground state can be calculated using the formula

$$P_{\rm GS}(\boldsymbol{r}, \boldsymbol{r}') = \sum_{s=1}^{N_{mbs}} A_s^{\rm GS} \sum_{s'=1}^{N_{mbs}} A_{s'}^{\rm GS} \langle \Psi_s | \hat{P}(\boldsymbol{r}, \boldsymbol{r}') | \Psi_{s'} \rangle, \tag{71}$$

with the matrix elements determined by Equations (55) and (56). Examples of the calculated function $P_{\rm GS}(\boldsymbol{r}, \boldsymbol{r}')$ are shown in Figure 7. Here, the colored distribution shows the probability of finding an electron at a point $\boldsymbol{r}$ under the condition that another electron is fixed at the point $\boldsymbol{r}'$ shown by small black circles on the panels. The panels (a), (b), and (c) illustrate the cases when the points $\boldsymbol{r}'$ are outside the disk center at the distance corresponding to the maxima of the electron density, Figure 6. Figure 7a illustrates the case of $N = 3$ particles. One sees a triangular structure which resembles the classical Wigner molecule configuration shown in Figure 3b. Starting from $N = 4$, crystalline electron–electron correlations are significantly weakened: they are still weakly seen Figure 7b corresponding to $N = 4$, but becomes invisible at a larger N, see Figure 7c for $N = 6$, where only one maximum is seen opposite the point $\boldsymbol{r}'$. This is a consequence of the significant overlap of single-particle wave functions and of the averaging of their positions over the angular coordinate.

Figure 7d shows the pair correlation function for the case $N = 7$ and $\boldsymbol{r}' = \boldsymbol{0}$. Now the function $P_{\mathrm{GS}}(\boldsymbol{r}, \boldsymbol{0})$ is circularly symmetric and has a maximum at $r \approx 1.16 a_0$. The behavior of $P(\boldsymbol{r}, \boldsymbol{0})$ at small r is quadratic, $P_{\mathrm{GS}}(\boldsymbol{r}, \boldsymbol{0}) \propto r^2$ at $r \to 0$.

Thus, although the ground state of the system at $\nu = 1/3$ resembles a Wigner molecule, its internal structure is not rigid like that of a real crystal. The analogy with the Wigner crystal appears only in the fact that the maxima of the electron density are located where they are expected according to the distribution of classical particles.

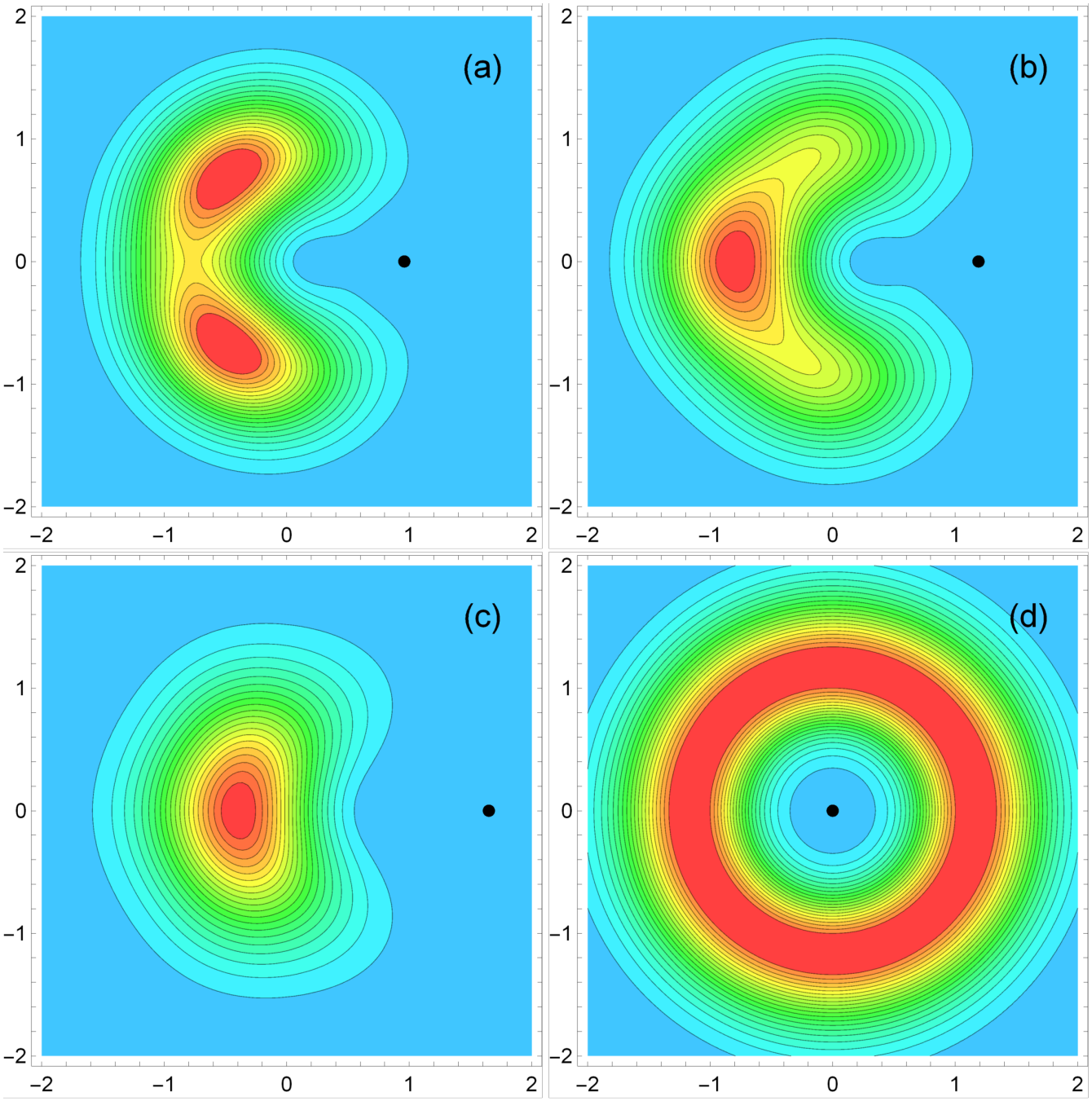

Figure 7. The pair correlation function $P_{\mathrm{GS}}(\boldsymbol{r}, \boldsymbol{r}')$ in the ground state, as a function of x/a_0 and y/a_0, for different N and different coordinates $\boldsymbol{r}'$: (**a**) $N = 3$ and $\boldsymbol{r}'/a_0 = (0.96, 0)$; (**b**) $N = 4$ and $\boldsymbol{r}'/a_0 = (1.19, 0)$; (**c**) $N = 6$ and $\boldsymbol{r}'/a_0 = (1.65, 0)$; and (**d**) $N = 7$ and $\boldsymbol{r}'/a_0 = (0, 0)$. The positions of the $\boldsymbol{r}'$ points are shown by small black circles; in (**a**–**c**), they correspond to the maxima of the electron density, see Figure 6.

5. Maximum Density Droplet State, $\nu = 1$

Using the mathematical apparatus developed in Section 2, one can now calculate the properties of the states (5) for few-electron systems and compare them with those of the exact ground state. But, before proceeding to the discussion of the case $m = 3$ ($\nu = 1/3$), it will be useful to briefly overview the physical properties of the MDD configuration [7], which is a special case of the function (5) at $m = 1$. Only results for the step-like profile of the uniform background are shown in this Section.

5.1. Wave Function

The MDD configuration

$$\Psi_{\rm mdd} = |0,1,2,\ldots,N-1\rangle = \frac{1}{\sqrt{N!}} \det \begin{vmatrix} \psi_0(\boldsymbol{r}_1) & \psi_0(\boldsymbol{r}_2) & \ldots & \psi_0(\boldsymbol{r}_N) \\ \psi_1(\boldsymbol{r}_1) & \psi_1(\boldsymbol{r}_2) & \ldots & \psi_1(\boldsymbol{r}_N) \\ \ldots & \ldots & \ldots & \ldots \\ \psi_{N-1}(\boldsymbol{r}_1) & \psi_{N-1}(\boldsymbol{r}_2) & \ldots & \psi_{N-1}(\boldsymbol{r}_N) \end{vmatrix}, \quad (72)$$

describes the ground state of the system at $\nu = 1$, if the influence of higher Landau levels is neglected, Ref. [7]. In this configuration, N electrons occupy the lowest Landau level single-particle states with the smallest possible individual angular momenta from $L = 0$ up to $L = N - 1$. Since $\psi_L(\boldsymbol{r})$ is proportional to z^L, the matrix in (72) has the form of the Vandermonde matrix, and its determinant can be presented in the form (5) with $m = 1$. The total angular momentum in the MDD state is $\mathcal{L} = \mathcal{L}_{\rm min} = N(N-1)/2$, Equation (30). The number of many-body configurations for a given N and $\mathcal{L} = \mathcal{L}_{\rm min}$ equals one, $N_{mbs}(N, \mathcal{L}_{\rm min}) = 1$.

5.2. Energy of an N-Particle System

The energy of the MDD state

$$E_{\rm mdd}(N) = \langle \Psi_{\rm mdd} | \hat{V}_{bb} + \hat{V}_{be} + \hat{V}_{ee} | \Psi_{\rm mdd} \rangle \quad (73)$$

can be calculated using the Coulomb matrix elements found in Section 2.5. The background–background interaction energy in this formula is given, for the step-like background density profile, by Equation (37); the calculation of the background–electron interaction energy in the MDD case gives

$$\langle \Psi_{\rm mdd} | \hat{V}_{be} | \Psi_{\rm mdd} \rangle = -N \frac{e^2}{a_0} 2 \frac{\Gamma\left(N + \frac{1}{2}\right)}{\Gamma(N)} {}_2F_2\left(-\frac{1}{2}, \frac{1}{2}; 2, \frac{1}{2} - N; -N\right), \quad (74)$$

see Appendix B.2, and the electron–electron (Hartree minus Fock) interaction energy is

$$\langle \Psi_{\rm mdd} | \hat{V}_{ee} | \Psi_{\rm mdd} \rangle = \frac{e^2}{a_0} \sqrt{\frac{\pi}{2}} \sum_{L=0}^{N-2} \sum_{L'=L+1}^{N-1} \Big[\mathcal{K}(L, L', 0) - \mathcal{K}(L, L, L' - L) \Big]. \quad (75)$$

The energy (73) (per particle) calculated for N up to $N = 100$ is shown in Figure 8 by the black curves and symbols, as a function of N in Figure 8a, and as a function of $N^{-1/2}$ in Figure 8b.

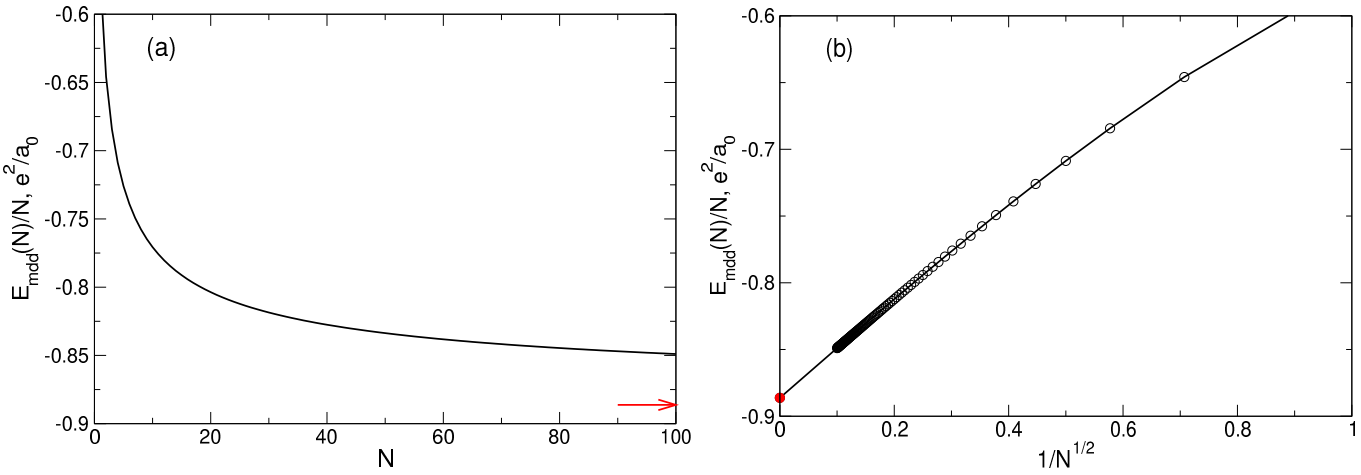

Figure 8. The energy per particle of the MDD state (72), measured in units e^2/a_0, (**a**) as a function of the number of electrons N and (**b**) as a function of $1/\sqrt{N}$. The red arrow in (**a**) and red point in (**b**) show the asymptotic value (82), reported in Ref. [6].

5.3. Electron Density

The density of the electrons in the MDD state (72), according to (34), is

$$n_e^{\mathrm{mdd}}(\boldsymbol{r}) = \sum_{L=0}^{N-1} |\psi_L(\boldsymbol{r})|^2 = \frac{1}{\pi\lambda^2} e^{-r^2/\lambda^2} \sum_{L=0}^{N-1} \frac{(r/\lambda)^{2L}}{L!} = n_s Q(N, r^2/\lambda^2). \tag{76}$$

The density $n_e^{\mathrm{mdd}}(r)$ is constant and equals n_s up to $r \simeq R - \lambda = R - a_0$, Figure 9. In the limit $N \to \infty$, the density $n_e^{\mathrm{mdd}}(r)$ becomes homogeneous in the whole 2D space. The state (72) thus describes an ideally uniform liquid. The structure typical for a Wigner crystal does not arise in this state, since the function (72) does not satisfy the many-body Schrödinger equation (57) with the Hamiltonian (22) , i.e., in the MDD state, the Coulomb interaction is completely ignored. In order to obtain a more accurate description of the ground state at $\nu = 1$, the single-particle states from the higher Landau levels should be taken into account.

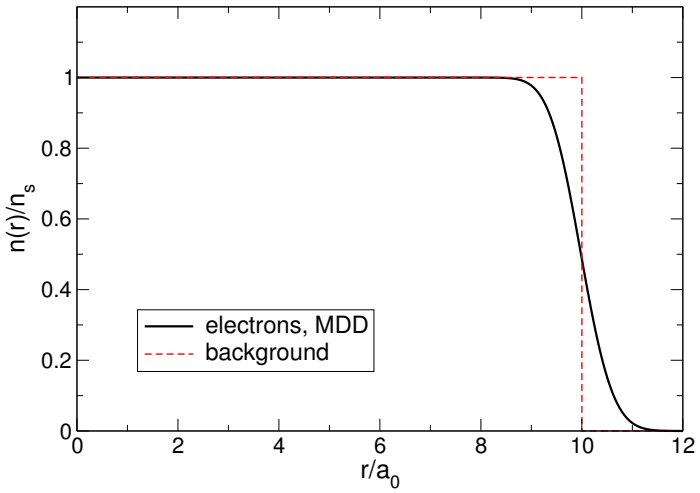

Figure 9. The density of the electrons in the MDD state at $\nu = 1$ (black solid curve) and the density of the positive background $n_b(r)$ (red dashed curve) for $N = 100$. The density is plotted as a function of r/a_0 or r/λ (at $\nu = 1$ $\lambda = a_0$).

5.4. Pair Correlation Function

The pair correlation function of the MDD configuration can be found by calculating the average value of the operator (54) with the wave function (72). It can be presented in the form

$$P(\boldsymbol{r},\boldsymbol{r}') = n_e(\boldsymbol{r})n_e(\boldsymbol{r}') + \delta P(\boldsymbol{r},\boldsymbol{r}'), \tag{77}$$

where

$$\delta P_{\rm mdd}(\boldsymbol{r},\boldsymbol{r}') = -n_s^2 e^{-|z-z'|^2} Q(N, zz'^{\star}) Q(N, z^{\star}z'), \tag{78}$$

and $z = (x - iy)/\lambda$. The dependence of $P_{\rm mdd}(\boldsymbol{r},\boldsymbol{r}')$ on x/a_0 and y/a_0 at $\boldsymbol{r}'/a_0 = (0,0)$ and $\boldsymbol{r}'/a_0 = (3,0)$ for $N = 30$ particles is shown in Figure 10. The pair correlation function tends to unity when $|\boldsymbol{r} - \boldsymbol{r}'|/a_0 \gg 1$ and both points, $\boldsymbol{r}$ and $\boldsymbol{r}'$, are far from the system boundaries. In the limit $|\boldsymbol{r} - \boldsymbol{r}'| \to 0$, the function $P_{\rm mdd}(\boldsymbol{r},\boldsymbol{r}')$ tends to zero as $|\boldsymbol{r} - \boldsymbol{r}'|^2$ due to the exchange "interaction".

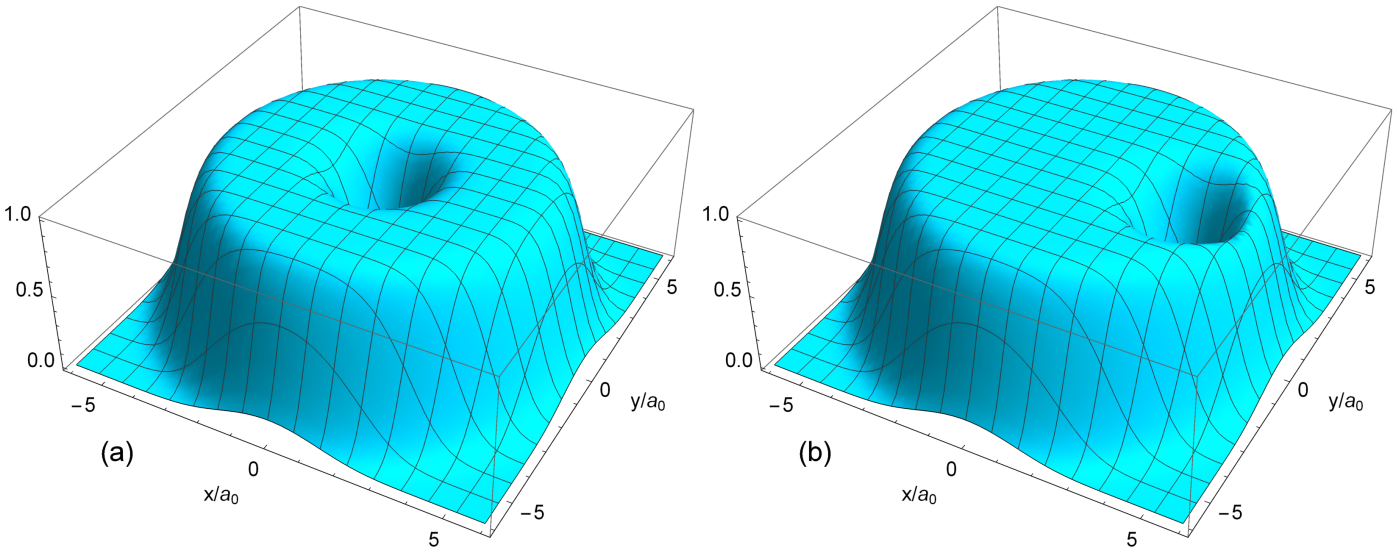

Figure 10. The pair correlation function of the MDD state (72), as a function of $\boldsymbol{r}/a_0$, at $N = 30$ and (**a**) $\boldsymbol{r}'/a_0 = (0,0)$ and (**b**) $\boldsymbol{r}'/a_0 = (3,0)$.

5.5. Thermodynamic Limit

If Ψ is a many-body wave function of an N-particle system, the average value of the energy in this state $E(N) = \langle\Psi|\hat{\mathcal{H}}|\Psi\rangle = \langle\Psi|\hat{V}_C|\Psi\rangle$ can be presented in the form (the kinetic energy contribution $N\hbar\omega_c/2$ is omitted)

$$E(N) = \langle\Psi|\hat{V}_C|\Psi\rangle = \frac{e^2}{2}\int\frac{d\boldsymbol{r}d\boldsymbol{r}'}{|\boldsymbol{r}-\boldsymbol{r}'|}\delta n(\boldsymbol{r})\delta n(\boldsymbol{r}') + \frac{e^2}{2}\int\frac{d\boldsymbol{r}d\boldsymbol{r}'}{|\boldsymbol{r}-\boldsymbol{r}'|}\delta P(\boldsymbol{r},\boldsymbol{r}'), \tag{79}$$

where $\delta n(\boldsymbol{r}) = n_e(\boldsymbol{r}) - n_b(\boldsymbol{r})$ and $\delta P(\boldsymbol{r},\boldsymbol{r}')$ is defined in Equation (77). The first term in (79) is the Hartree energy, which vanishes if the electron and positive background densities are identical. This condition is satisfied at $\nu = 1$ in the MDD state in the limit $N \to \infty$, when the density of electrons $n_e^{\rm mdd}(r)$ becomes ideally uniform in the whole 2D space, $n_e^{\rm mdd}(r) \to n_s$. The regularized incomplete Gamma function $Q(N,x)$ tends to unity at $N \to \infty$, and the pair correlation function (78) becomes a function of only the inter-particle distance $|\boldsymbol{r} - \boldsymbol{r}'|$,

$$\delta P_{\rm mdd}(\boldsymbol{r} - \boldsymbol{r}') = -n_s^2 e^{-|\boldsymbol{r}-\boldsymbol{r}'|^2/a_0^2}. \tag{80}$$

For the MDD energy, one then obtains from (79)

$$E_{\rm mdd}(N) \approx \frac{e^2}{2}\int d\boldsymbol{r}\int\frac{d\boldsymbol{r}'}{|\boldsymbol{r}-\boldsymbol{r}'|}\delta P_{\rm mdd}(|\boldsymbol{r}-\boldsymbol{r}'|) \approx \frac{e^2}{2}\pi R^2\int\frac{d\boldsymbol{r}'}{|\boldsymbol{r}'|}\delta P_{\rm mdd}(|\boldsymbol{r}'|). \tag{81}$$

Since $\pi R^2 n_s = N$, this gives the energy per particle in the thermodynamic limit $N \to \infty$

$$\frac{E_{\rm mdd}(N)}{N} = \frac{\pi e^2}{n_s}\int_0^\infty dr \delta P_{\rm mdd}(r) = -\frac{e^2}{a_0}\frac{\sqrt{\pi}}{2}. \tag{82}$$

This formula was reported for $\nu = 1$ in Ref. [6]. The asymptotic value (82) is shown by the red arrow and red point in Figures 8a,and b, respectively. Notice that the formulas (81) and (82) are valid only if the density of electrons is uniform in the whole 2D space—only in this case does the Hartree energy in (79) vanish and the pair correlation function $P_{\rm mdd}(\boldsymbol{r}, \boldsymbol{r}')$ becomes a function of $|\boldsymbol{r} - \boldsymbol{r}'|$.

6. Laughlin State at $\nu = 1/3$

6.1. General Remarks

Now, let us calculate the energy, electron density, and other physical properties of the system in the state (5) at $\nu = 1/m = 1/3$. To do this, I proceed as follows.

The function (5) is the eigenfunction of the angular momentum operator with the eigenvalue

$$\mathcal{L} = m\frac{N(N-1)}{2} = 3\frac{N(N-1)}{2}. \tag{83}$$

For any given N and $\mathcal{L}$, I determine N_{mbs} many-body states, formed from the lowest Landau level single-particle functions (8), and expand the function (5) in these basis states,

$$\Psi_{\rm LS}^{(m=3)} = \sum_{s=1}^{N_{mbs}} A_s^{\rm LS}\Psi_s. \tag{84}$$

The coefficients $A_s^{\rm LS}$ here are real numbers, and the function (84) is assumed to be normalized, i.e., $\sum_{s=1}^{N_{mbs}}\left(A_s^{\rm LS}\right)^2 = 1$. After the coefficients $A_s^{\rm LS}$ are found, any physical quantity F can be calculated as the average

$$F = \langle\Psi_{\rm LS}^{(m=3)}|\hat{F}|\Psi_{\rm LS}^{(m=3)}\rangle = \sum_{s=1}^{N_{mbs}}\sum_{s'=1}^{N_{mbs}} A_s^{\rm LS}A_{s'}^{\rm LS}\langle\Psi_s|\hat{F}|\Psi_{s'}\rangle, \tag{85}$$

where the matrix elements $\langle\Psi_s|\hat{F}|\Psi_{s'}\rangle$ are found in Section 2.5 for commonly used operators. How to calculate the coefficients $A_s^{\rm LS}$?

6.2. Expansion Coefficients of the Laughlin Function

The coefficients $A_s^{\rm LS}$ in (84) can be found as follows. First, using the binomial expansion of the polynomial factors in the function (5), I obtain integer binomial coefficients C_s, as in the following example for two particles:

$$(z_1 - z_2)^3 = z_1^3 - 3z_1^2z_2 + 3z_1z_2^2 - z_2^3 = (-1)\det\begin{vmatrix} z_1^0 & z_2^0 \\ z_1^3 & z_2^3 \end{vmatrix} + 3\det\begin{vmatrix} z_1^1 & z_2^1 \\ z_1^2 & z_2^2 \end{vmatrix}; \tag{86}$$

I denote the coefficients C_s as

$$C_{|0,3\rangle} = -1 \text{ and } C_{|1,2\rangle} = 3. \tag{87}$$

The determinants in (86) are proportional to the basis functions $|0,3\rangle$ and $|1,2\rangle$. For example,

$$|0,3\rangle = \frac{1}{\sqrt{2!}}\det\begin{vmatrix} \psi_0(\boldsymbol{r}_1) & \psi_0(\boldsymbol{r}_2) \\ \psi_3(\boldsymbol{r}_1) & \psi_3(\boldsymbol{r}_2) \end{vmatrix} = \frac{1}{\sqrt{2!}}\det\begin{vmatrix} z_1^0 & z_2^0 \\ z_1^3 & z_2^3 \end{vmatrix}\frac{e^{-(|z_1|^2+|z_2|^2)/2}}{\pi\lambda^2\sqrt{0!3!}}, \tag{88}$$

so that one obtains

$$\det \begin{vmatrix} z_1^0 & z_2^0 \\ z_1^3 & z_2^3 \end{vmatrix} \propto \sqrt{0!3!}\,|0,3\rangle. \tag{89}$$

Then, the expansion of the function (5) for two particles takes the form

$$(z_1 - z_2)^3 e^{-(|z_1|^2+|z_2|^2)/2} \propto D_{|0,3\rangle}|0,3\rangle + D_{|1,2\rangle}|1,2\rangle, \tag{90}$$

where

$$D_{|L_1,L_2\rangle} = \sqrt{L_1!L_2!}C_{|L_1,L_2\rangle}. \tag{91}$$

Thus, in order to calculate (for any N) the real coefficients A_s^{LS} in the expansion (84), one needs to find, first, the integers binomial coefficients $C_s = C_{|L_1,L_2,\ldots,L_N\rangle}$ in the expansions of the polynomial factors in (5), then calculate the D_s factors according to the formula

$$D_{|L_1,L_2,\ldots,L_N\rangle} = \sqrt{L_1!L_2!\ldots L_N!}C_{|L_1,L_2,\ldots,L_N\rangle}, \tag{92}$$

and finally determine the real coefficients A_s^{LS} using the normalization condition

$$A_s^{\mathrm{LS}} = \frac{D_s}{\sqrt{\sum_{p=1}^{N_{mbs}} D_p^2}}. \tag{93}$$

Now, I apply the described algorithm to the Laughlin wave function for a few values of the particle number N.

6.2.1. Two Particles

If $N = 2$, then the angular momentum (83) at $\nu = 1/3$ equals $\mathcal{L} = 3$. The number of many-body states in this case is $N_{mbs} = 2$, and they are $|0,3\rangle$ and $|1,2\rangle$, see Table 1. Expanding the factor $(z_1 - z_2)^3$ as in (86), I obtain the coefficients C_s, Equation (87), D_s, A_s^{LS}, and $\left(A_s^{\mathrm{LS}}\right)^2$. The results are shown in Table 8.

Table 8. Many-body configurations for $N = 2$ and $\mathcal{L} = 3$, with the expansion coefficients C_s, A_s^{LS}, and $\left(A_s^{\mathrm{LS}}\right)^2$. The coefficients D_s can be found using Equation (92).

No.	Configuration	C_s	A_s^{LS}	$\left(A_s^{\mathrm{LS}}\right)^2$
1	$\|0,3\rangle$	-1	-0.5	0.25
2	$\|1,2\rangle$	3	0.86603	0.75

6.2.2. Three Particles

If $N = 3$, then the angular momentum (83) equals $\mathcal{L} = 9$. Now one has $N_{mbs} = 7$ many-body states, see Table 2. Using again the binomial expansion

$$(z_1 - z_2)^3(z_1 - z_3)^3(z_2 - z_3)^3 \propto -\Delta_{|0,3,6\rangle} + 3\Delta_{|0,4,5\rangle} + 3\Delta_{|1,2,6\rangle} - 6\Delta_{|1,3,5\rangle} + 15\Delta_{|2,3,4\rangle}, \tag{94}$$

where

$$\Delta_{|j,k,l\rangle} = \det \begin{vmatrix} z_1^j & z_2^j & z_3^j \\ z_1^k & z_2^k & z_3^k \\ z_1^l & z_2^l & z_3^l \end{vmatrix}, \tag{95}$$

I get the coefficients C_s, A_s^{LS}, and $\left(A_s^{\mathrm{LS}}\right)^2$ shown in Table 9. Not all possible basis functions Ψ_s are represented in the LS (5). Two configurations, $|0,1,8\rangle$ and $|0,2,7\rangle$, have zero weights in $\Psi_{\mathrm{LS}}^{(m=3)}$.

Table 9. Many-body configurations for $N = 3$ and $\mathcal{L} = 9$, with the expansion coefficients C_s, A_s^{LS}, and $\left(A_s^{\mathrm{LS}}\right)^2$. The coefficients D_s can be found using Equation (92).

No.	Configuration	C_s	A_s^{LS}	$\left(A_s^{\mathrm{LS}}\right)^2$
1	$\|0,1,8\rangle$	0	0.0	0.0
2	$\|0,2,7\rangle$	0	0.0	0.0
3	$\|0,3,6\rangle$	-1	-0.17961	0.03226
4	$\|0,4,5\rangle$	3	0.43994	0.19355
5	$\|1,2,6\rangle$	3	0.31109	0.09677
6	$\|1,3,5\rangle$	-6	-0.43994	0.19355
7	$\|2,3,4\rangle$	15	0.69561	0.48387

6.2.3. Four Particles

If $N = 4$, then the total angular momentum (83) equals $\mathcal{L} = 18$, and the number of many-body states is $N_{mbs} = 34$. Applying the binomial expansion procedure I calculate the numbers C_s. Only 16 of them are nonzero; these states, the corresponding integer binomial coefficients C_s, as well as the numbers A_s^{LS} and $\left(A_s^{\mathrm{LS}}\right)^2$, are shown in Table 10. The other 18 states, namely

$$\begin{aligned}
&|0,1,2,15\rangle,\ |0,1,3,14\rangle,\ |0,1,4,13\rangle,\ |0,1,5,12\rangle,\ |0,1,6,11\rangle,\ |0,1,7,10\rangle,\ |0,1,8,9\rangle,\\
&|0,2,3,13\rangle,\ |0,2,4,12\rangle,\ |0,2,5,11\rangle,\ |0,2,6,10\rangle,\ |0,2,7,9\rangle,\\
&|0,3,4,11\rangle,\ |0,3,5,10\rangle,\\
&|1,2,3,12\rangle,\ |1,2,4,11\rangle,\ |1,2,5,10\rangle,\\
&|1,3,4,10\rangle
\end{aligned}$$

have zero weights $C_s = 0$ in the LS.

Table 10. Many-body configurations for $N = 4$ and $\mathcal{L} = 18$, with the expansion coefficients C_s, A_s^{LS}, and $\left(A_s^{\mathrm{LS}}\right)^2$. The coefficients D_s can be found using Equation (92).

No.	Configuration	C_s	A_s^{LS}	$\left(A_s^{\mathrm{LS}}\right)^2$
15	$\|0,3,6,9\rangle$	1	0.05322	0.00283
16	$\|0,3,7,8\rangle$	-3	-0.14082	0.01983
17	$\|0,4,5,9\rangle$	-3	-0.13037	0.01700
18	$\|0,4,6,8\rangle$	6	0.21290	0.04533
19	$\|0,5,6,7\rangle$	-15	-0.42078	0.17705
23	$\|1,2,6,9\rangle$	-3	-0.09219	0.00850
24	$\|1,2,7,8\rangle$	9	0.24391	0.05949
26	$\|1,3,5,9\rangle$	6	0.13037	0.01700
27	$\|1,3,6,8\rangle$	-12	-0.21290	0.04533
28	$\|1,4,5,8\rangle$	-9	-0.13037	0.01700
29	$\|1,4,6,7\rangle$	27	0.33872	0.11473
30	$\|2,3,4,9\rangle$	-15	-0.20614	0.04249
31	$\|2,3,5,8\rangle$	27	0.27656	0.07649
32	$\|2,3,6,7\rangle$	-6	-0.05322	0.00283
33	$\|2,4,5,7\rangle$	-45	-0.32593	0.10623
34	$\|3,4,5,6\rangle$	105	0.49787	0.24788

6.2.4. Five-to-Eight Particles

The cases of $N = 5,\ldots,8$ particles can be analyzed similarly. The full tables with all many-body configurations and their weights are very large and not shown here; they can be found in Ref. [37], see Appendix C. Here, I give only a brief overview of some key features of the Laughlin function expansions that are useful for the subsequent analysis of the problem.

The number of many-body configurations which are *not* used in the LS dramatically grows with the number of particles N. Table 11 shows the total number of many-body configurations for a given N and $\mathcal{L}$, $N_{mbs}(N,\mathcal{L})$, the number of states $N_{mbs}^{=0}$ which do not contribute to the LS, the number of states which give a nonzero contribution to $\Psi_{\rm LS}^{(m=3)}$, $N_{mbs}^{\neq 0}$, and the percentage of many-body configuration *not contributing* to the function (5) (denoted by "% zero" in Table 11). One sees that, while for $N=3$ "only" 28.57% of all possible many-body configurations are not used in the LS, at $N=8$, this number increases up to 90.54%.

Table 11. The total number of many-body states N_{mbs}, the number of states contributing ($N_{mbs}^{\neq 0}$) and not contributing ($N_{mbs}^{=0}$) to the Laughlin function, as well as the percentage of non-contributing many-body configurations ('% zero'). N is the number of particles and $\mathcal{L}$ is the total angular momentum (83) corresponding to $\nu=1/3$ and $m=3$ in Equation (5).

N	$\mathcal{L}$	N_{mbs}	$N_{mbs}^{=0}$	$N_{mbs}^{\neq 0}$	% Zero
2	3	2	0	2	00.00
3	9	7	2	5	28.57
4	18	34	18	16	52.94
5	30	192	133	59	69.27
6	45	1206	959	247	79.52
7	63	8033	6922	1111	86.17
8	84	55974	50680	5294	90.54

The first nonzero-weight many-body configurations for N particles at $\nu=1/3$ have the form $|0,3,\ldots,3(N-1)\rangle$, e.g., $|0,3,6,9,12,15,18\rangle$ for seven particles. The angular momenta of individual particles in these states are $L_j=3(j-1)$ for $j=1,\ldots,N$. The largest angular momentum of individual particles in all possible many-body configurations which contribute to the LS equals $L_{\max}=L_N=3(N-1)$. In general, if $\nu=1/m$ in Equation (5), $m=3,5,7$, then $L_{\max}=L_N=m(N-1)$.

Having obtained the expansion coefficients C_s, D_s, and $A_s^{\rm LS}$ for different numbers of particles, I can now calculate physical properties of the LS (5).

6.3. Energy of the Laughlin State

The energy of the LS is determined by the formula (the constant kinetic energy contribution $N\hbar\omega_c/2$ is omitted)

$$E_{\rm LS}^{(m=3)}(N)=\langle\Psi_{\rm LS}^{(m=3)}|\hat{\mathcal{H}}|\Psi_{\rm LS}^{(m=3)}\rangle=\sum_{s=1}^{N_{mbs}}\sum_{s'=1}^{N_{mbs}}A_s^{\rm LS}A_{s'}^{\rm LS}\langle\Psi_s|\hat{V}_{bb}+\hat{V}_{eb}+\hat{V}_{ee}|\Psi_{s'}\rangle \tag{96}$$

in which all required matrix elements are calculated above. The calculated values of the energy (96), as well as the energy differences $E_{\rm LS}^{(m=3)}-E_{\rm GS}$ between the LS and the true ground state are given in Table 5 in the last two columns. The difference $E_{\rm LS}^{(m=3)}-E_{\rm GS}$ increases significantly with the growth of N (by more than 90 times when N changes from $N=2$ to $N=7$), see Figure 11a. In order to quantitatively estimate how big the deviation of the Laughlin energy from the true ground state energy is, I introduce a dimensionless quantity

$$\eta=\frac{E_{\rm LS}^{(m=3)}-E_{\rm GS}}{E_{\rm 1st}-E_{\rm GS}} \tag{97}$$

which measures the difference $E_{\rm LS}^{(m=3)}-E_{\rm GS}$ in units of the energy gap $E_{\rm 1st}-E_{\rm GS}$ between the true first excited state and the true ground state at $\nu=1/3$. The value of η is plotted as a function of N in Figure 11b. For $N=4$, 5, and 7, the value of η is greater than 1, i.e., the energy of the LS is not only greater than the energy of the ground state, which is

understandable for the trial wave function, but also greater than the energy of the first excited state. For $N = 7$, the value of η equals 5.8825 at $\nu = 1/3$.

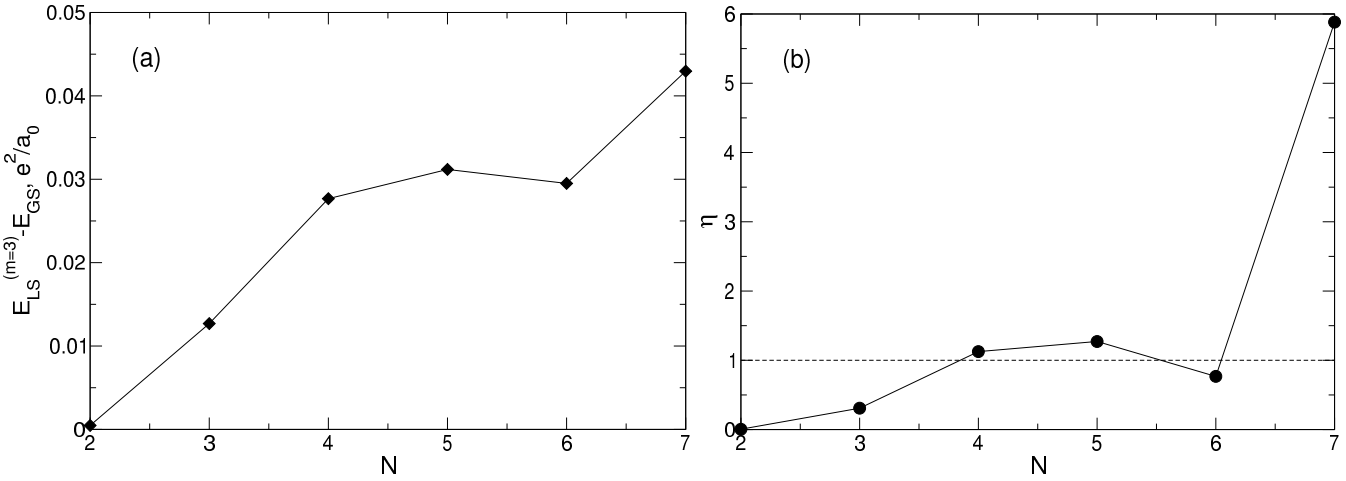

Figure 11. (**a**) The energy difference $E_{\mathrm{LS}}^{(m=3)} - E_{\mathrm{GS}}$ between the Laughlin state and the true ground state of a system of N particles as a function of N; the energy unit is e^2/a_0. (**b**) The value of η defined by Equation (97), as a function of N.

For $N = 6$, the wave functions of the LS and the true ground state are accidentally close to each other; this can be seen from the comparison of the electron densities in both states in Section 6.5. This is the reason why both the absolute and relative energy differences between the LS and the true ground state are smaller at $N = 6$ compared to the neighboring values of N.

6.4. Deviation of the Laughlin Wave Function from the True Ground State Wave Function

The energy difference between the LS and the exact ground state is very large. How big is the difference between the wave functions? Figure 12 shows the expansion coefficients of the true ground state wave function and the Laughlin wave function, A_s^{GS} and A_s^{LS}, for several many-body basis states, in the intervals $4482 \le s \le 4496$ and $3230 \le s \le 3290$ selected as examples. One sees a large difference between the vectors A_s^{GS} and A_s^{LS}. In the first example, Figure 12a, both coefficients are finite, and A_s^{GS} can be almost twice as big as A_s^{LS}. For example, for $s = 4493$ and 4494 (the states $|0,7,9,10,11,12,14\rangle$ and $|0,8,9,10,11,12,13\rangle$), the ratio $A_s^{\mathrm{GS}}/A_s^{\mathrm{LS}}$ equals 1.819 and 1.858, respectively. In the second example, Figure 12b, the coefficients A_s^{GS} of all ~ 60 s-states are on the order of 0.005–0.01, i.e., are close to the average value $\bar{A}_s = N_{mbs}^{-1/2} \simeq 0.011157$, while the coefficients A_s^{LS} for these states are identically zero.

In order to quantitatively characterize the overall discrepancy between the states Ψ_{GS} and $\Psi_{\mathrm{LS}}^{(m=3)}$, I calculate the standard deviation

$$D = \sqrt{\sum_{s=1}^{N_{mbs}} \left(A_s^{\mathrm{GS}} - A_s^{\mathrm{LS}}\right)^2}. \tag{98}$$

Table 12 shows the quantity D for N varying from $N = 2$ up to $N = 7$. The second column of Table 12 shows the projection of the LS onto the true ground state

$$P = \langle \Psi_{\mathrm{LS}}^{(m=3)} | \Psi_{\mathrm{GS}} \rangle = \sum_{s=1}^{N_{mbs}} A_s^{\mathrm{LS}} A_s^{\mathrm{GS}} = 1 - D^2/2. \tag{99}$$

For $N = 2$, the deviation (98) is quite small, about 3.3%, but as N increases, it substantially grows and exceeds $\sim 40\%$ for $N = 7$.

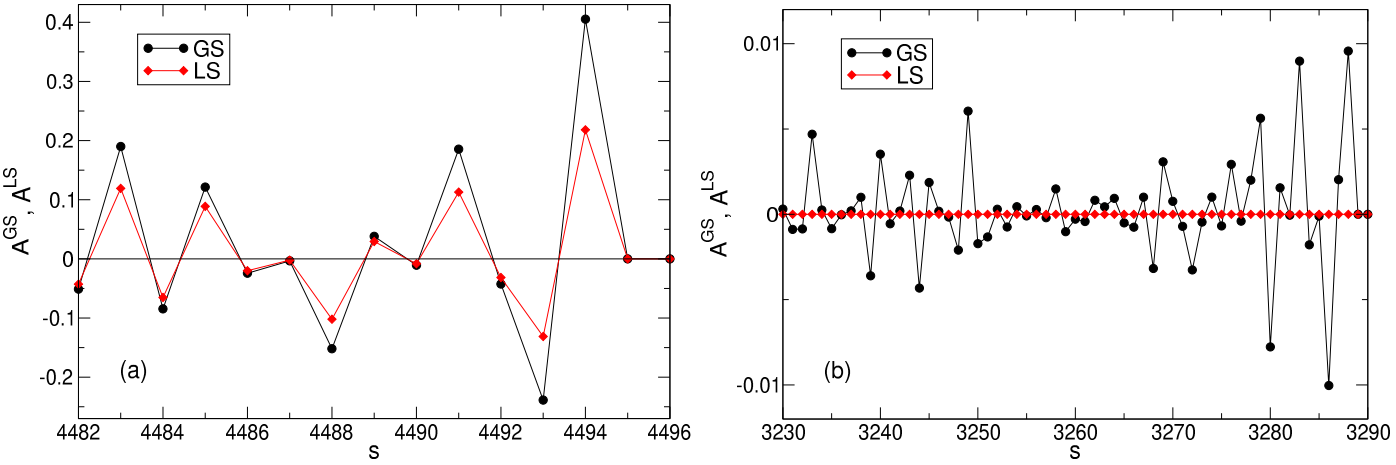

Figure 12. The expansion coefficients $A_s^{\rm GS}$ and $A_s^{\rm LS}$ of the true ground state wave function (58) and of the Laughlin state (84) for a few selected many-body basis states: (**a**) $4482 \le s \le 4496$ and (**b**) $3230 \le s \le 3290$. The Landau level filling factor is $\nu = 1/3$, the number of particles is $N = 7$, the total angular momentum is $\mathcal{L} = 63$, and the total number of many-body basis states is $N_{mbs} = 8033$.

Table 12. The standard deviation (98) and the projection (99) of the Laughlin wave function (5) from/onto the ground state wave function (58) at $\nu = 1/3$.

N	***D***	***P***
2	0.0334	0.9994
3	0.1755	0.9846
4	0.2978	0.9557
5	0.3500	0.9387
6	0.2960	0.9562
7	0.4021	0.9191

In Ref. [6], Laughlin gave the following numbers for the projections of his function on the numerically calculated ground state at $\nu = 1/3$: $P_3 = 0.99946$ for $N = 3$ and $P_4 = 0.979$ for $N = 4$. My calculations do not confirm these numbers. As seen from Table 12, the values of $P_2 = 0.9994$ and $P_3 = 0.9846$ in the first two lines are close to the numbers given in Ref. [6], but they refer to $N = 2$ and $N = 3$, respectively. When $N = 4$, the projection P is less than 95.6% which corresponds to the deviation D of almost 30%.

6.5. Electron Density in the Laughlin State

The density of electrons in the LS (5) at $\nu = 1/3$ is determined by the formula similar to (70),

$$n_e^{\rm LS}(r) = \sum_{s=1}^{N_{mbs}} \left(A_s^{\rm LS}\right)^2 \sum_{j=1}^{N} |\psi_{L_j^{(s)}}(\boldsymbol{r})|^2. \tag{100}$$

The normalized density (100) is shown in Figure 13a for $2 \le N \le 8$. At $N \le 4$, my results coincide with those obtained by Ciftja et al. in Ref. [25] by a different method.

If $N \lesssim 5$, the density of the state (5) behaves qualitatively similar to the exact electron density, Figure 6a: both have a maximum at a finite r, and this maximum shifts to a larger r as N increases. However, quantitatively, the density difference at $r/a_0 \ll 1$ becomes very large already at $N \ge 3$, as can be seen in Figure 13b. While at $N = 2$, the Laughlin density differs from the exact one "only" by $\sim 8.5\%$, at $N = 3$, the difference is already about 34%, and at $N = 4$ and 5, it approaches 50%. At $N = 6$, the densities of electrons in the both states become close to each other, but this is a coincidental result of two different trends. While for Laughlin electrons, $n_{\rm LS}(0)/n_s$ tends to unity at $N \to \infty$, as shown in Refs. [23,24], the ratio $n_{\rm GS}(0)/n_s$ is close to 1 only because the maximum in the disk center is not yet

sufficiently developed. When N grows further, the local density difference becomes huge, approaching $\sim 70\%$ for $N = 7$ at $r \ll a_0$, and the coordinate dependencies of the exact and Laughlin densities becomes *qualitatively* different, see Figure 13c. While the exact density shows the formation of a structure resembling a sliding Wigner crystal, with a large density maximum arising in the disk center, the Laughlin density flattens out in the inner part of the disk.

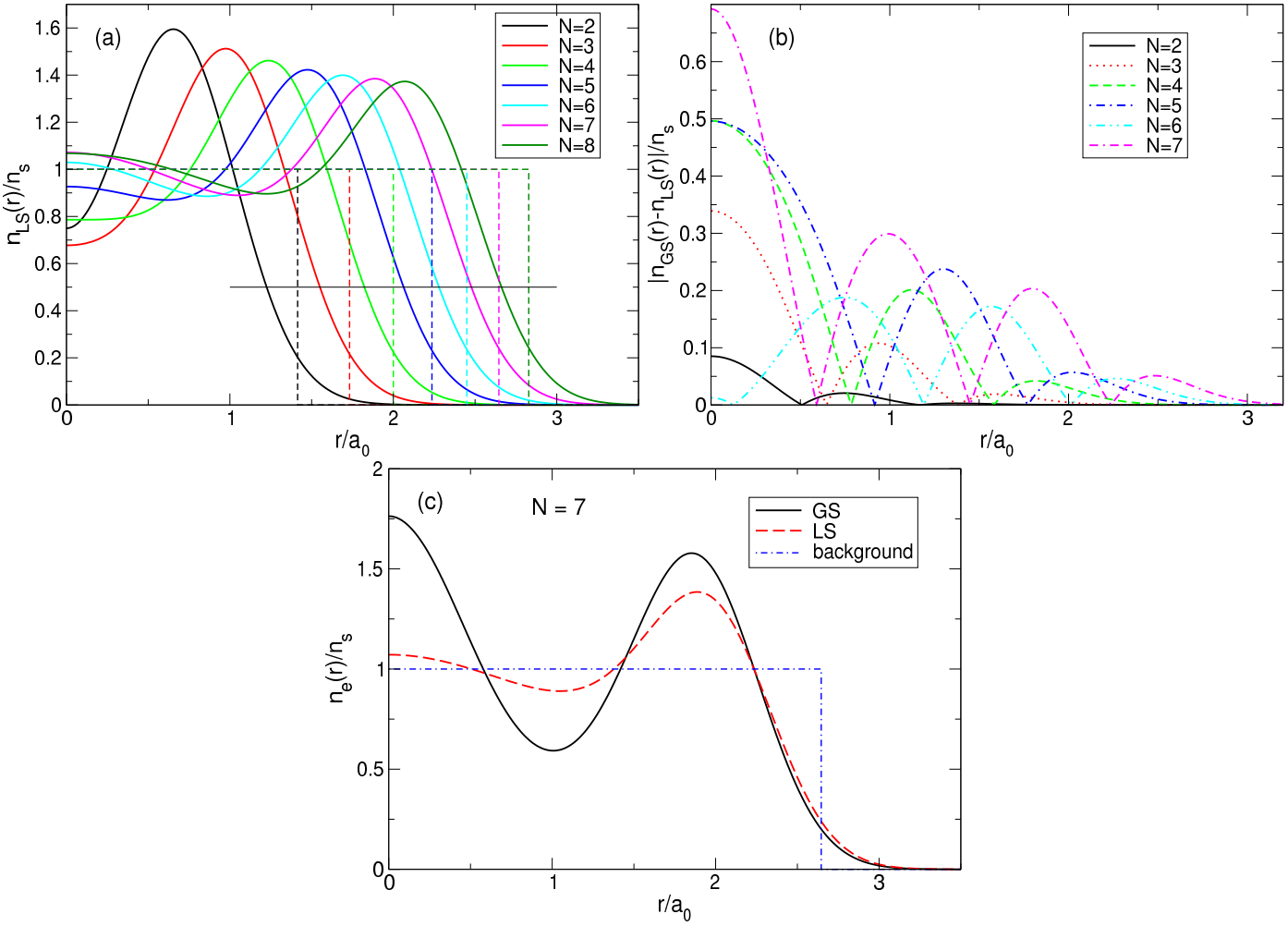

Figure 13. (**a**) The density of electrons $n_e^{\mathrm{LS}}(r)$ (solid curves) in the Laughlin state (5) at $\nu = 1/3$, as a function of the radial coordinate for $N = 2$–8. The dashed lines show the corresponding positive background densities; the thin horizontal black line indicates the level 0.5, which determines the radii of the electron disks. (**b**) The absolute value of the density difference between the true ground state and the LS for different N. (**c**) The density of electrons in the true ground state (GS) and the Laughlin state (LS) at $N = 7$.

6.6. Pair Correlation Function in the Laughlin State

The pair correlation function $P_{\mathrm{LS}}(\boldsymbol{r}, \boldsymbol{r}')$ in the LS at $\nu = 1/3$ can be calculated using a formula similar to (71); only the coefficients A_s^{GS} should be replaced by A_s^{LS}. In general, the function $P_{\mathrm{LS}}(\boldsymbol{r}, \boldsymbol{r}')$ looks similarly to the plots of Figure 7. But there exists a very large quantitative difference at small $|\boldsymbol{r} - \boldsymbol{r}'|$, when $|\boldsymbol{r} - \boldsymbol{r}'|/a_0 \lesssim 0.6$, see Figure 14. While the exact pair correlation function tends to zero at $|\boldsymbol{r} - \boldsymbol{r}'| \to 0$ as $P_{\mathrm{GS}}(\boldsymbol{r}, \boldsymbol{r}') \propto |\boldsymbol{r} - \boldsymbol{r}'|^2$, the LS pair correlation function vanishes as $P_{\mathrm{LS}}(\boldsymbol{r}, \boldsymbol{r}') \propto |\boldsymbol{r} - \boldsymbol{r}'|^6$ at $|\boldsymbol{r} - \boldsymbol{r}'| \to 0$. This is a direct consequence of the unphysical assumption in (5), that the wave function contains only the polynomials $(z_j - z_k)^3$. In the real world, this is not the case; see an additional discussion of this point in Sections 6.10 and 8.

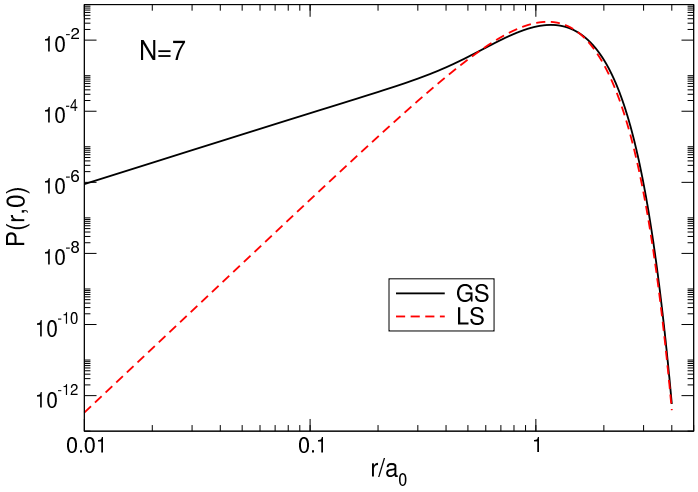

Figure 14. The pair correlation functions $P(\boldsymbol{r}, \boldsymbol{0})$ for the exact ground state (GS) and the Laughlin state (LS), for a system of $N = 7$ particles.

6.7. Additional Remark to the Case of $N = 7$ Particles

Results obtained for the energy of the ground and the first excited states of a seven-electron system need a little more discussion. Laughlin assumed [6] that the ground state of an N-particle system at $\nu = 1/3$ should have the total angular momentum $\mathcal{L} = 3N(N-1)/2$. For $N = 7$, this is $\mathcal{L} = 63$. My exact results show that the ground state of the seven-particle system has the angular momentum $\mathcal{L} = 63$ indeed, while the first excited states has the angular momentum $\mathcal{L} = 57$, as shown in Table 5. The difference between the energies of the first excited and the ground state is very small and equals $E_{1st} - E_{GS} = 0.0073e^2/a_0$.

However, Kasner et al. [18] also performed the exact diagonalization calculations for N electrons in the disk geometry. Their calculations showed that the ground state of the seven-particle system at $\nu = 1/3$ has the angular momentum $\mathcal{L} = 57$. This *exact* result contradicted the variational theory of Laughlin, but the authors of [18] could not resolve this "dilemma" and decided just to "disregard this difficulty".

Questions arise: Why do the exact results of Ref. [18] contradict my exact results and the assumption of Laughlin? Were the results of Ref. [18] correct?

This "dilemma" has a simple explanation. Results for the energy shown in Section 4.1 (Table 5) are obtained for the positive background density having the step-like form (11). Kasner et al. [18] performed their exact diagonalization calculations assuming the smooth density profile (13). I have also performed calculations for the smooth density profile (13) and my results *confirm* those of Ref. [18]. For $N = 7$ and $\nu = 1/3$, my results are shown in Table 13. One sees that, in agreement with [18], in the case of the smooth density profile the ground state has the total angular momentum $\mathcal{L} = 57$, while the first excited state has $\mathcal{L} = 63$. Moreover, the LS energy not only exceeds the energy of the first excited state, but is larger than the energy of the second excited state; see an additional discussion of this point in Section 7.1.7. Also notice that, for the smooth density profile, the projection of the LS onto the true ground state wave function is zero, since these functions have different angular momenta $\mathcal{L}$ and are therefore orthogonal.

Table 13. The energies of the ground state, first and second excited states, as well as of the Laughlin state, at $\beta = 1/\nu = 3$, in the case of the smooth density profile. All energies are in units e^2/a_0.

State	$\mathcal{L}$	E_{state}	$E_{state} - E_{GS}$
Laughlin	63	−6.6363835	0.0431284
2nd excited	51	−6.6407409	0.0387709
1st excited	63	−6.6613834	0.0181285
Ground	57	−6.6795119	0.0

6.8. About the Variational Principle in the Thermodynamic Limit

The results obtained above show that the trial wave function (5) proposed in Ref. [6] for the ground state of the FQHE system has very little in common with the true ground state wave function. The argument of [6] about sufficiently large projections of the wave function (5) onto the numerically calculated exact ground state for $N = 3$ and 4 loses its persuasiveness when the number of particles increases up to $N = 7$. Another Laughlin argument, that seemed to be rather strong, was that the function (5) gives the lowest energy per particle at $N \to \infty$, $E_{\rm LS}^{(m=3)}/N = -0.4156 e^2/l_B$ at $\nu = 1/3$, compared to all other trial functions. How convincing is this argument?

Let us assume that the true ground ($s = 1$) and excited ($s = 2, 3, \dots$) states of the system are known. Their energies and the wave functions are E_s and Ψ_s. Let an arbitrary trial wave function be a linear combination of the ground ($\Psi_1 \equiv \Psi_{\rm GS}$) and several low-lying excited states,

$$\Psi_{\rm trial} = \alpha_1 \Psi_{\rm GS} + \sum_{s>1} \alpha_s \Psi_s. \tag{101}$$

The energy of the trial state $E_{\rm trial}$ will then be

$$E_{\rm trial} = \alpha_1^2 E_{\rm GS} + \sum_{s>1} \alpha_s^2 E_s = E_{\rm GS} + \sum_{s>1} \alpha_s^2 (E_s - E_{\rm GS}), \tag{102}$$

where the normalization condition $\sum_s \alpha_s^2 = 1$ is taken into account.

The energy differences between the low-lying excited states and the ground state $E_s - E_{\rm GS}$ do not depend on N and are determined by typical energies of the FQHE problem, e^2/a_0, e^2/l_B, or $\hbar\omega_c$, which are all on the meV scale. But the energy $E_{\rm GS}$ is proportional to the number of particles N and tends to minus infinity in the thermodynamic limit. Under typical experimental conditions ($N \simeq 10^{11}$), it is on the GeV scale. Therefore, the energy per particle in the limit $N \to \infty$ will be the same both for the true ground state and *for any* trial wave function:

$$\lim_{N\to\infty} \frac{E_{\rm trial}}{N} = \lim_{N\to\infty} \frac{E_{\rm GS}}{N} + \sum_{s>1} \alpha_s^2 \lim_{N\to\infty} \frac{E_s - E_{\rm GS}}{N} = \lim_{N\to\infty} \frac{E_{\rm GS}}{N}. \tag{103}$$

This conclusion also holds in the case $\alpha_1 = 0$, when the trial and the ground state wave functions are orthogonal. Thus, while the "thermodynamic limit" argument may give a correct estimate for the ground state energy per particle, it completely fails to determine the correct ground state wave function. The quantum-mechanical variational principle, that perfectly works for one- or few-particle systems, is useless in the limit $N \to \infty$. Relying on this principle, one can mistakenly take any arbitrarily unreasonable wave function as a correct ground state wave function. This can be illustrated by a simple quantitative example.

In Section 5, the properties of the MDD configuration $|\Psi_{\rm mdd}\rangle = |0, 1, \dots, N-1\rangle$, Equation (72), have been analyzed, in particular the energy, Figure 8, and the density, Figure 9, of this state. Let us now consider two other quantum states, which I will call "MDD-plus" and "MDD-shift". The MDD-plus state $|\Psi_{\rm mdd}^{+}\rangle = |0, 1, \dots, N-2, N\rangle$ differs from $|\Psi_{\rm mdd}\rangle$ by the angular momentum of only one, N-th electron: $L_N = N - 1 \;\to\; L_N = N$. In the MDD-shift state, $|\Psi_{\rm mdd}^{\Rightarrow}\rangle = |1, 2, \dots, N-1, N\rangle$, the individual angular momenta of all particles are increased by one as compared to their MDD L's: $L_j = j - 1 \;\to\; L_j = j$, $j = 1, \dots, N$. The total angular momenta of the plus- and shift-states are $\mathcal{L} = N(N-1)/2 + 1$ and $\mathcal{L} = N(N+1)/2$, respectively, and hence, these two states are orthogonal to the ground MDD state: their projections onto the ground state are zero. What are the energy and the density of these two configurations? This question can be easily answered for any N with the help of the formulas obtained above.

Figure 15 shows the electron density in the MDD, MDD-plus, and MDD-shift states. The densities of the first two states are very close to each other. But the density of the MDD-shift state has a deep hole in the disk center and differs significantly from both the MDD and MDD-plus states. If nothing was known about the ground state of the system,

then the MDD-shift state would definitely be excluded from the list of potential candidates for the role of the ground state wave function, since it does not give a physically reasonable coordinate dependence of the electron density.

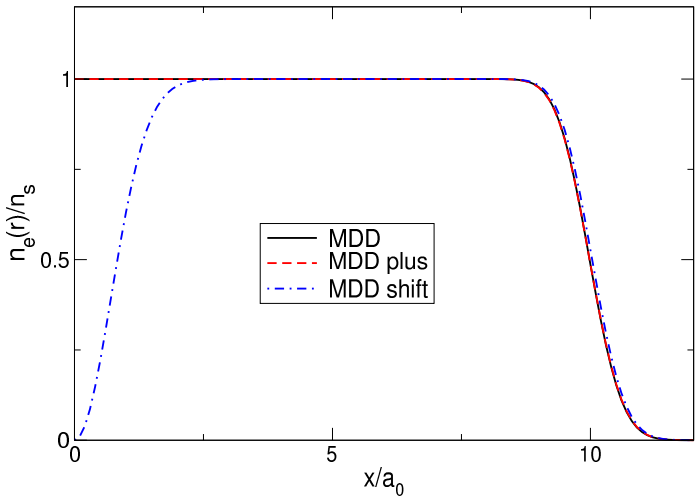

Figure 15. The density of electrons in the MDD, MDD-plus, and MDD-shift states as a function of r/a_0 for $N = 100$.

What about the energy of these three states? Figure 16a shows the energy per particle of the MDD, MDD-plus, and MDD-shift configurations, as a function of $1/\sqrt{N}$, for N varying from 1 to 100. One sees that, at small N, the energy difference between both the excited and the ground (MDD) states is very large. But when N grows, this difference quickly tends toward zero. Figure 16b shows the energy differences $\delta E^{+}_{\rm mdd}/N$ and $\delta E^{\Rightarrow}_{\rm mdd}/N$ in dependence of $1/N$. In spite of the MDD-shift state has an evidently incorrect coordinate dependence of the electron density, both energy differences linearly tend to zero with $1/N$. This implies that $\delta E^{+}_{\rm mdd}$ and $\delta E^{\Rightarrow}_{\rm mdd}$ are constants at $N \to \infty$: $\delta E^{+}_{\rm mdd} \approx 0.118050 e^2/a_0$ and $\delta E^{\Rightarrow}_{\rm mdd} \approx 0.8973 e^2/a_0$. Obviously, there exist an infinite number of different wave functions whose energy per particle will tend to the same limit as $N \to \infty$.

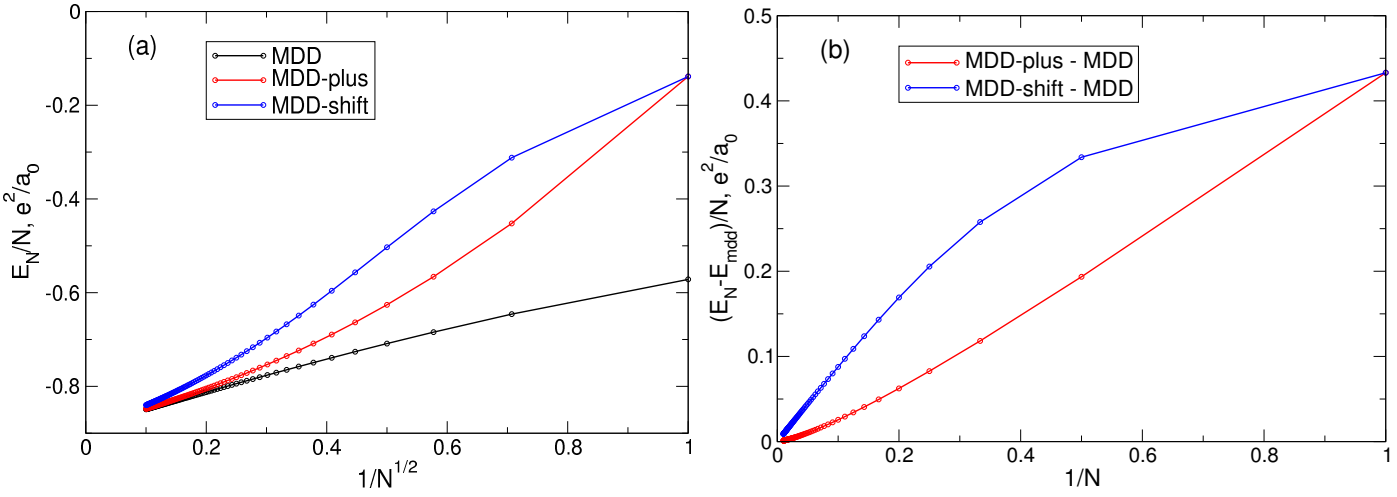

Figure 16. (**a**) The energy of the MDD, MDD-plus, and MDD-shift states, as a function of $1/\sqrt{N}$. (**b**) The energy differences as a function of $1/N$.

6.9. Electron Density in the Laughlin State at Large N

The density of electrons in the MDD-shift state, Figure 15, is "physically unreasonable"; therefore, one should exclude the state $|\Psi^{\Rightarrow}_{\rm MDD}\rangle$ from the list of potential candidates for the ground state wave function. Could one, for similar reasons, exclude the Laughlin

wave function (5) from the list of potential candidates for the role of the ground state wave function at $\nu = 1/m$? This question can be answered due to the studies of Ciftja and co-authors [23,24], who calculated, using Monte Carlo simulations, the density of electrons $n_e^{\mathrm{LS}}(r)$ in the $\nu = 1/3$ Laughlin states for $N = 64$, 100, 144, and 196 [23], and in the 1/5 and 1/7 states for $N = 196$ [24].

As seen in Figure 13a, the normalized LS density at small r tends to unity as N increases, and has a rather large peak near the edge of the disk at $r \approx R - a_0$. The value of the normalized density n_e^{LS}/n_s in this peak varies from ∼1.6 for $N = 2$ to ∼1.37 for $N = 8$. Do these features remain when N grows further? Figure 17 shows the results of Refs. [23,24] (curves with symbols) replotted as a function of r/a_0 (in Refs. [23,24], these data were plotted in dependence of r/l_B). At $r/a_0 \lesssim 11$ (not shown in Figure 17), the normalized density n_e^{LS}/n_s calculated in Refs. [23,24] is very close to 1, which agrees with the statement of [6] that the Laughlin function describes a uniform liquid. However, near the disk edge, this "liquid" becomes strongly inhomogeneous. The ring of the high electron density, which is seen in Figure 13 for $N \leq 8$, is also preserved for N up to $N = 196$, see Figure 3 in Ref. [23] and Figure 1 in Ref. [24]. Consider this LS feature in more detail.

It is possible to fit the numerical data of Ciftja et al. [23] for $\nu = 1/\beta = 1/3$ by a linear combination

$$\frac{n_e^{\mathrm{fit}}(r)}{n_s} = \sum_{L=0}^{L_{\max}(N)} \Phi_L\left(\sqrt{\beta}\frac{r}{a_0}\right) + \sum_{k=1}^{3}(-1)^{k-1}A_k(N)\Phi_{L_k(N)}\left(\sqrt{\beta}\frac{r}{a_0}\right) \tag{104}$$

of functions

$$\Phi_L(x) = \frac{x^{2L}}{L!}e^{-x^2}, \tag{105}$$

which are related to the single-particle states (9),

$$|\psi_L(\boldsymbol{r})|^2 = \frac{1}{\pi\lambda^2}\Phi_L\left(\frac{r}{\lambda}\right). \tag{106}$$

The angular momenta $L_{\max}(N)$ and $L_k(N)$, as well as the coefficients $A_k(N)$ in Equation (104) are

$$L_{\max}(N) = 3N - 1 - \sqrt{N}, \quad L_k(N) = 3N - 2(3k-1)\sqrt{N} - 13 + 12k, \tag{107}$$

$$A_1(N) = 1.205\sqrt{N} + 0.07, \quad A_2(N) = 0.2525\sqrt{N} - 0.115, \quad A_3(N) = \sqrt{N} - A_1(N) + A_2(N). \tag{108}$$

The fitting function (104) is not unique and not exact, but it shows excellent agreement with the numerical data [23], see Figure 18. Remarkably, the data for different N can be equally well fitted by a single formula (104), which implies that Equation (104) should also successfully work at an even larger N, in the thermodynamic limit.

Apart from the data of Ref. [23] and the fitting function (104), I also show in Figure 18a–d, by black solid curves, the density of a "uniform liquid" (UL)

$$\frac{n_e^{\mathrm{UL}}(r)}{n_s} = \sum_{L=0}^{\beta N-1}\Phi_L\left(\sqrt{\beta}\frac{r}{a_0}\right) = Q(\beta N, \beta r^2/a_0^2), \tag{109}$$

which is similar to the density of the MDD state (76) but is defined for $\beta = 1/\nu = 3$. The function (109) satisfies the condition

$$\int_0^{2\pi} d\phi \int_0^{\infty} r dr n_e^{\mathrm{UL}}(\boldsymbol{r}) = N \tag{110}$$

and is ideally flat at $r \lesssim R - a_0$. As seen from Figure 18a–d, the radius of the electron disk in the "uniform liquid" state (109), defined as the point where $n_e^{\mathrm{UL}}(r)/n_s = 1/2$, is very close to the radius $R = a_0\sqrt{N}$ of the positively charged background disk.

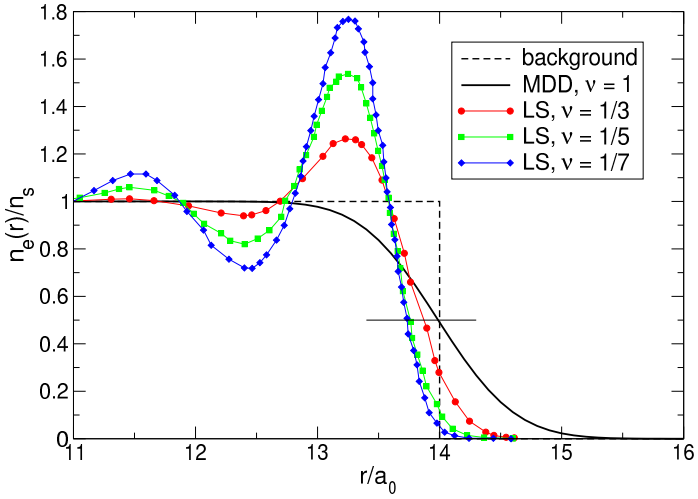

Figure 17. The coordinate dependencies of the density of electrons in the Laughlin states (5) at $\nu = 1/3, 1/5$, and $1/7$, calculated for $N = 196$ by Ciftja et al. in Refs. [23,24]; the discrete numerical data points are connected by lines to guide the eye. The thick black solid curve shows the MDD density at $\nu = 1$. At $r/a_0 \lesssim 11$ (not shown in the Figure), the normalized electron density equals 1 according to Refs. [23,24]. A thin horizontal line at the level of 0.5 visualizes the change of the electron disk radius when ν decreases from $\nu = 1$ to $\nu = 1/7$.

If the Laughlin wave function (5) really described a homogeneous liquid state, it would have to have a density close to (109). But, as seen from Figure 18a–d, the radii of the electron disks in the LS (5) are always noticeably smaller than the radii of the "uniform liquid" and of the positive background. Since all densities should satisfy the electroneutrality condition (110), the decrease in diameter of the "Laughlin liquid" disk should be compensated by a strong increase in its density in the interior of the system. This is indeed the case, i.e. the LS (5) describes not a uniform liquid, but a highly inhomogeneous state, which is never realized in the experiments.

Mathematically, one can evaluate this redistribution of the electron density by comparing the "uniform liquid" density (109) with the "Laughlin liquid" density, calculated for a large N in Ref. [23] and fitted by the formula (104). The "uniform liquid" density consists of a sum of the functions Φ_L with L running from $L = 0$ up to $L = 3N - 1$. The LS density also contains a similar sum, but L in the first term of Equation (104) runs from $L = 0$ up to $L = L_{\max} = 3N - 1 - \sqrt{N}$, Equation (107). A *macroscopically* large number ($\propto \sqrt{N}$) of the L-states are lost from the Laughlin function. To compensate this loss and to describe the oscillating behavior of the LS density near the edge of the disk, three additional terms with *macroscopically* large amplitudes $A_k(N) \propto \sqrt{N}$, Equation (108), have to be added to the fitting function (104). Note that the high density ring lies approximately at $R - 1.2a_0 \lesssim r \lesssim R - 0.4a_0$, with the density maximum at $r \approx R - 0.8a_0$, that is all changes in the local electron density occur inside the sample, at $r \lesssim R - a_0$, which means that they also take place in the thermodynamic limit $N \to \infty$.

The above discussion refers to the case $\nu = 1/3$. At $\nu = 1/5$ and $1/7$, the Laughlin function (5) demonstrates the even stronger inhomogeneity of the local electron density near the edge of the system, as can be seen in Figure 17. The electron disk radius becomes smaller, and the maximum of the electron density near $r \approx R - 0.8a_0$ increases. Thus, not only is the LS characterized by a non-physical feature of a strongly inhomogeneous density, but, in addition, this inhomogeneity significantly depends on the magnetic field.

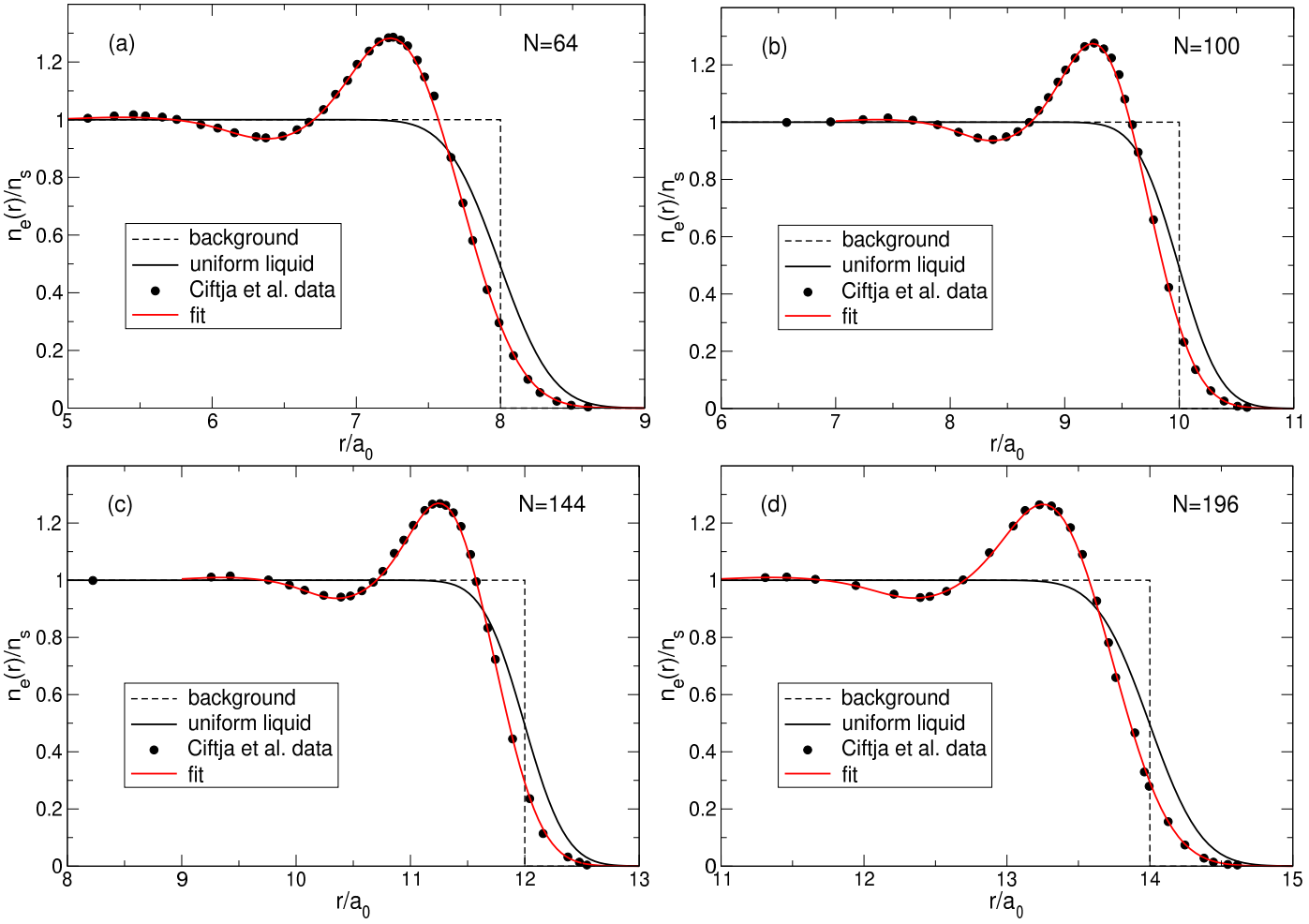

Figure 18. Fitting of the numerical data [23] for the density of electrons in the $\nu = 1/3$ LS by the analytical function (104) for (**a**) $N = 64$; (**b**) $N = 100$; (**c**) $N = 144$; and (**d**) $N = 196$.

Let us imagine a macroscopic 2DEG sample with an electron density on the order of 10^{11} cm^{-2} [3]. In equilibrium at $B = 0$, the sample is locally electroneutral, i.e., the density of electrons equals the density of the positive background at any point. Now, one switches the magnetic field on and increases it up to the value of ∼50 kG [3], corresponding to the Landau level filling factor $\nu = 1$. One obtains the MDD ground state with a perfectly uniform density of electrons (76) at all $r \lesssim R - a_0$, Figure 19a. Then, one further increases the magnetic field up to ∼150 kG [3] which corresponds to the filling factor $\nu = 1/3$. If the wave function (5) corresponded to reality, a ring with a strongly enhanced electron density ($\sim 1.27 \times 10^{11}$ cm^{-2}) would have to grow near the edge of the sample, Figure 19b. If after that, the B-field is further increased up to $\nu = 1/5$ and $\nu = 1/7$, then the local electron density in the edge ring should increase to $\sim 1.55 \times 10^{11}$ cm^{-2} and $\sim 1.77 \times 10^{11}$ cm^{-2}, respectively, as can be seen in Figure 19c,d.

Such a strong redistribution of the electron density would require enormous energy costs, which can be estimated as follows. The density of the uncompensated charge can be modeled as

$$\delta\rho(\boldsymbol{r}) = \gamma e n_s \Theta(R - r)\Theta(r - R + a_0) \tag{111}$$

where γ is a number on the order of unity: $\gamma \approx 0.27$, 0.55, and 0.78 at $\nu = 1/3$, $1/5$, and $1/7$, respectively. The electrostatic energy of this uncompensated charge is

$$\delta E = \int \frac{\delta\rho(\boldsymbol{r})\delta\rho(\boldsymbol{r}')}{|\boldsymbol{r} - \boldsymbol{r}'|} d\boldsymbol{r} d\boldsymbol{r}' = \int \frac{d\boldsymbol{q}}{2\pi q} |\delta\rho_{\boldsymbol{q}}|^2, \tag{112}$$

where the Fourier transform of $\delta\rho(\boldsymbol{r})$ equals

$$\delta\rho_{\boldsymbol{q}} = \frac{2\pi\gamma e n_s}{q^2} qR\Big((1-\xi)J_1(qR(1-\xi)) - J_1(qR)\Big), \tag{113}$$

and

$$\xi = \frac{a_0}{R} = \frac{1}{\sqrt{N}} \tag{114}$$

is a small parameter. Substituting Equation (113) into (112) gives in the limit $\xi \ll 1$ ($N \gg 1$)

$$\delta E \approx \frac{e^2}{R}(2\gamma N)^2 \frac{\xi^2}{2\pi}\left(3 + 2\ln\frac{8}{\xi}\right) = \left(\frac{e^2}{a_0}\frac{6\gamma^2}{\pi}\right)\sqrt{N}\left[1 + \frac{1}{3}\ln(64N)\right]. \tag{115}$$

The electrostatic energy (115) grows as $\sqrt{N}\ln(N)$ in the thermodynamic limit. If the density of electrons assumes a typical value $n_s = 3 \times 10^{11}$ cm^{-2} and the dielectric permittivity, which should be taken into account here, is $\epsilon = 12.8$, the energy $(e^2/a_0\epsilon)(6\gamma^2/\pi)$ equals 1.52 meV for $\nu = 1/3$ ($\gamma = 0.27$). Then, for the macroscopic number of particles $N \simeq 10^{11}$, the electrostatic energy (115) exceeds 2.5 keV at $\nu = 1/3$, ~ 10 keV at $\nu = 1/5$, and about 20 keV at $\nu = 1/7$. The "Laughlin liquid" requires too much energy for its existence.

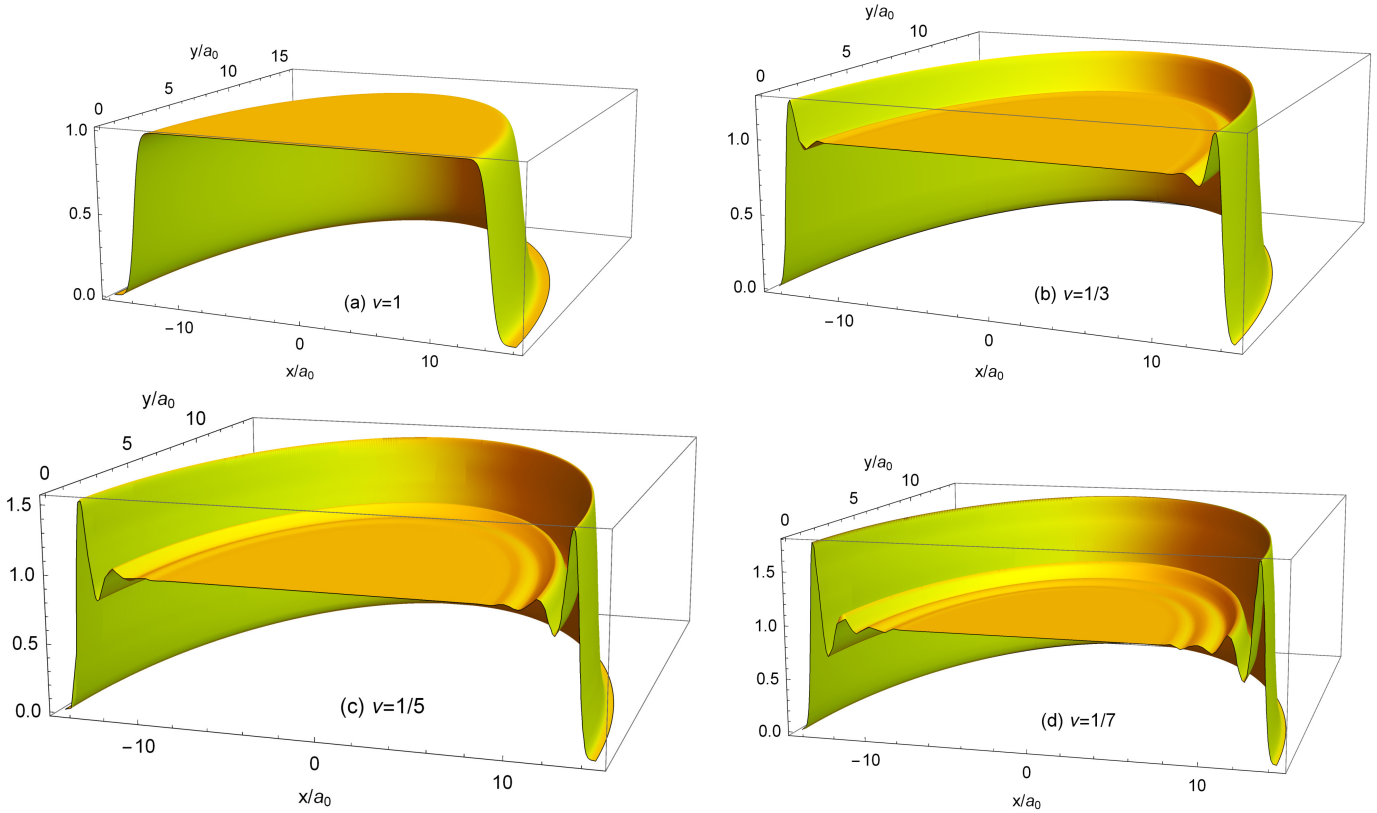

Figure 19. The density of electrons in the MDD ($\nu = 1$) and in the Laughlin states (5) with $\nu = 1/3$, $1/5$, and $1/7$. The number of particles is $N = 196$. The data for the Laughlin electron densities are taken from Refs. [23,24].

6.10. Behavior of the Laughlin Function at $\boldsymbol{r}_j \to \boldsymbol{r}_k$

Another reason for which the Laughlin wave function is inappropriate for the description of the ground state of the FQHE system is as follows. The behavior of the many-body wave function at $|\boldsymbol{r}_j - \boldsymbol{r}_k| \to 0$ is governed by the Coulomb interaction terms $\sum_{jk} \Psi/|\boldsymbol{r}_j - \boldsymbol{r}_k|$ in the many-body Schrödinger equation. To compensate the $1/r$-singularity in this equation, the wave function should be proportional to $|\boldsymbol{r}_j - \boldsymbol{r}_k|$ at $|\boldsymbol{r}_j - \boldsymbol{r}_k| \to 0$. This is indeed the case for the MDD solution at $\nu = 1$ and the true ground state solution at $\nu = 1/3$.

The Laughlin assumption $\Psi_{\rm LS}^{(m)} \propto |\boldsymbol{r}_j - \boldsymbol{r}_k|^m$ with $m = 3, 5, 7$ actually suggests that electrons repel each other substantially stronger than needed in the world of Coulomb forces, as if the electron–electron interaction potential were proportional to $1/|\boldsymbol{r}_j - \boldsymbol{r}_k|^m$. As a result, electrons are pushed out of the disk center, with forces proportional to $1/|\boldsymbol{r}_j - \boldsymbol{r}_k|^{m+1}$, and have to accumulate near the disk edge with a local electron density growing with m, see Figures 17 and 19.

In Ref. [43], it was argued that, in the case of two particles, there is only one analytical function describing the motion of electrons on the lowest Landau level, and that this function is proportional to $(z_1 - z_2)^m$ with m odd. Then, the work [6] aimed to generalize this statement to the case of N particles, resulting in Equation (5). However, the statement of [43] is not applicable to real physical systems with a neutralizing positive background and leads to physically unreasonable conclusions in such systems. Further discussion of this point can be found in Section 8.2.

In this Section, I only discussed the properties of the wave function (5). A similar analysis of the *excited* Laughlin states, the fractionally charged quasiholes and quasielectrons, can also be carried out. I present the results of such an analysis in Section 8.1, after clarifying the physics of the true excited states in the next Section.

7. Exact Solutions at Filling Factors $\nu \leq 1$

As shown in Section 4, not only the ground state at $\nu = 1/3$ has the spatial particle distribution like in a floating Wigner molecule, but also the excited state, see Figure 6b. In order to better understand the nature of the ground and excited states, I now calculate the spectra and the electron densities of the system at arbitrary values of the Landau level filling factor $\nu \leq 1$. The total angular momenta from $\mathcal{L} = \mathcal{L}_{\rm min} = N(N-1)/2$ up to $\mathcal{L} = \mathcal{L}_{\rm max} = 4\mathcal{L}_{\rm min}$ will be considered, and the magnetic field parameter $\beta = 1/\nu$ will be varied in the range $1 \leq \beta \lesssim 4$.

As in the previous Sections, here I continue to assume that all electrons are spin-polarized and occupy only the lowest Landau level states. In general, this implies that the typical Coulomb interaction energy e^2/a_0 is smaller than the inter-Landau-level distance $\hbar\omega_c$,

$$\frac{e^2/a_0}{\hbar\omega_c} \ll 1, \quad \text{or} \quad \nu \ll 2\sqrt{\pi n_s a_B^2} = 2\frac{a_B}{a_0}; \tag{116}$$

here, $a_B = \hbar^2/m^\star e^2$ is the effective Bohr radius and it is implicitly assumed that the dielectric constant of the medium ϵ is included in the definition of charge, $e^2 \to e^2/\epsilon$. The approximation (116) is very accurate for $\beta = 1/\nu = 3$, but begins to fail as β approaches $1+$. Indeed, in order to obtain accurate results, the expansion of the Ψ function (58) over the basis many-body states should contain a sufficiently large number of terms, $N_{mbs} \gg 1$. But if $\mathcal{L} = \mathcal{L}_{\rm min}$ (the MDD state) or $\mathcal{L} = \mathcal{L}_{\rm min} + 1$ (the MDD-plus state), this number is $N_{mbs} = 1$. As will be seen below, under the assumption made, the MDD state is the ground state in certain intervals of the B-field, $\beta < \beta_0$, where β_0 depends on N and for $N = 7$ is about 1.5. In these magnetic fields, the results obtained only provide an upper bound on the ground state energy and should be improved in the future by taking into account states from higher Landau levels.

The positive background density profile is assumed to be step-like everywhere in this Section, except the Sections 7.1.7 and 7.2.3.

7.1. Energy Spectra, Energy Gaps, and Excited States

7.1.1. Two Particles

If $N = 2$, the total angular momenta considered vary from $\mathcal{L}_{\rm min} = 1$ up to $\mathcal{L}_{\rm max} = 4$. The many-body configurations for these $\mathcal{L}$ and the number of these configurations N_{mbs} are given in Table 1. If (for any N) $\mathcal{L} \leq \mathcal{L}_{\rm min} + 1$, there exists only one many-body state, $N_{mbs} = 1$, and there exists only one energy-vs.-B curve $E_{\mathcal{L}}(\beta)$. If $\mathcal{L} > \mathcal{L}_{\rm min} + 1$, the number of many-body state is bigger than one, $N_{mbs} > 1$, and the energy-vs.-B curves $E_{\mathcal{L},s}(\beta)$ will be enumerated by an additional index $s = 1, 2, \ldots$. The goal is to determine, for each

β-value, the energies of the ground $E_{\rm GS}(\beta)$ and the first excited $E_{\rm 1st}(\beta)$ states, as well as the values of the quantum numbers $(\mathcal{L},s)$ corresponding to these states.

Figure 20a shows the energies of all many-body states with $\mathcal{L}$ varying from 1 to 4 and $s=1,2$, for the system of $N=2$ electrons. If $\beta=1/\nu=1$, the ground state is characterized by the quantum numbers $(\mathcal{L},s)=(1,1)$ and is the MDD state $|0,1\rangle$. As β increases, the energy of this state, shown by the black curve in Figure 20a, decreases, reaches a minimum at $\beta\approx 2.73$, and then starts to slowly grow. When β becomes larger than $\beta_0=2.5559$, the role of the ground state $(\mathcal{L},s)=(1,1)$ is transferred to the state $(\mathcal{L},s)=(3,1)$, shown by the green solid curve in Figure 20a. The energies of the states with $\mathcal{L}=2$ and $\mathcal{L}=4$ are higher, at all β, than the energies of the states with $\mathcal{L}=1$ and $\mathcal{L}=3$, but the states $(\mathcal{L},s)=(2,1)$ (the red dashed curve) and $(\mathcal{L},s)=(4,1)$ (the blue dashed curve) may be the first excited state in certain intervals of the magnetic field, see Table 14. For all ground and first excited states the value of the second quantum number is $s=1$, i.e., the states with $s>1$ ($s=2$ in the case of two particles) cannot be the first excited state at any β. This feature remains valid for any N. Figure 20b shows the energy gap between the first excited and the ground state as a function of the magnetic field parameter β. The gap vanishes at $\beta=2.5559$ and reaches the value of about $0.164e^2/a_0$ at $\beta=3.3567$. The energy of the LS with $m=3$ is shown in Figure 20a by a small red circle at $\beta=3$.

Table 14. The total angular momenta of the ground state $\mathcal{L}_{\rm GS}$ and of the first excited state $\mathcal{L}_{\rm 1st}$ assume the values shown in the last two columns in the intervals from $\beta_{\rm from}$ to $\beta_{\rm to}$ shown in the first two columns. The number of particles is $N=2$, the density profile is step-like.

$\beta_{\rm from}$	$\beta_{\rm to}$	$\mathcal{L}_{\rm GS}$	$\mathcal{L}_{\rm 1st}$
1.0000	1.5986	1	2
1.5986	2.5559	1	3
2.5559	3.3567	3	1
3.3567	4.0000	3	4

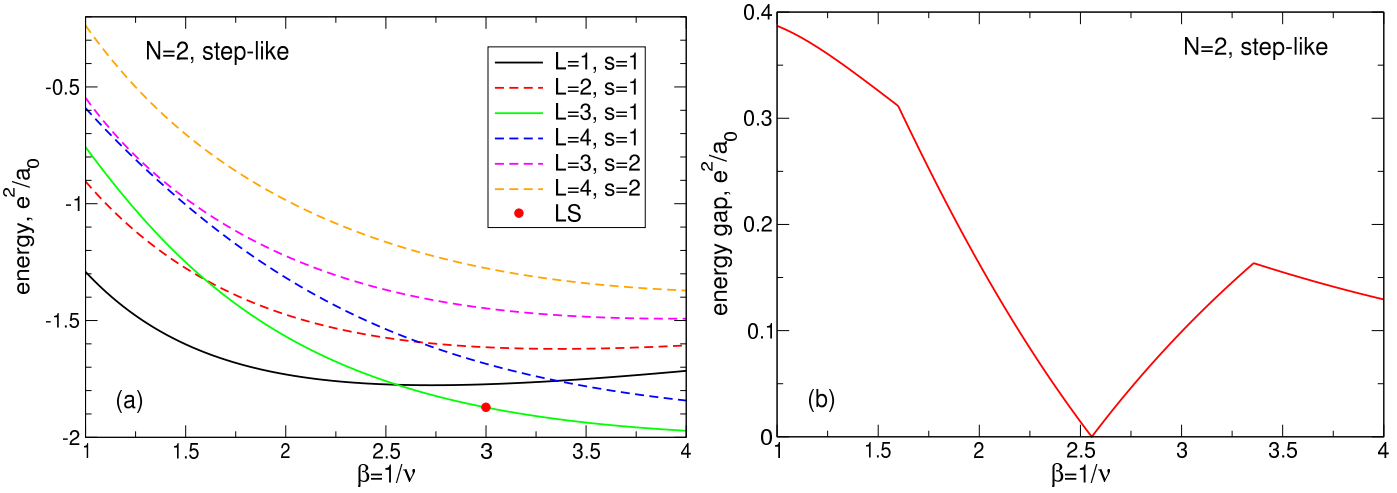

Figure 20. (**a**) The energy of the many-body states with the total angular momenta from $\mathcal{L}=\mathcal{L}_{\rm min}=1$ up to $\mathcal{L}=\mathcal{L}_{\rm max}=4$ in the system of $N=2$ 2D electrons as a function of the magnetic field parameter $\beta=1/\nu$. The index s enumerates different states with the same $\mathcal{L}$. The LS energy at $\nu=1/3$ is shown by a small red circle. (**b**) The energy gap between the ground and the first excited states as a function of β. The positive background density profile is step-like.

7.1.2. Three Particles

If $N=3$, I consider the total angular momenta between $\mathcal{L}_{\rm min}=3$ and $\mathcal{L}_{\rm max}=12$, see Table 2. Figure 21a shows the energies $E_{\mathcal{L},s}(\beta)$ for all many-body states with $\mathcal{L}$ varying from 3 to 12 and for $s=1$. The states with $s\geq 2$ are not shown, since they are neither the ground state nor the first excited state for any β. States that are the ground states in some

region of the magnetic field are shown by solid curves, and all other states are shown by dashed curves.

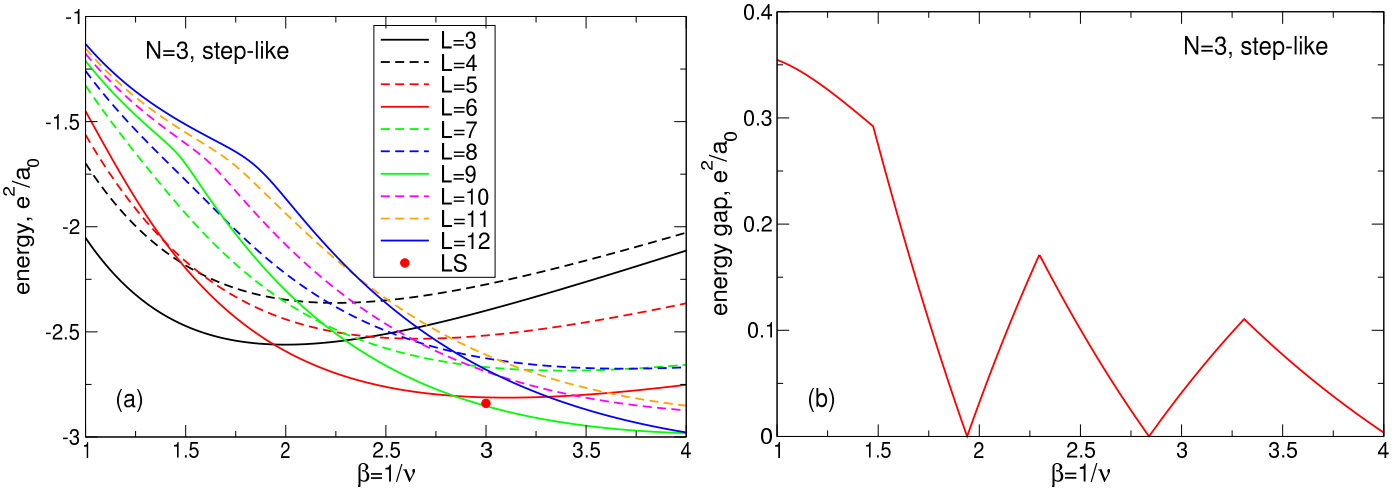

Figure 21. (**a**) The energy of the many-body states with the total angular momenta from $\mathcal{L} = \mathcal{L}_{\min} = 3$ up to $\mathcal{L} = \mathcal{L}_{\max} = 12$ in the system of $N = 3$ 2D electrons as a function of the magnetic field parameter $\beta = 1/\nu$. For all shown states, the index s equals $s = 1$; the states with $s > 1$ are not shown. The LS energy at $\nu = 1/3$ is shown by a small red circle. (**b**) The energy gap between the ground and the first excited states as a function of β. The positive background density profile is step-like.

The behavior of the curves $E_{\mathcal{L},1}(\beta)$ is similar to the case of $N = 2$. The MDD configuration $|0,1,2\rangle$ with $(\mathcal{L}, s) = (3,1)$ is the ground state in the interval from $\beta = 1$ to $\beta = \beta_0 = 1.9397$ (black solid curve) and then transfers its role of the ground state to the state $(\mathcal{L}, s) = (6,1)$ (red solid curve). After $\beta = 2.8392$, the state $(\mathcal{L}, s) = (9,1)$ becomes the ground state (green solid curve), see Table 15. The next state that will become the ground state at β that is slightly bigger than 4 is the state $(\mathcal{L}, s) = (12,1)$ (blue solid curve). As can be seen from Figure 21a and Table 15, the states with $\mathcal{L}$ other than 3, 6, 9, and 12 are also not the first excited states at any magnetic field. The only exception is the $\mathcal{L} = 4$ state, which is the first excited state for β close to 1, but in this region the problem needs to be reconsidered by including higher Landau levels as discussed above. The energy of the LS with $m = 3$ is shown by a small orange circle at $\beta = 3$.

Table 15. The total angular momenta of the ground state $\mathcal{L}_{\text{GS}}$ and of the first excited state $\mathcal{L}_{1\text{st}}$ assume the values shown in the last two columns in the intervals from β_{from} to β_{to} shown in the first two columns. The number of particles is $N = 3$, the density profile is step-like.

β_{from}	β_{to}	$\mathcal{L}_{\text{GS}}$	$\mathcal{L}_{1\text{st}}$
1.0000	1.4751	3	4
1.4751	1.9397	3	6
1.9397	2.2971	6	3
2.2971	2.8392	6	9
2.8392	3.3096	9	6
3.3096	4.0000	9	12

Figure 21b shows the energy gap between the first excited and the ground state as a function of the magnetic field parameter β. The gap vanishes at two β-points and is about $0.17e^2/a_0$ at $\beta = 2.2971$ and $0.11e^2/a_0$ at $\beta = 3.3096$.

Note that the angular momenta values corresponding to the ground states in different β intervals ($\mathcal{L} = 3, 6, 9$) satisfy the rule

$$\mathcal{L}_k^{\text{GS}} = \mathcal{L}_{\min} + n^{\text{st}}(N)k, \tag{117}$$

where $n^{\mathrm{st}}(N)$ is given by Equation (65) and $k = 0, 1, 2, \ldots$ is integer. The reason for the sequence (117) is that the quantum solution should be formed from the $\mathcal{L}$ states that have the same circular symmetry as the classical Wigner molecule. The states from the sequence (117) satisfy this requirement, and therefore, they have a lower energy and serve as the ground states in different β-intervals. The rule (117) is also valid for $N = 2$ and $N > 3$, as shown below.

7.1.3. Four Particles

If $N = 4$, the total angular momenta that I consider lie between $\mathcal{L}_{\mathrm{min}} = 6$ and $\mathcal{L}_{\mathrm{max}} = 24$. In order not to overload the graph with too many curves, I show in Figure 22a only the energies of the states $(\mathcal{L}, s)$ that are either the ground or the first excited state in any interval of β. The rule (117) for the ground-states angular momenta remains valid for $N = 4$. The $(\mathcal{L}, s)$-states with $\mathcal{L} = 8, 11 \ldots 13, 15 \ldots 17, 19 \ldots 21, 23 \ldots 24$, and $s = 1$, as well as all states with $s > 1$, which can be only the second or higher excited state, are not shown in the Figure. The angular momenta of the ground and first excited states, with the corresponding β intervals, are given in Table 16. The energy of the LS with $\nu = 1/3$ is shown by a small red circle at $\beta = 3$ in Figure 22a. It lies slightly above the green curve corresponding to the first excited state $\mathcal{L} = 14$ at $\nu = 1/3$.

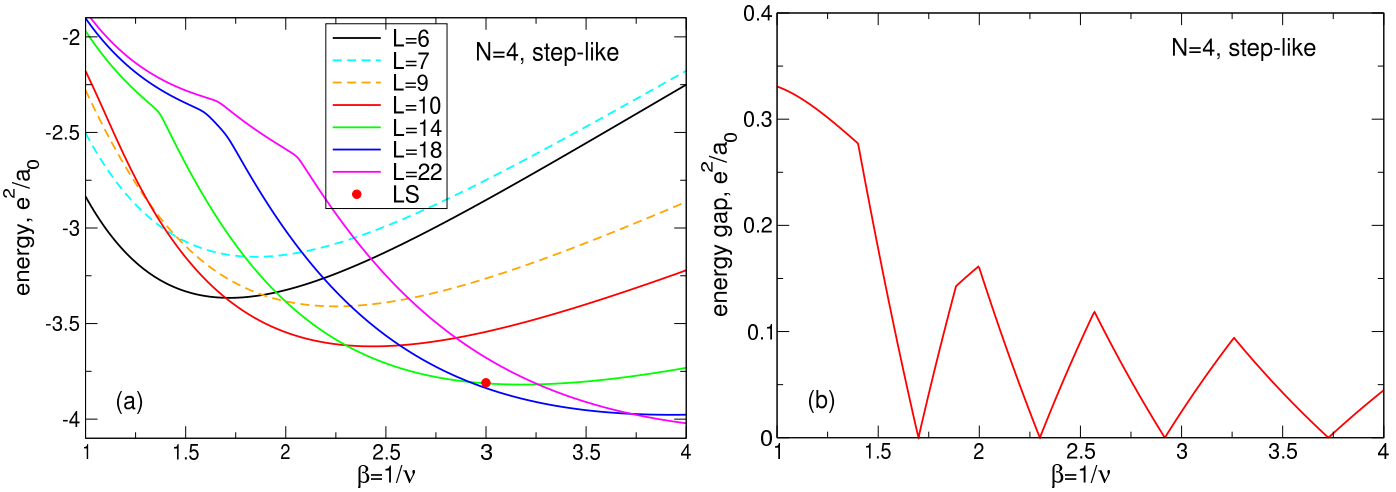

Figure 22. (**a**) The energy of the many-body states with the total angular momenta from $\mathcal{L} = \mathcal{L}_{\mathrm{min}} = 6$ up to $\mathcal{L} = 22$ in the system of $N = 4$ 2D electrons as a function of the magnetic field parameter $\beta = 1/\nu$. For all shown states, the index s equals $s = 1$. Only the states which are either ground or first excited states are shown. The LS energy at $\nu = 1/3$ is shown by a small red circle. (**b**) The energy gap between the ground and the first excited states as a function of β. The positive background density profile is step-like.

Table 16. The total angular momenta of the ground state $\mathcal{L}_{\mathrm{GS}}$ and of the first excited state $\mathcal{L}_{\mathrm{1st}}$ assume the values shown in the last two columns in the intervals from β_{from} to β_{to} shown in the first two columns. The number of particles is $N = 4$, and the density profile is step-like.

β_{from}	β_{to}	$\mathcal{L}_{\mathrm{GS}}$	$\mathcal{L}_{\mathrm{1st}}$
1.0000	1.4006	6	7
1.4006	1.6991	6	10
1.6991	1.8850	10	6
1.8850	1.9972	10	9
1.9972	2.2994	10	14
2.2994	2.5689	14	10
2.5689	2.9173	14	18
2.9173	3.2593	18	14
3.2593	3.7263	18	22
3.7263	4.0000	22	18

Figure 22b shows the energy gap between the first excited and the ground state as a function of the magnetic field parameter β. The gap vanishes in a few β-points and has local maxima varying from $\approx 0.15 e^2/a_0$ at $\beta = 1.9972$ to $\approx 0.094 e^2/a_0$ at $\beta = 3.2593$.

7.1.4. Five Particles

As in the case of $N = 4$, Figure 23a shows the energies $E_{\mathcal{L},1}(\beta)$ only for those $\mathcal{L}$ that are either the ground state or the first excited state in some intervals of β. These intervals and the corresponding angular momenta $\mathcal{L}_{\rm GS}$ and $\mathcal{L}_{\rm 1st}$ are given in Table 17. The rule (117) for $\mathcal{L}_j^{\rm GS}$ remains valid for $N = 5$. The energy of the LS with $m = 3$ is shown by a small red circle at $\beta = 3$. It lies above the blue curve corresponding to the first excited state $\mathcal{L} = 25$ at $\nu = 1/3$.

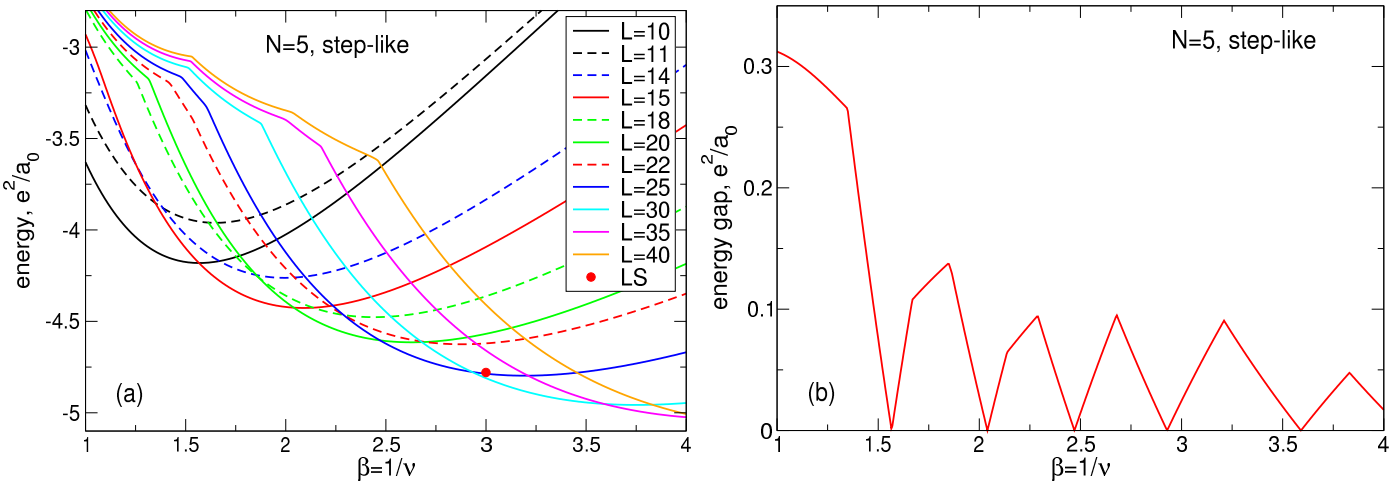

Figure 23. (**a**) The energy of the many-body states with the total angular momenta from $\mathcal{L} = \mathcal{L}_{\rm min} = 10$ up to $\mathcal{L} = \mathcal{L}_{\rm max} = 40$ in the system of $N = 5$ 2D electrons as a function of the magnetic field parameter $\beta = 1/\nu$. For all shown states, the index s equals $s = 1$. Only the states which are either ground or first excited states are shown. The LS energy at $\nu = 1/3$ is shown by a small red circle. (**b**) The energy gap between the ground and the first excited states as a function of β. The positive background density profile is step-like.

Table 17. The total angular momenta of the ground state $\mathcal{L}_{\rm GS}$ and of the first excited state $\mathcal{L}_{\rm 1st}$ assume the values shown in the last two columns in the intervals from $\beta_{\rm from}$ to $\beta_{\rm to}$ shown in the first two columns. The number of particles is $N = 5$, the density profile is step-like.

$\beta_{\rm from}$	$\beta_{\rm to}$	$\mathcal{L}_{\rm GS}$	$\mathcal{L}_{\rm 1st}$
1.0000	1.3483	10	11
1.3483	1.5666	10	15
1.5666	1.6688	15	10
1.6688	1.8486	15	14
1.8486	1.8647	15	18
1.8647	2.0402	15	20
2.0402	2.1372	20	15
2.1372	2.2887	20	18
2.2887	2.2890	20	22
2.2890	2.4705	20	25
2.4705	2.6791	25	20
2.6791	2.9287	25	30
2.9287	3.2100	30	25
3.2100	3.5904	30	35
3.5904	3.8305	35	30
3.8305	4.0000	35	40

Figure 23b shows the energy gap between the first excited and the ground state as a function of β. Its value in the local maxima varies from $\approx 0.137 e^2/a_0$ at $\beta = 1.8486$ to $\approx 0.048 e^2/a_0$ at $\beta = 3.8305$.

7.1.5. Six Particles

For $N = 6$, Figure 24a shows the energies $E_{\mathcal{L},1}(\beta)$ for those $\mathcal{L}$ which are either the ground state or the first excited state in some intervals of β. These intervals and the corresponding angular momenta $\mathcal{L}_{\rm GS}$ and $\mathcal{L}_{\rm 1st}$ are given in Table 18. In the case of six particles, the overall picture of the energy spectra is more complex than for $N < 6$. Firstly, the number of $\mathcal{L}$-states that take on the role of the ground state in the interval $1 \le \beta \le 4$ is ten, which is substantially larger than one would expect from the evolution of plots from Figures 20–23. Secondly, the length of the β intervals in which the ground state angular momenta remain constant becomes shorter, and these intervals are less uniformly distributed along the β-axis. Thirdly, although the rule (117) is satisfied for some values of $\mathcal{L}$, it is violated for some other $\mathcal{L}$'s.

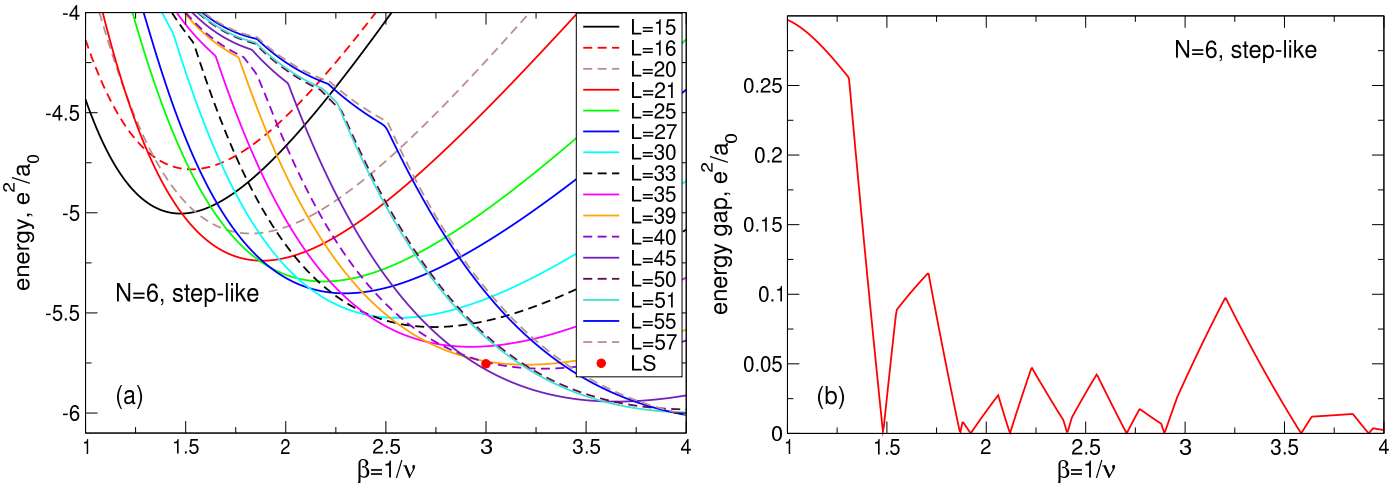

Figure 24. (**a**) The energy of the many-body states with the total angular momenta from $\mathcal{L} = \mathcal{L}_{\rm min} = 15$ up to $\mathcal{L} = 57$ in the system of $N = 6$ 2D electrons as a function of the magnetic field parameter $\beta = 1/\nu$. For all shown states, the index s equals $s = 1$. Only the states which are either ground or first excited states are shown. The LS energy at $\nu = 1/3$ is shown by a small red circle. (**b**) The energy gap between the ground and the first excited states as a function of β. The positive background density profile is step-like.

What are the reasons for such unusual behavior of the spectra at $N = 6$?

As has been seen in Section 3, for $N = 6$, the energies of the classical shell configurations $(1, N-1)$ and $(0, N)$ are very close to each other. Therefore, the configurations with the symmetry C_5 (five particles on the outer shell) can compete in energy with the configurations with the symmetry C_6 (six particles on the outer shell). Indeed, in the case of the $(1,5)$ shell configuration, the expected $\mathcal{L}$ sequence (117) would be

$$\mathcal{L}_{\rm GS}^{(1,5)} = 15,\ 20,\ 25,\ 30,\ 35,\ 40,\ 45,\ 50,\ 55. \tag{118}$$

In the case of the $(0,6)$ shell configuration, the expected ("underlined") $\mathcal{L}$ sequence would be

$$\mathcal{L}_{\rm GS}^{(0,6)} = \underline{15},\ \underline{21},\ \underline{27},\ \underline{33},\ \underline{39},\ \underline{45},\ \underline{51},\ \underline{57}. \tag{119}$$

Calculations show that, for $N = 6$, a mixture of the sequences (118) and (119),

$$\mathcal{L}_{\rm GS} = \underline{15},\ \underline{21},\ 25,\ \underline{27},\ 30,\ 35,\ \underline{39},\ \underline{45},\ \underline{51},\ 55, \tag{120}$$

is actually realized, while the states with

$$\mathcal{L}_{1st} = 20,\ \underline{33},\ 40,\ 50,\ \underline{57} \tag{121}$$

serve as the first excited states. Thus, the complicated structure of the levels at $N = 6$ is explained by the competition of one-shell and two-shell configurations which have very close energies already in the classical approach.

Table 18. The total angular momenta of the ground state $\mathcal{L}_{GS}$ and of the first excited state $\mathcal{L}_{1st}$ assume the values shown in the last two columns in the intervals from β_{from} to β_{to} shown in the first two columns. The number of particles is $N = 6$, and the density profile is step-like.

β_{from}	β_{to}	$\mathcal{L}_{GS}$	$\mathcal{L}_{1st}$
1.0000	1.3094	15	16
1.3094	1.4812	15	21
1.4812	1.5480	21	15
1.5480	1.7089	21	20
1.7089	1.8685	21	25
1.8685	1.8813	25	21
1.8813	1.9215	25	27
1.9215	2.0598	27	25
2.0598	2.1190	27	30
2.1190	2.2284	30	27
2.2284	2.3883	30	33
2.3883	2.4072	30	35
2.4072	2.4303	35	30
2.4303	2.5560	35	33
2.5560	2.7060	35	39
2.7060	2.7714	39	35
2.7714	2.8798	39	40
2.8798	2.8965	39	45
2.8965	2.9606	45	39
2.9606	3.2029	45	40
3.2029	3.5837	45	51
3.5837	3.6374	51	45
3.6374	3.8437	51	50
3.8437	3.9236	51	55
3.9236	3.9456	55	51
3.9456	4.0000	55	57

Figure 24b shows the energy gap between the first excited and the ground state as a function of the magnetic field parameter β. It is noticeable that the largest energy gaps and the largest distances between the gap nodes are seen in the ranges $1.48 \lesssim \beta \lesssim 1.87$ and $2.8965 \lesssim \beta \lesssim 3.58$, which are close to $\nu = 2/3$ and $\nu = 1/3$. The gap maxima in these intervals are $\approx 0.115 e^2/a_0$ at $\beta = 1.6688$ and $\approx 0.097 e^2/a_0$ at $\beta = 3.21$, which are about twice as large as the other local gap maxima between $\beta \simeq 2$ and 3 ($\lesssim 0.05 e^2/a_0$). If it were possible to show that the Hall conductivity is constant in the β-intervals, where the gaps are finite (this still needs to be performed in a future theory), the widths of the plateaus would be maximal around $\nu = 1/3$ and $2/3$. So, some correlations with the FQHE experiment in a macroscopic sample arise already at $N = 6$.

7.1.6. Seven Particles, Step-like Density Profile

For $N = 7$, the energy-vs.-β curves for the angular momenta $\mathcal{L}$ which are either the ground or the first excited state in some intervals of β are shown in Figure 25. The corresponding intervals and the angular momenta $\mathcal{L}_{GS}$ and $\mathcal{L}_{1st}$ are given in Table 19. As compared to the case of six particles, the spectra look simpler again, with $N + 1 = 8$ angular momenta, corresponding to the ground states in the different intervals of β. The rule

(117) is satisfied with one exception: in the expected sequence of the ground state $\mathcal{L}$'s ($= \mathcal{L}_{\min} + (N-1)k$),

$$21, 27, 33, 39, 45, 51, 57, 63,$$

the second number is replaced by 28 ($= \mathcal{L}_{\min} + N$). The state with $\mathcal{L} = 28$ is the ground state of the seven-particle system at $1.4211 \leq \beta \leq 1.721$. The reason for these deviations is very interesting and is discussed in Section 7.2.2.

The energy of the state (5) with $m = 3$ is shown by a small red circle at $\beta = 3$ in Figure 25a. In the case $N = 7$, the ground ($\mathcal{L} = 63$) and the first excited states ($\mathcal{L} = 57$) are very close in energy, while the LS energy is substantially larger than both E_{GS} and $E_{1\mathrm{st}}$, as can also be seen in Table 5.

Figure 25b shows the energy gap between the first excited and the ground state as a function of β. The values of the gap lie between $\sim 0.1 e^2/a_0$ at $\beta = 1.617$ and 2.0512 and $\sim 0.0375 e^2/a_0$ at $\beta = 2.8819$.

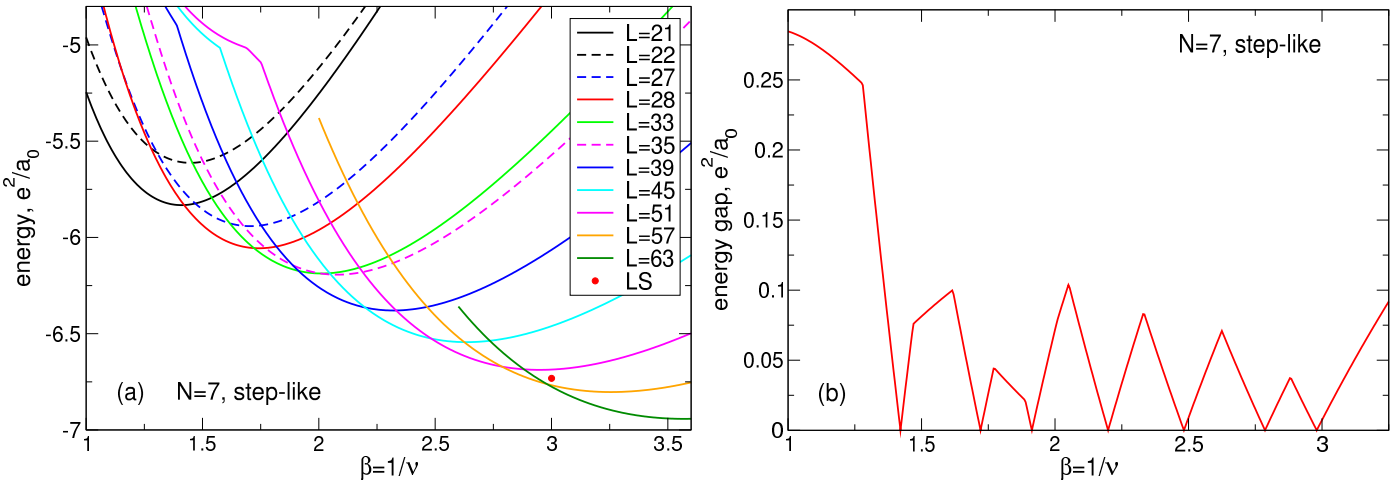

Figure 25. (**a**) The energy of the many-body states with the total angular momenta from $\mathcal{L} = \mathcal{L}_{\min} = 21$ up to $\mathcal{L} = 63$ in the system of $N = 7$ 2D electrons as a function of the magnetic field parameter $\beta = 1/\nu$. For all shown states, the index s equals $s = 1$. Only the states which are either ground or first excited states are shown. The LS energy at $\nu = 1/3$ is shown by a small red circle. (**b**) The energy gap between the ground and the first excited states as a function of β. The positive background density profile is step-like.

Table 19. The total angular momenta of the ground state $\mathcal{L}_{\mathrm{GS}}$ and of the first excited state $\mathcal{L}_{1\mathrm{st}}$ assume the values shown in the last two columns in the intervals from β_{from} to β_{to} shown in the first two columns. The number of particles is $N = 7$, the density profile is step-like.

β_{from}	β_{to}	$\mathcal{L}_{\mathrm{GS}}$	$\mathcal{L}_{1\mathrm{st}}$
1.0000	1.2795	21	22
1.2795	1.4211	21	28
1.4211	1.4690	28	21
1.4690	1.6170	28	27
1.6170	1.7210	28	33
1.7210	1.7708	33	28
1.7708	1.8886	33	35
1.8886	1.9132	33	39
1.9132	2.0082	39	33
2.0082	2.0512	39	35
2.0512	2.1988	39	45
2.1988	2.3323	45	39
2.3323	2.4828	45	51
2.4828	2.6249	51	45
2.6249	2.7866	51	57
2.7866	2.8819	57	51
2.8819	2.9803	57	63
2.9803	3.2500	63	57

7.1.7. Seven Particles, Smooth Density Profile

As has been shown in Section 6.7, at $\beta = 1/\nu = 3$, the angular momenta of the ground ($\mathcal{L} = 63$) and the first excited state ($\mathcal{L} = 57$) in the system with the step-like profile are reversed when the profile is smooth. It is interesting to see how the energy spectra look over a wide range of the magnetic field in a system with a smooth density profile (13).

Figure 26a shows these spectra. In general, the curves $E_{\rm GS}(\beta)$ and $E_{\rm 1st}(\beta)$ look qualitatively similar to the case of the step-like profile, but some details are quantitatively different. In particular, the intervals of β corresponding to different $\mathcal{L}$ values differ from the case of the step-like profile, see Table 20. The rule (117) is also satisfied for $N = 7$ and a smooth density profile, with the exception of the region of small β, where the ground state has $\mathcal{L} = 28$ instead of the expected $\mathcal{L}$ =27.

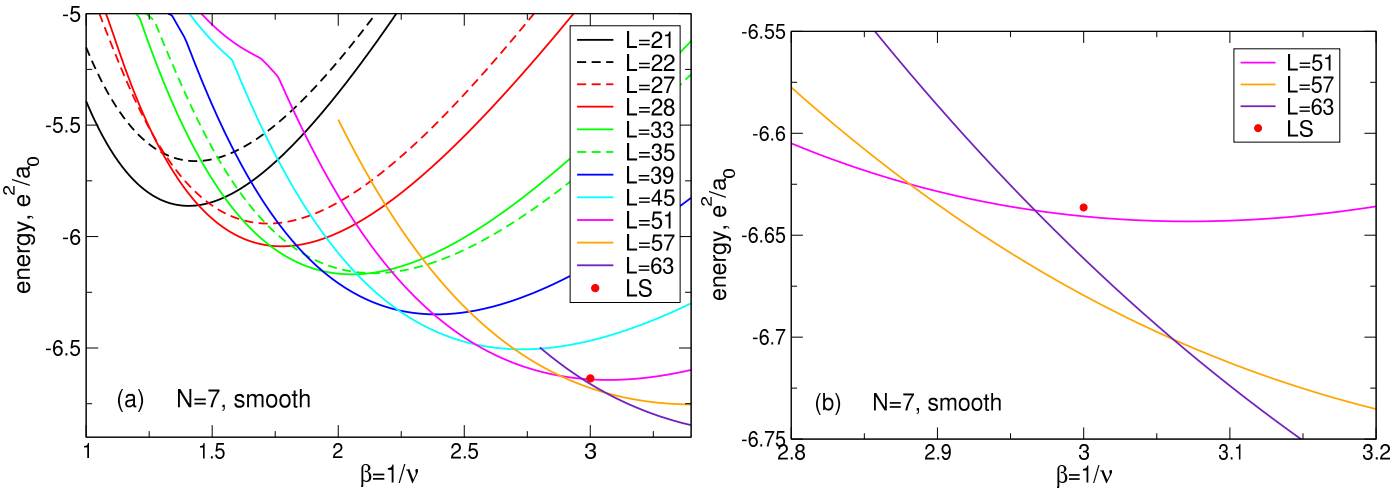

Figure 26. (**a**) The energy of the many-body states with the total angular momenta from $\mathcal{L} = \mathcal{L}_{\rm min} = 21$ up to $\mathcal{L} = 63$ in the system of $N = 7$ 2D electrons as a function of the magnetic field parameter $\beta = 1/\nu$. For all shown states, the index s equals $s = 1$. Only the states which are either ground or first excited states are shown. The LS energy at $\nu = 1/3$ is shown by a small red circle. (**b**) The vicinity of the point $\beta = 3$ on a larger scale. The positive background density profile is smooth.

Table 20. The total angular momenta of the ground state $\mathcal{L}_{\rm GS}$ and of the first excited state $\mathcal{L}_{\rm 1st}$ assume the values shown in the last two columns in the intervals from $\beta_{\rm from}$ to $\beta_{\rm to}$ shown in the first two columns. The number of particles is $N = 7$, the density profile is smooth.

$\beta_{\rm from}$	$\beta_{\rm to}$	$\mathcal{L}_{\rm GS}$	$\mathcal{L}_{\rm 1st}$
1.0000	1.3016	21	22
1.3016	1.4455	21	28
1.4455	1.4849	28	21
1.4849	1.6180	28	27
1.6180	1.7293	28	33
1.7293	1.8142	33	28
1.8142	1.8689	33	35
1.8689	1.9380	33	39
1.9380	2.0744	39	33
2.0744	2.2388	39	45
2.2388	2.3790	45	39
2.3790	2.5443	45	51
2.5443	2.6990	51	45
2.6990	2.8809	51	57
2.8809	2.9667	57	51
2.9667	3.0613	57	63
3.0613	3.4000	63	57

The neighborhood of the point $\beta = 3$ is shown in Figure 26b. One sees that, around the point $\beta = 3$, at $2.8809 < \beta < 3.0613$, the ground state has the angular momentum $\mathcal{L}_{\rm 1st} = 57$, as was found in Ref. [18] and discussed in Section 6.7. The state $\mathcal{L}_{\rm GS} = 63$ becomes the

ground state at a larger $\beta > 3.0613$. The LS point lies above the second excited state which has $\mathcal{L}_{2nd} = 51$.

7.2. Electron Density

The magnetic field dependencies of the energy levels investigated in Section 7.1 show that the ground state energy decreases with increasing B, oscillating due to a stepwise increase in the total angular momentum $\mathcal{L}_{GS}$ in the ground states. The physical reasons of such oscillations are explained below. Here, I analyze the density of electrons $n_e(r)$ in a number of different $\mathcal{L}$-states for two cases, $N = 5$ and $N = 7$, representing the one-shell and two-shell configurations.

7.2.1. Five Particles

The energy spectra of the system of $N = 5$ electrons are shown in Figure 23a. One of the states, shown there by the blue solid curve, has the total angular momentum $\mathcal{L} = 25$. Let us consider the density of electrons in this state at different magnetic fields.

Figure 27a shows the normalized function $n_e(r)$ for the state $\mathcal{L} = 25$ and for β varying from $\beta = 2.0$ up to $\beta = 3.6$ with the step 0.2. At all values of β, the function $n_e(r)$ has a maximum at a certain distance from the origin, i.e., the electron density has the shape of a ring. The position of the maximum, i.e., the ring radius, as well as the width of the maximum, are large at small β and decrease when β grows. This is caused by a decrease in the magnetic length with an increasing magnetic field. If the $\mathcal{L} = 25$ state is the ground state of the system at a given β, the corresponding density functions are shown by solid curves; otherwise they are shown by dashed curves.

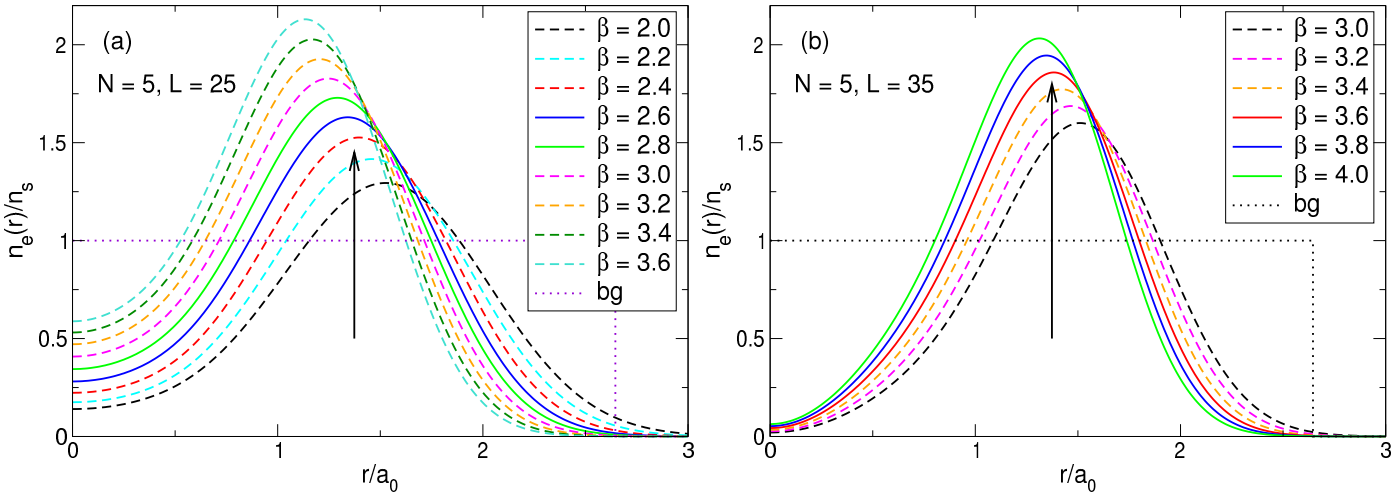

Figure 27. The density of electrons in the system of $N = 5$ particles at different magnetic fields and at (**a**) $\mathcal{L} = 25$ and (**b**) $\mathcal{L} = 35$. For β-values, for which the corresponding $\mathcal{L}$ state is the ground state (one of the excited states), the function $n_e(r)$ is shown by solid (dashed) curves. The vertical arrow at $r/a_0 = R_s/a_0 = 1.373422$ shows the position of the shell radius in the classical Wigner molecule. The positive background density profile is step-like and shown by the black dotted curve in both panels.

The classical shell radius at $N = 5$ equals $R_s = 1.3734a_0$. It is shown by the vertical arrow in Figure 27. When $\beta = 2.0$ (the rightmost curve in Figure 27a), the density maximum is located at $r = R_{max} \approx 1.525a_0$, which is noticeably larger than the classical shell radius. In this magnetic field, the state $\mathcal{L} = 25$ is not the ground, but the fifth excited state. Then, when the magnetic field increases, the wave function shrinks, and the density maximum shifts to smaller values of r. At $\beta = 2.2$ and 2.4, the state $\mathcal{L} = 25$ is the fourth and first excited state, respectively, and the maximum of the electron density is still located at the points larger than R_s.

When the B-field continues to grow, the density maximum $R_{\max}$ passes through the position of the shell radius R_s, and the state $\mathcal{L} = 25$ becomes the ground state. In Figure 27a, this is the case for the curves labeled by $\beta = 2.6$ and 2.8. The maxima of the electron density then lie at $R_{\max} \approx 1.34a_0$ and $1.29a_0$, respectively, close to the position of R_s. As the β-parameter increases further, the ring radius $R_{\max}$ becomes too small compared to the classical shell radius R_s, and the state with $\mathcal{L} = 25$ ceases to be the ground state.

In order to return the ring radius $R_{\max}$ back to the classical shell radius R_s, a state with a larger $\mathcal{L}$ should take over the role of the ground state. The ground state angular momentum jumps up by the value $\delta\mathcal{L} = n^{\rm st}(N) = 5$, and the radius of the electron density ring turns out to be again close to or slightly larger than R_s.

Figure 27b confirms this simple physical picture. This shows the density of electrons for the state $\mathcal{L} = 35$ and for β varying from $\beta = 3.0$ up to $\beta = 4.0$ with the step 0.2. Again, at all values of β, the density of the electrons has the shape of a ring, but the ring radius $R_{\max}$ is larger (at the same values of β) than in panel (a) since the angular momentum is now bigger. At $\beta = 3.0$, the state with $\mathcal{L} = 35$ is the second excited state, and the density maximum lies well outside the shell radius R_s. When β increases up to $\beta = 3.2$ and 3.4, the density maxima become smaller, $R_{\max} = 1.46a_0$ and $1.42a_0$, respectively, but they are still larger than R_s. At even larger β's, $\beta = 3.6$, 3.8, and 4.0, the ring radii become almost equal or slightly smaller than R_s, $R_{\max}/a_0 \approx 1.38$, 1.35, and 1.31, respectively, and the state $\mathcal{L} = 35$ becomes the ground state.

7.2.2. Seven Particles, Step-like Density Profile

Let us now consider the system of $N = 7$ particles which illustrates the case of the two-shell configuration. I first consider relatively large magnetic fields $\beta \geq 1.7$. Figure 28a–f show the density of electrons for the ground state angular momenta from $\mathcal{L} = 33$ to $\mathcal{L} = 63$ and for β from 1.7 to 3.4 with the step 0.1.

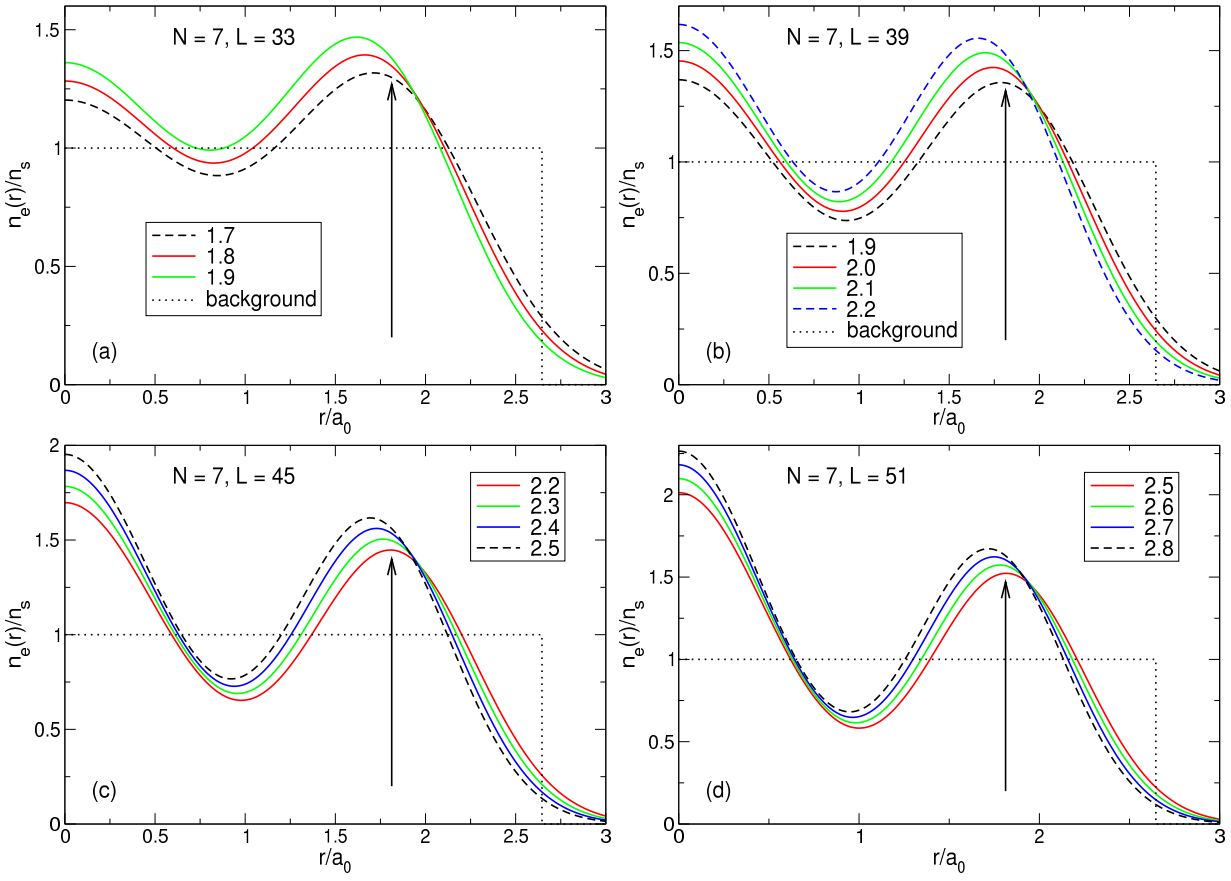

Figure 28. *Cont.*

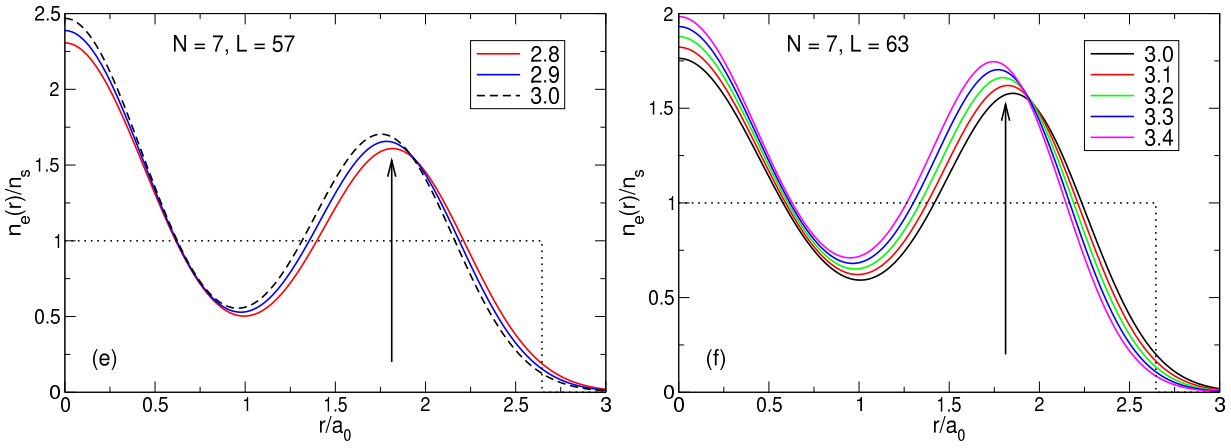

Figure 28. The density of electrons in the system of $N = 7$ particles at different magnetic fields and at (**a**) $\mathcal{L} = 33$, (**b**) $\mathcal{L} = 39$, (**c**) $\mathcal{L} = 45$, (**d**) $\mathcal{L} = 51$, (**e**) $\mathcal{L} = 57$, and (**f**) $\mathcal{L} = 63$. For β-values, for which the corresponding $\mathcal{L}$ state is the ground state, the function $n_e(r)$ is shown by solid curves. The arrow at $r/a_0 = R_s/a_0 = 1.8126$ shows the position of the shell radius in the classical Wigner molecule. The step-like positive background density profile is shown by the black dotted curve in all panels.

As expected, all density curves have two maxima, one at $r = 0$ and the other at a finite $r = R_{\max}$. The behavior of the density curves is similar to the case of $N = 5$ particles. As the magnetic field increases, the maxima of the density curves $R_{\max}$ pass through the position of the classical shell radius R_s. When, for a given $\mathcal{L}$, $R_{\max}$ becomes close to or slightly smaller than R_s, this state becomes the ground state. When $R_{\max}$ becomes too small compared to R_s, the role of the ground state is taken over by the next state with the angular momentum increased by $\delta\mathcal{L} = n^{\mathrm{st}}(N) = 6$. The oscillations of $R_{\max}$ around the fixed value of R_s are shown in Figure 29. The quantum-mechanically calculated radii of the rings $R_{\max}$ are on average smaller than the classical shell radius R_s. This is because the potential energy of the attractive positively charged background is higher at $r > R_s$ and lower at $r < R_s$ compared to $V_b(r = R_s)$, see Figure 2.

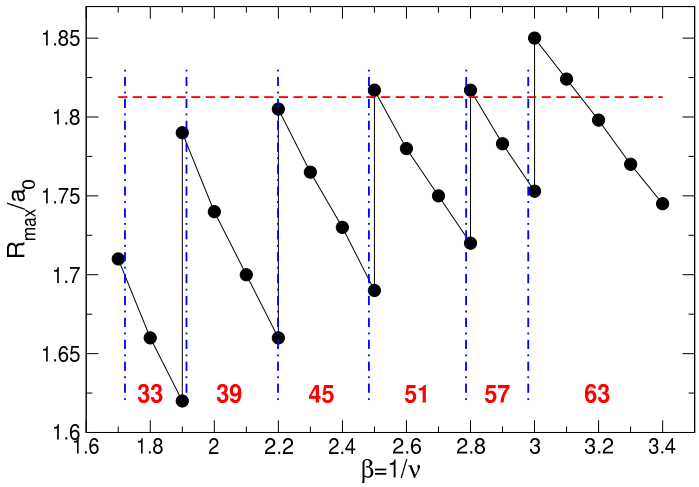

Figure 29. Positions of the maxima of the density curves shown in Figure 28 at different β-values and different angular momenta $\mathcal{L}$. The red dashed line at $R/a_0 = 1.8126$ shows the position of the shell radius in the classical Wigner molecule. The blue dash-dotted lines separate the areas where the ground states have different angular momenta indicated by the numbers 33, 39, ..., 63 in the corresponding β-intervals.

At lower magnetic fields $\beta \lesssim 1.72$, the shape of the electron density in the ground state changes significantly, as shown in Figure 30a. Here, one should consider two different situations. If $1.0 \leq \beta \leq 1.4211$, the ground state has the total angular momentum $\mathcal{L} = 21$,

the expansion of the many-body wave function (58) contains only one Slater determinant, $N_{mbs} = 1$, and the wave function is the MDD state $|0,1,2,3,4,5,6\rangle$. The electron density in this state, as shown in Figure 30a, does not have an internal structure typical for a Wigner molecule, but has the form of a uniform liquid, Figure 9. The radius of the MDD-liquid spot decreases, while the density on the plateau increases with increasing β. As I discussed at the beginning of Section 7, this solution is not accurate enough and should be improved by taking higher Landau level states into account. As seen from Figure 30a, this should be done at least at $1.0 \leq \beta \lesssim 1.42$. Here, I show the density $n_e(r)$ for the state $\mathcal{L} = 21$ for completeness only.

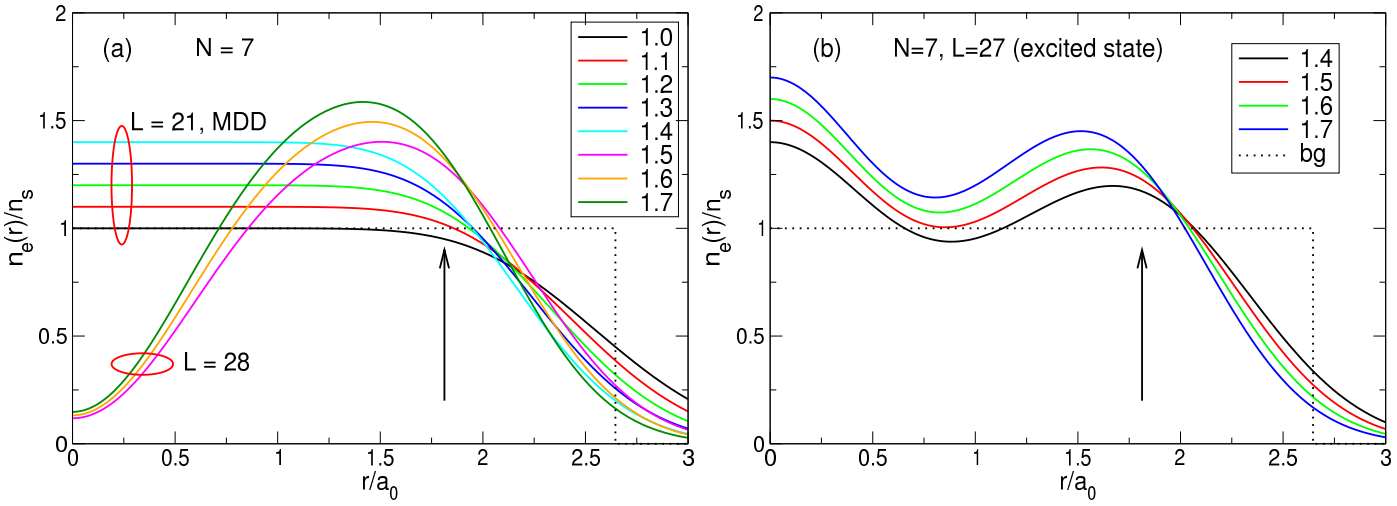

Figure 30. The density of electrons in the system of $N = 7$ particles at different magnetic fields and (**a**) in the ground states with $\mathcal{L} = 21$ and 28, and (**b**) in the excited state with $\mathcal{L} = 27$. The arrow at $r/a_0 = R_s/a_0 = 1.8126$ shows the position of the shell radius in the classical Wigner molecule. The step-like positive background density profile is shown by the black dotted curve in both panels.

In intermediate magnetic fields, $1.4211 \leq \beta < 1.721$, the total angular momentum in the ground state is $\mathcal{L} = 28$, and the density $n_e(r)/n_s$ assumes the form of a broad ring with a *single* density maximum at a finite r, Figure 30a. That is, in this β-region, instead of the "usual" $(1, N-1)$ Wigner molecule configuration, the configuration $(0, N)$ is realized. The state $\mathcal{L} = 27$, corresponding to the "correct" configuration $(1, N-1)$, has the density profile with two maxima, Figure 30b, but is the first excited state.

There are two possible explanations for this "unusual" behavior of the electron density. First, it is not entirely clear whether the solution in this β-range is sufficiently accurate. If $\mathcal{L} = 28$, the number of many-body basis states in the expansion (58) is $N_{mbs} = 15$. Although this number is much larger than one, it is worth checking whether this result still holds when higher Landau level states are taken into account.

If this result is correct, it can be explained as follows. In strong magnetic fields, the size of the wave functions $\lambda \propto 1/\sqrt{\beta}$ is small, and "thin" electrons are more like point-like classical particles. Trying to find the configuration with the lowest energy in the field of the attractive potential, Figure 2, six electrons push one of their comrades into the center of the disk, and themselves form a ring around it. As the magnetic field decreases, the length λ grows, and the electrons become "fat". A "fat" electron cannot fit in the center of the potential well, and therefore, all seven electrons are located at its edge, creating a single-shell $(0,7)$ configuration.

To answer the question of which of the two described situations is actually the case, one should develop a more general theory that takes into account the higher Landau level states.

7.2.3. Seven Particles, Smooth Density Profile

In the case of the smooth background density profile (13), the density of electrons at $\beta = 3$ is shown in Figure 31 for the ground, first and second excited states, $\mathcal{L} = 57$, 63, and 51, as well as for the Laughlin state. The density of electrons in all three exact states has the shape of the Wigner molecule, with the high maximum in the center and the second maximum at $r = R_{\max} \simeq R_s$. The density in the three exact states differs only in the position of the second maximum and the heights of both maxima.

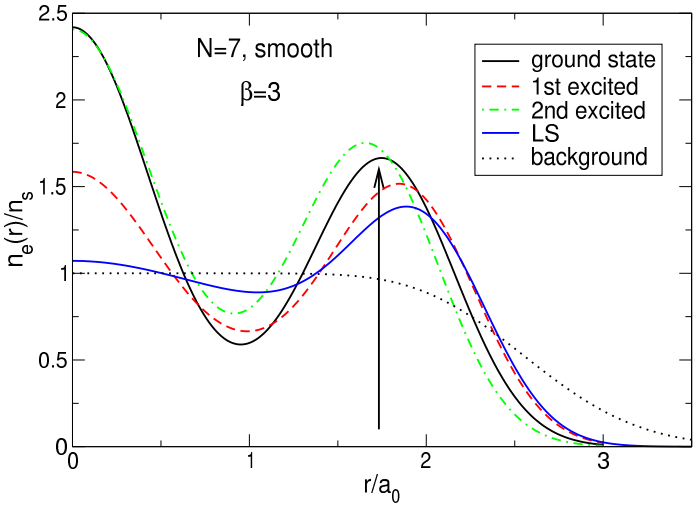

Figure 31. The density of electrons in the ground state ($\mathcal{L} = 57$), first ($\mathcal{L} = 63$) and second ($\mathcal{L} = 51$) excited states, and in the LS in a system of $N = 7$ particles at $\beta = 3$. The positive background density profile is smooth. The arrow at $r/a_0 = R_s/a_0 = 1.732047$ shows the position of the outer shell of the classical Wigner molecule in the case of the smooth background density. The density of the LS at $r = 0$ is 2.2576 times smaller than the density of the ground state.

The difference between the electron densities in the LS and in the true ground state at $\beta = 3$ in the smooth background case is even greater than in the previously considered case of the step-like profile, Figure 13c. At $r = 0$, the ratio $n_e^{\mathrm{GS}}(0)/n_e^{\mathrm{LS}}(0)$ is equal to 2.2576. The density maximum in the LS is located at the point $R_{\max}^{\mathrm{LS}}/a_0 = 1.888$, which is significantly further from the center than the classical shell radius $R_s/a_0 = 1.732$. Thus, while in the exact solution one of the electrons jumps to the bottom of the deep potential well, Figure 2, lowering the energy of the system, in the LS all seven electrons accumulate at the edge of the well, increasing its energy.

7.3. Exact Solutions: Summary

Thus, the B-dependencies of the energy of the ground and excited states, as well as the corresponding electron densities, give a simple and clear picture of the FQHE physics. The interplay of the Coulomb forces and the compressive action of the B-field leads to the alternating opening and closing of the energy gaps in the many-body spectrum of the system as the magnetic field changes, as shown in Figures 20–26. It is reasonable to assume that, in a macroscopic 2D electron system, the diagonal conductivity will tend to zero in the finite-gap regions of B, while the Hall conductivity will take quantized values there. It is also clear from the spectra of Figures 20–26, that the point $\nu = 1/3$ (or any other fractional ν point) is not something special; this is just a single point in the B-field interval where the energy gap is finite. This fact is fully consistent with the FQHE experiments in which it is not the filling factor that is quantized, but the Hall conductivity.

It is clear that the physical picture similar to that described in this Section should also occur at larger values of the filling factor ν, when the higher Landau levels are also occupied. Moreover, one sees from the described analysis that, in order to explain the Hall quantization, both integer and fractional, there is no need to assume the presence of a

disorder in the system. Both effects can be explained from a unified position within the framework of the many-body theory, as it has been performed in the present Section.

Let us now discuss some further statements of the currently accepted theory of the FQHE effect.

8. Further Comments on the Currently Accepted FQHE Theory

8.1. Fractionally Charged Excitations in the Laughlin Theory

Apart from the wave function (5), which was designed for the ground state of the FQHE system at $\nu = 1/m$, Laughlin also "generated" trial many-body wave functions for the excited states. According to [6], these wave functions should have the form

$$\Psi_{\rm LS}^{(m),+z_0}(\boldsymbol{r}_1,\boldsymbol{r}_2,\ldots,\boldsymbol{r}_N,\boldsymbol{r}_0) \propto \exp\left(-\frac{1}{2}\sum_{j=1}^{N}|z_j|^2\right)\left(\prod_{1\le i\le N}(z_i-z_0)\right)\left(\prod_{1\le j<k\le N}(z_j-z_k)^m\right) \tag{122}$$

for particles that were called "quasiholes", and the form

$$\Psi_{\rm LS}^{(m),-z_0}(\boldsymbol{r}_1,\boldsymbol{r}_2,\ldots,\boldsymbol{r}_N,\boldsymbol{r}_0) \propto \exp\left(-\frac{1}{2}\sum_{j=1}^{N}|z_j|^2\right)\left(\prod_{1\le i\le N}\left(\frac{\partial}{\partial z_i}-\frac{z_0}{l_B^2}\right)\right)\left(\prod_{1\le j<k\le N}(z_j-z_k)^m\right) \tag{123}$$

for particles that were called "quasielectrons". Projections of these wave functions "onto the analogous ones computed numerically", for four particles and $m = 3$, were found to be 0.998 for $\Psi_{\rm LS}^{(m),-0}$ and 0.982 for $\Psi_{\rm LS}^{(m),+0}$ (at $z_0 = 0$). Laughlin also stated that these quasiparticles have fractional charges e/m. Let us explore the properties of the quasiparticles (122) and (123) in somewhat more detail. For simplicity, I will also consider only the case $z_0 = 0$.

In Section 6, I expanded the Laughlin function (5) in a set of many-body basis states Ψ_s, as shown in Equation (84). A similar expansion can also be performed for the "quasihole" and "quasielectron" wave functions (122) and (123). For example, for three particles and $m = 3$, the LS function (5) is expanded as

$$\begin{aligned}\Psi_{\rm LS}^{(m=3)} &\propto e^{-(|z_1|^2+|z_2|^2+|z_3|^2)/2}[(z_1-z_2)(z_1-z_3)(z_2-z_3)]^3\\ &\propto -\sqrt{0!3!6!}\Psi_{|0,3,6\rangle}+3\sqrt{0!4!5!}\Psi_{|0,4,5\rangle}+3\sqrt{1!2!6!}\Psi_{|1,2,6\rangle}-6\sqrt{1!3!5!}\Psi_{|1,3,5\rangle}+15\sqrt{2!3!4!}\Psi_{|2,3,4\rangle},\end{aligned} \tag{124}$$

with the coefficients C_s ($= -1, 3, 3, -6$ and 15) from Table 9. The similar expansions of the "quasihole" and "quasielectron" states (122) and (123) have the form

$$\begin{aligned}\Psi_{\rm LS}^{(m=3),+0} &\propto e^{-(|z_1|^2+|z_2|^2+|z_3|^2)/2}z_1z_2z_3[(z_1-z_2)(z_1-z_3)(z_2-z_3)]^3\\ &\propto -\sqrt{1!4!7!}]\Psi_{|1,4,7\rangle}+3\sqrt{1!5!6!}\Psi_{|1,5,6\rangle}+3\sqrt{2!3!7!}\Psi_{|2,3,7\rangle}-6\sqrt{2!4!6!}]\Psi_{|2,4,6\rangle}+15\sqrt{3!4!5!}\Psi_{|3,4,5\rangle}\end{aligned} \tag{125}$$

and

$$\begin{aligned}\Psi_{\rm LS}^{(m=3),-0} &\propto e^{-(|z_1|^2+|z_2|^2+|z_3|^2)/2}\left(\partial_{z_1}\partial_{z_2}\partial_{z_3}[(z_1-z_2)(z_1-z_3)(z_2-z_3)]^3\right)\\ &\propto 3\cdot1\cdot2\cdot6\cdot\sqrt{0!1!5!}\Psi_{|0,1,5\rangle}-6\cdot1\cdot3\cdot5\sqrt{0!2!4!}\Psi_{|0,2,4\rangle}+15\cdot2\cdot3\cdot4\sqrt{1!2!3!}\Psi_{|1,2,3\rangle}.\end{aligned} \tag{126}$$

As seen from the definition (122) and from the example (125), the "quasihole" wave function $\Psi_{\rm LS}^{(m=3),+0}$ is an eigenfunction of the total angular momentum operator with

$$\mathcal{L}_{\rm Q-hole} = \frac{3N(N-1)}{2} + N. \tag{127}$$

The statement (127) is valid for any number of particles N. Similarly, the "quasielectron" wave function $\Psi_{\rm LS}^{(m=3),-0}$ is an eigenfunction of the total angular momentum operator with

$$\mathcal{L}_{\rm Q-elec} = \frac{3N(N-1)}{2} - N \tag{128}$$

for any N. This obviously shows that the wave functions (122) and (123) can in no case describe the real low lying excitations of the system. As it was seen from the exact solution of the problem, Sections 4 and 7, the angular momenta of the lowest excited states differ from the angular momenta of the ground states by a small number $\delta\mathcal{L} \leq 6$, see Equations (68) and (117). But according to (127) and (128), the angular momenta difference between the ground and the excited state is *macroscopically large*. For example, in real samples with $N \simeq 10^{11}$ (in the thermodynamic limit), $\delta\mathcal{L}$ would be about $\delta\mathcal{L} = N \simeq 10^{11}$. This is evidently incorrect.

Using the expansions like (125) and (126), I calculated the energy and the density of electrons in the "quasihole" and "quasielectron" states (122) and (123) for $N = 7$. The results are shown in Figure 32. One sees that, Figure 32a, while the LS energy lies between the first and the second exact excited states, see also Figure 25, the energy of the Laughlin "quasielectron" is between the fourth and fifth exact excited states. As for the energy of the "quasihole" state, it lies above at least 24 different exact excited states shown by thin green (the states with different $\mathcal{L}$ and $s = 1$) and thin blue states (the states with different $\mathcal{L}$ and $s = 2$). Note that the number of different exact states lying below the "quasihole" state is definitely larger, since I did not check *all* possible $(\mathcal{L}, s)$ states that could have a lower energy than the "quasihole" state (122).

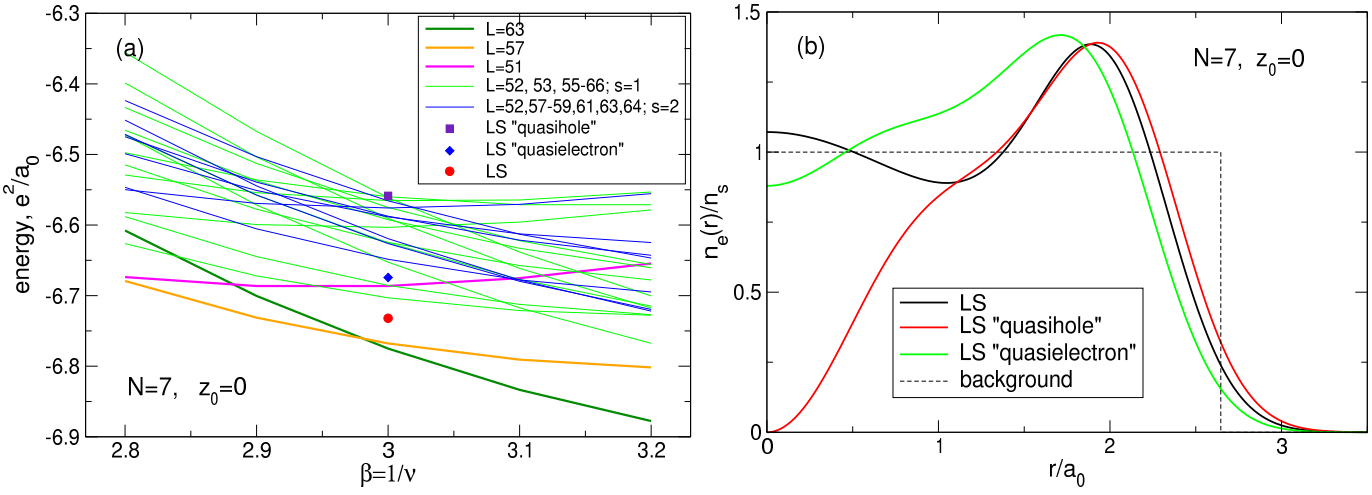

Figure 32. (**a**) The energy of the Laughlin state and the Laughlin excitations ("quasiholes" and "quasielectrons"), together with the energies of the exact ground and excited states in the vicinity of the filling factor $\nu = 1/3$. The green (blue) thin curves show the energy of the $s = 1$ ($s = 2$) exact excited states with different $\mathcal{L}$; not all exact excited states with energies lower than the energy of the Laughlin "quasihole" are shown. (**b**) The density of electrons in the Laughlin "quasiholes" and "quasielectrons" states (122) and (123).

Figure 32b shows the density of electrons in the Laughlin "quasihole" and "quasielectron" states (127) and (128), together with the density of the LS (5). One sees that the "quasihole" and "quasielectron" curves are qualitatively different from the densities of the exact low-lying excited states, compare with Figures 6b and 31.

Since the total angular momenta of the "quasihole" and "quasielectron" states (127) and (128) for $N = 7$ equal $\mathcal{L}_{\mathrm{Q-hole}} = 70$ and $\mathcal{L}_{\mathrm{Q-elec}} = 56$, respectively, the projections of the both states onto the first exact excited state $\mathcal{L}_{\mathrm{1st}} = 57$ are identically equal to zero.

Thus, the "fractionally charged quasiparticles" generated in Ref. [6] have no relation to physical reality.

8.2. Can the FQHE Problem be Studied in Models without a Positively Charged Background?

Electrons repel each other by strong and long-range Coulomb forces. To hold them together requires a positively charged background, which is always present in real physical systems. However, in many publications, e.g., in Refs. [15,19,20,27,44,45], the FQHE

problem was considered in systems without edges, i.e., without taking into account the positively charged background. In some works [15,20,44], it has been assumed that electrons are on the surface of a sphere. In other papers, e.g., Refs. [19,27,45], electrons were assumed to occupy a 2D plane, but the background–electron interaction was removed from the Hamiltonian. Are such models suitable for describing the FQHE effect in real physical systems?

8.2.1. Two-Dimensional Electrons on the Surface of a Sphere

By considering 2D electrons on the surface of a sphere, one is actually dealing with a different problem. Let us consider two particles, A and B, separated by a polar angle θ, on the surface of a sphere, see inset to Figure 33. The Coulomb force acting on the particle B from the particle A is shown as the vector $\boldsymbol{F}_C$, where

$$|\boldsymbol{F}_C| = \frac{e^2}{|AB|^2} = \frac{e^2}{(2R)^2 \sin^2(\theta/2)}. \tag{129}$$

However, the projection of the force $\boldsymbol{F}_C$ on the direction perpendicular to the sphere surface does not matter for 2D electrons. The force that matters, i.e., the force that really acts on electrons in the direction parallel to the sphere surface, equals

$$F_{C,\parallel} = F_C \cos\frac{\theta}{2} = \frac{e^2}{(2R)^2} \frac{\cos(\theta/2)}{\sin^2(\theta/2)}. \tag{130}$$

This force equals zero at $\theta = \pi$, although the real Coulomb force is always finite and decreases very slowly with r.

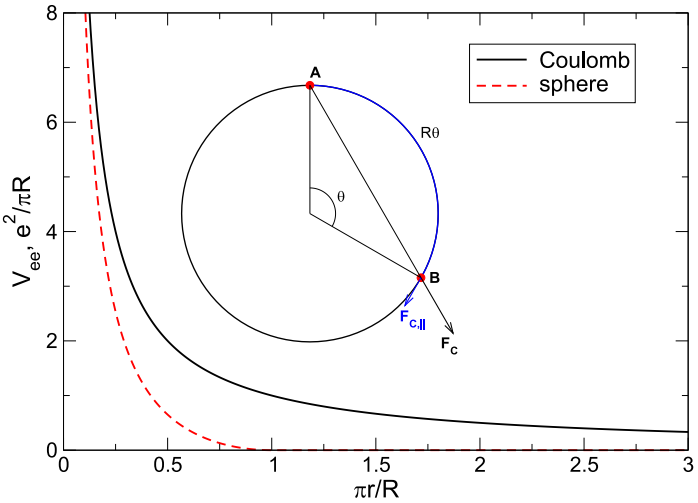

Figure 33. The Coulomb interaction potential (black curve) and the potential (132). The energy is in units $e^2/\pi R$. Inset shows a sphere with two interacting electrons A and B separated by a polar angle θ.

In addition, since the final goal is to model the behavior of the 2D electrons on a plane, the distance r between them should be counted not along the chord AB [15,44], but along the ark, shown by the blue curve, so that $r = R\theta$. Thus, the force acting on the 2D electrons along the 2DEG surface equals

$$F_{C,\parallel} = \frac{e^2}{(2R)^2} \frac{\cos(r/2R)}{\sin^2(r/2R)}, \quad \text{if } r < \pi R, \tag{131}$$

and zero otherwise. The corresponding interaction potential energy of particles on the sphere,

$$V_{ee}^{\text{sphere}} = \frac{e^2}{2R}\left(\frac{1}{\sin(r/2R)} - 1\right)\theta(\pi - r/R), \tag{132}$$

is shown in Figure 33 together with the Coulomb interaction energy e^2/r of real 2D electrons. The difference is significant. The potential (132) is actually short range, in contrast to the real Coulomb potential. Therefore, the results of calculations in the spherical geometry can hardly correctly describe the real systems of Coulomb interacting electrons.

8.2.2. No Positively Charged Background for 2D Electrons on a Plane

In the case of a flat geometry without the positive background the electrons are assumed to be at the lowest Landau level and are held together due to the angular momentum conservation [27,43]. The idea to ignore the positive background potential in this situation can lead to incorrect results and physically unreasonable conclusions. Let us consider, following [27,43], two particles with the relative angular momentum m and the center of mass angular momentum M in the plane $z = 0$. The particles are at the lowest Landau level. Under these conditions, according to [27,43], the *unique* analytic wave function that describes the two-body problem is

$$\psi_{mM}(z_1, z_2) \propto (z_1 - z_2)^m (z_1 + z_2)^M e^{-(|z_1|^2 + |z_2|^2)/2}. \tag{133}$$

Furthermore, it is stated "Remarkably, this is the exact (neglecting Landau level mixing) solution for the Schrödinger equation for *any* central potential $V(|z_1 - z_2|)$ acting between the two particles" [27].

This statement is formally correct, but it obviously contradicts common sense if we think about real systems of electrons. Let us assume that the interaction of the two particles is described by the screened Coulomb potential

$$V_{ee}^{\text{scr}} = \frac{e^2}{r} e^{-r/b}. \tag{134}$$

If $b \to \infty$, then V_{ee}^{scr} tends to the usual long-range Coulomb potential, which strongly repels electrons from each other. If b tends to zero, the potential becomes short range and the repulsive forces weaken significantly. In any real system, this will cause the distance between particles to decrease. But from the statement [27,43], it follows that the wave function describing the motion of two particles is completely independent of the screening parameter b.

The contradiction arises because the above consideration does not take into account the attractive potential of a positively charged background, which is always present in real physical systems. If to add to the V_{ee}^{scr} the *be* and *bb* interactions, Equation (23), the relative and center-of-mass angular momenta are not conserved separately. Only the total angular momentum is conserved, and the two-particle problem should be solved as described in Section 4. If $N = 2$ and $m = 3$, the solution should be sought as a linear combination

$$\Psi(\boldsymbol{r}_1, \boldsymbol{r}_2) = A_{|0,3\rangle}|0,3\rangle + A_{|1,2\rangle}|1,2\rangle. \tag{135}$$

Having solved the problem for the screened Coulomb potential (134), I obtained the coefficients $A_{|0,3\rangle}$ and $A_{|1,2\rangle}$ shown in Table 21 for different values of the parameter b/λ. The wave function (135) with the coefficients from Table 21 describes a physically correct solution in which electrons come closer to each other when b/λ tends to zero. In contrast, if the background–electron interaction is ignored, the coefficients A_s equal to $A_{|0,3\rangle} = -1/2$ and $A_{|1,2\rangle} = \sqrt{3}/2$ *for any value* of the screening parameter b/λ. These coefficients give the Laughlin wave function $\propto (z_1 - z_2)^3$, but this does not describe the physical reality.

Table 21. The coefficients A_s^{GS} in the true ground state for the system of $N = 2$ electrons with the screened Coulomb potential.

b/λ	$A_{\|0,3\rangle}$	$A_{\|1,2\rangle}$
10.0	−0.47033	0.88249
1.0	−0.44351	0.89627
0.6	−0.40232	0.91550
0.2	−0.12297	0.99241
0.1	−0.02107	0.99978

8.2.3. Contradiction in the Thermodynamic Limit

The fact that the positively charged background cannot be neglected when solving the FQHE problem, especially in the thermodynamic limit, can be seen from the following consideration. The energies of the electron–electron (*ee*) and background–background (*bb*) interactions are positive and grow as $N^{3/2}$ in the limit $N \to \infty$. The energy of the background–electron (*be*) interaction is negative and its absolute value also grows as $N^{3/2}$ in the same limit. The ground state energy E_{GS} of the real physical system is determined by the sum of all three contributions. It is negative and its absolute value grows linearly with N at $N \to \infty$. The energy per particle E_{GS}/N in the true ground state (proportional to N^0) is thus determined, in the real physical system, by the difference of two huge (proportional to $N^{1/2}$) contributions.

By replacing the actual physical problem with the problem of interacting electrons in a sample without edges and/or without the positively charged background, one minimizes only the energy of one large *ee* contribution ($\sim N^{3/2}$) and ignores two other contributions *of the same order*. It is obvious that, mathematically, this procedure is more than doubtful and can lead to noticeable quantitative errors and incorrect qualitative conclusions about the nature of the true ground state of FQHE systems.

8.3. Is the Laughlin Function Exact for the Short-Range Interaction Potential?

In a number of publications it was stated that the Laughlin wave function is an exact solution of the problem with a short-range interaction potential, see, e.g., Refs. [15,44–46]. It was first formulated in Ref. [15] in the form of an *observation*, i.e., without any proof, and later in Ref. [44], it was mentioned that "a formal proof (of this statement) has not yet been found". Later, the clear statement "Laughlin's states ψ_m are shown to be exact for any number of particles in the limit in which the particles have a repulsive interaction of vanishing range" was formulated in Ref. [46], see also [45]. The authors of [45,46] considered the FQHE problem ignoring the presence of the background potential—the point already criticized in Section 8.2. Nevertheless, let us determine whether this statement is correct and how relevant it is to the FQHE problem.

The statement formulated in Ref. [46] sounds very general, but raises questions and doubts. For example, does it apply to *any* type of short-range interaction with a vanishing range? Let us consider the well-known Lennard–Jones potential

$$V_{LJ}(r) = 4\epsilon\left[\left(\frac{\sigma}{r}\right)^{12} - \left(\frac{\sigma}{r}\right)^{6}\right]; \tag{136}$$

where σ and ϵ are the characteristic length and energy scales of the interaction, respectively. The parameter σ can be chosen to be much smaller than the magnetic length, so that this is truly a short-range potential. But it is obvious that the function (5) does not satisfy the many-body Schrödinger equation

$$\frac{1}{2}\sum_{j\neq k=1}^{N} V_{LJ}(\boldsymbol{r}_j - \boldsymbol{r}_k)\Psi_{LS}^{(m)}(\boldsymbol{r}_1, \boldsymbol{r}_2, \ldots, \boldsymbol{r}_N) = E\Psi_{LS}^{(m)}(\boldsymbol{r}_1, \boldsymbol{r}_2, \ldots, \boldsymbol{r}_N), \tag{137}$$

because at $|\boldsymbol{r}_j - \boldsymbol{r}_k| \to 0$, the left-hand side of this equation tends to infinity (as $|\boldsymbol{r}_j - \boldsymbol{r}_k|^{m-12}$), while the right-hand side tends to zero (as $|\boldsymbol{r}_j - \boldsymbol{r}_k|^m$, $m = 3, 5, 7$).

Then, one can show that for any $N \geq 3$ the Laughlin function does not satisfy the Schrödinger equation

$$\frac{1}{2}\sum_{j\neq k=1}^{N} V_{ee}^{\mathrm{scr}}(\boldsymbol{r}_j - \boldsymbol{r}_k)\Psi(\boldsymbol{r}_1, \boldsymbol{r}_2, \ldots, \boldsymbol{r}_N) = E\Psi(\boldsymbol{r}_1, \boldsymbol{r}_2, \ldots, \boldsymbol{r}_N), \tag{138}$$

with the screened Coulomb interaction (134). Using the methods developed in Section 2 and recalculating the matrix elements $\langle \Psi_s | \hat{V}_{ee} | \Psi_{s'} \rangle$ for the screened Coulomb interaction potential (134), one can solve the problem exactly for a small number of particles. The results show, for example, that for $N = 3$, the exactly calculated expansion coefficients A_s do not tend to those of the LS (Table 9) at $b/\lambda \ll 1$.

In principle, one can consider a short-range repulsive potential that is formally described by the δ-function. Then, the Schrödinger equation

$$\frac{1}{2}\sum_{j\neq k=1}^{N} \delta(\boldsymbol{r}_j - \boldsymbol{r}_k)\Psi(\boldsymbol{r}_1, \boldsymbol{r}_2, \ldots, \boldsymbol{r}_N) = E\Psi(\boldsymbol{r}_1, \boldsymbol{r}_2, \ldots, \boldsymbol{r}_N) \tag{139}$$

is indeed satisfied by the function (5), but it is also satisfied by *any* antisymmetric wave function Ψ. To obtain a more meaningful result, the authors of Ref. [46] expanded some real short-range potential $V_b^{\mathrm{sr}}(\boldsymbol{r})$ in powers of its range b,

$$V_b^{\mathrm{sr}}(\boldsymbol{r}) = \sum_{s=0}^{\infty} c_s b^{2s} \Delta^s \left[\delta(\boldsymbol{r})\right] \tag{140}$$

and omitted all terms higher than the term $\sim b^2$. Then, the Schrödinger equation is satisfied because $b^2 \Delta \Psi_{\mathrm{LS}}^{(m=3)} = 0$, that is, simply because the Laughlin wave function is by construction proportional to $|\boldsymbol{r}_j - \boldsymbol{r}_k|^3$ at $|\boldsymbol{r}_j - \boldsymbol{r}_k| \to 0$. But, if we are talking about a *real* interaction potential, for example, the screened Coulomb interaction (134), then *all* terms in the expansion (140) must be taken into account. Then, the Schrödinger equation is not satisfied because, for example, $b^6 \Delta^3 \Psi_{\mathrm{LS}}^{(m=3)} \neq 0$.

Thus, the statement of Ref. [46] can only be proved for the artificial strongly singular interaction potentials

$$V_{pp}(\boldsymbol{r} - \boldsymbol{r}') \equiv c_0 \delta(\boldsymbol{r} - \boldsymbol{r}') + c_2 b^2 \Delta \left[\delta(\boldsymbol{r} - \boldsymbol{r}')\right] \tag{141}$$

that do not exist in nature. The procedure of terminating the series like (140) on terms of order $\sim b^2$ is mathematically incorrect for realistic potentials. In addition, the corresponding eigenenergy which has been obtained in [46] is $E = 0$, which means that the interaction has no effect on the wave function. It can then be chosen as an arbitrary eigenfunction of the kinetic energy operator, which can hardly help in understanding the FQHE problem.

8.4. Is There an Edge Reconstruction of the Laughlin State?

The exact calculations by Ciftja et al. [23,24], performed for a macroscopically large number of electrons, showed that the density of electrons in the LS is perfectly flat in the bulk of the 2DEG, but strongly deviates from the positive background density near its edge, Figures 18 and 19. Perhaps because of this problem, the currently accepted FQHE theory states that the Laughlin function (5) well describes the bulk properties of the 2DEG (an unproved claim), but undergoes a "reconstruction" near its edge.

The edge reconstruction of the fractional $\nu = 1/3$ state has been discussed in detail in the paper [19], where the authors performed an exact diagonalization study of the systems with up to $N = 12$ electrons and interpreted their results as "formation of an edge striped phase (ESP) with wave vector $q_{ESP} \approx \pi/2l_B$, possibly smectic liquid crystal, at the edge of a FQH system". Do the results obtained in Ref. [19] really indicate some reconstruction of the electronic state at the sample edge?

If $N \leq 7$, the density of electrons calculated in [19] (Figure 1 there) looks very similar to the electron density calculated in this work, see Figures 6b, 13c, 28 and 31. That is, the results of [19] for $N \leq 7$ evidently suggest the formation of Wigner molecules in the 2D disks. What happens when $N > 7$?

At larger N, the $n_e(r)$ curves in Ref. [19] begin to change qualitatively. Starting from $N = 10$, a second maximum appears at a finite distance from the center. At $N = 12$, the maxima are at the distances $\sim 2.5 l_B$ and $\sim 6.5 l_B$ from the disk center. Does one need to treat these changes of the electron density by the formation of edge striped phases and smectic liquid crystals?

Obviously, these changes have a much simpler explanation. At $N \sim$ 7–8, the Coulomb interaction arranges electrons into the Wigner molecule in the $(1, N-1)$ shell structure, as shown in Figure 3g,h. At a larger N, $N \sim$10–12, the shell structure $(1, N-1)$ costs too much energy and the electrons are rearranged into the structure $(3, N-3)$ with three electrons dancing around the common center and other surrounding them at a larger distance, see the classical result for this case in Ref. [47]. Figure 34 shows the $(1, N-1)$ and $(3, N-3)$ fragments of the triangular lattice with 7 and 12 electrons, respectively. The red circles show the boundaries of the disks containing this number of particles; their radii equal to $R = \sqrt{N/\pi n_s} = 3^{1/4} a \sqrt{N/2\pi}$, where a is the distance between the triangular lattice points. The blue dashed circles correspond to the maxima of the electron density calculated in Ref. [19]. In both cases, $N = 7$ and $N = 12$, they ideally coincide with the positions of the classical particles in the Wigner lattice.

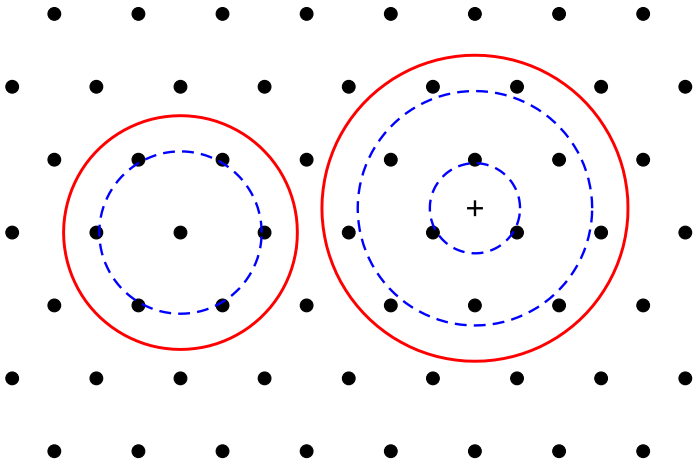

Figure 34. Wigner crystal fragments of the macroscopic lattice with $N = 7$ and $N = 12$ electrons. The red circles show the boundaries of the disks containing N electrons, and the blue dashed circles correspond to the maxima of the electron density calculated in [19]. The common center of all 12 electrons is shown by a small cross in the right part of the figure.

In Ref. [19] it was noted that the amplitude of the density peaks noticeably decreases with the distance from the edge of the disk to its center. This is completely consistent with what is expected in the case of a Wigner crystal. In a macroscopic system, it is reasonable to expect that, due to the presence of the edge, which is inevitable in any real structure, small density fluctuations with a period of the order of $a_0 = 1/\sqrt{\pi n_s}$ should be observed near it. As one moves away from the edge toward the sample center, weak density oscillations should decay over a distance of the order of several a_0, as seen from the exact calculations of Ref. [19], so that inside the sample, the density becomes uniform. In the LS, on the contrary, a macroscopically large part of the electrons ($\sim\sqrt{N}$) remains near the edge, violating the principle of local electroneutrality, Figures 18 and 19. Thus, the exact diagonalization results of Ref. [19] perfectly confirm the formation of a Wigner-crystal-type structure in the FQHE system, which is in full agreement with the results of this paper. There is no need to invent an alternative interpretation of the results of [19], such as an edge reconstruction.

9. Summary and Conclusions

I have presented the results of a detailed theoretical study of the ground and excited states of the system of few 2D electrons at the Landau level filling factors varying from $\nu = 1$ to $\nu \simeq 1/4$. The obtained results show that

1. Both the ground and low-lying excited states of the system have the form resembling a sliding Wigner molecule at any $\nu \lesssim 0.7$ ($\beta \gtrsim 1.42$): the maxima of the quantum-mechanically calculated electron density are at the same distance from the disk center as the radii of the shells in the classical Wigner molecules.
2. When the magnetic field changes, energy gaps between the ground and the first excited states arise and disappear as a result of the competition between repulsive Coulomb forces and compressive action of the magnetic field; the positions of the energy gaps on the magnetic field axis and their values are in reasonable agreement with experimental observations.
3. Both the Laughlin wave function (5) and the fractionally charged excitations (122) and (123) do not describe the physical reality, neither at small N nor in the thermodynamic limit. The experimental results of Refs. [31–33] on the observation of "fractionally charged quasiparticles" need to be reinterpreted.

This work represents the first step towards the development of a new, well-founded theory of the fractional quantum Hall effect.

Funding: This research received no external funding.

Data Availability Statement: The data presented in this study are available in Ref. [37], for details see Appendix C.

Acknowledgments: The author thanks Elliott Lieb for useful discussions, Orion Ciftja for providing details and additional information about his works published in Refs. [23–25], Blagoje Oblak for a useful remark, and Nadya Savostiyanova for reading the manuscript and useful comments on it.

Conflicts of Interest: The author declares no conflicts of interest.

Abbreviations

The following abbreviations are used in this manuscript:

2D	Two-dimensional
EG	Electron gas
FQHE	Fractional quantum Hall effect
GS	Ground state
LS	Laughlin state
MDD	Maximum density droplet
MOSFET	Metal-oxide semiconductor field effect transistor

Appendix A. Integral $\mathcal{J}$

The matrix elements of the different operators in this work can be expressed in terms of the integral $\mathcal{J}$ defined as

$$\mathcal{J}(n_1, n_2, l_1, l_2, k; \alpha, \beta) = \sqrt{\frac{8}{\pi}} \int_0^\infty dx x^{2k} L_{n_1}^{l_1}\left(\alpha x^2\right) L_{n_2}^{l_2}\left(\beta x^2\right) e^{-(\alpha+\beta)x^2}, \tag{A1}$$

where n_1, n_2, l_1, l_2, and k are integers, α and β are real numbers, and $L_n^l(x)$ are Laguerre polynomials. Substituting the explicit expression for the generalized Laguerre polynomial into the definition (A1), one obtains a finite sum of integrals of the type $\int_0^\infty x^{2n} e^{-ax^2} dx$, which can be analytically calculated. The final result can be written in the form

$$\mathcal{J}(n_1,n_2,l_1,l_2,k;\alpha,\beta)=\sqrt{\frac{2}{\pi(\alpha+\beta)}}\sum_{m_1=0}^{n_1}\begin{pmatrix} n_1+l_1 \\ m_1+l_1 \end{pmatrix}\frac{(-\alpha)^{m_1}}{m_1!}\sum_{m_2=0}^{n_2}\begin{pmatrix} n_2+l_2 \\ m_2+l_2 \end{pmatrix}\frac{(-\beta)^{m_2}}{m_2!}\frac{\Gamma\left(m_1+m_2+k+\frac{1}{2}\right)}{(\alpha+\beta)^{m_1+m_2+k}}. \quad \text{(A2)}$$

The integrals $\mathcal{K}(n_1,n_2,k)$ are related to $\mathcal{J}$ as follows

$$\mathcal{K}(n_1,n_2,k)=\sqrt{\frac{n_1!}{(n_1+k)!}\frac{n_2!}{(n_2+k)!}}\mathcal{J}(n_1,n_2,k,k,k;1,1). \quad \text{(A3)}$$

Appendix B. Matrix Elements of the Background–Electron Interaction Energy

The formulas derived here are obtained for the step-like density profile (11).

Appendix B.1. General Formulas

The matrix elements of the background–electron interaction energy are determined by Equation (39). In that formula, by substituting the Fourier transforms of the background and the electron densities from Equations (16) and (36) and replacing the variable $q\lambda/2=x$, I obtain

$$\langle\Psi_s|\hat{V}_{be}|\Psi_{s'}\rangle=-\delta_{ss'}\frac{e^2}{R}2N\sum_{j=1}^{N}\int_0^\infty\frac{dx}{x}J_1(x2R/\lambda)e^{-x^2}L^0_{L_j^{(s)}}\left(x^2\right). \quad \text{(A4)}$$

Using the definition of the Laguerre polynomials,

$$L_n^l(x)=\sum_{m=0}^{n}(-1)^m\begin{pmatrix} n+l \\ m+l \end{pmatrix}\frac{x^m}{m!}, \quad \text{(A5)}$$

I obtain

$$\langle\Psi_s|\hat{V}_{be}|\Psi_{s'}\rangle=-\delta_{ss'}\frac{e^2}{R}2N\sum_{j=1}^{N}\sum_{m=0}^{L_j^{(s)}}\begin{pmatrix} L_j^{(s)} \\ m \end{pmatrix}\frac{(-1)^m}{m!}\int_0^\infty dxJ_1(x2R/\lambda)e^{-x^2}x^{2m-1}. \quad \text{(A6)}$$

The integral in this formula is known (Ref. [48], integral 2.12.9.3),

$$\int_0^\infty dxJ_1(cx)e^{-x^2}x^{2m-1}=\frac{c}{4}\frac{\Gamma\left(m+\frac{1}{2}\right)}{\Gamma(2)}{}_1F_1\left(m+\frac{1}{2},2;-\frac{c^2}{4}\right), \quad \text{(A7)}$$

so that I obtain

$$\langle\Psi_s|\hat{V}_{be}|\Psi_{s'}\rangle=-\delta_{ss'}\frac{e^2}{\lambda}N\sum_{j=1}^{N}\sum_{m=0}^{L_j^{(s)}}\begin{pmatrix} L_j^{(s)} \\ m \end{pmatrix}\frac{(-1)^m}{m!}\Gamma\left(m+\frac{1}{2}\right){}_1F_1\left(m+\frac{1}{2},2;-\frac{R^2}{\lambda^2}\right). \quad \text{(A8)}$$

Taking into account that

$$\frac{R^2}{\lambda^2}=\frac{\pi n_sR^2}{\pi n_s\lambda^2}=\frac{N}{\nu}=N\beta \quad \text{(A9)}$$

and

$$\frac{a_0}{\lambda}=\sqrt{\frac{\pi n_sa_0^2}{\pi n_s\lambda^2}}=\sqrt{\frac{1}{\nu}}=\sqrt{\beta} \quad \text{(A10)}$$

I obtain the formula (40) in the main text.

Appendix B.2. Maximum Density Droplet State

In the case of the MDD state, the matrix elements (40) of the background–electron interaction energy can be transformed further. In this case, $\beta = 1/\nu = 1$, and one has only one state $|s\rangle = |\Psi_{\rm mdd}\rangle = |0, 1, \ldots, N-1\rangle$, so that $L_j^{\rm mdd} = j - 1$. Then, Equation (A8) gives

$$\frac{\langle\Psi_{\rm mdd}|\hat{V}_{be}|\Psi_{\rm mdd}\rangle}{Ne^2/a_0} = -\sum_{j=1}^{N}\sum_{m=0}^{j-1}\left(\begin{array}{c} j-1 \\ m \end{array}\right)\frac{(-1)^m}{m!}\Gamma\left(m+\frac{1}{2}\right){}_1F_1\left(m+\frac{1}{2},2;-N\right). \quad \text{(A11)}$$

First, I change the order of summation over j and m,

$$\frac{\langle\Psi_{\rm mdd}|\hat{V}_{be}|\Psi_{\rm mdd}\rangle}{Ne^2/a_0} = -\sum_{m=0}^{N-1}\frac{(-1)^m}{m!}\Gamma\left(m+\frac{1}{2}\right){}_1F_1\left(m+\frac{1}{2},2;-N\right)\sum_{j=m+1}^{N}\left(\begin{array}{c} j-1 \\ m \end{array}\right). \quad \text{(A12)}$$

The sum of binomial coefficients here gives

$$\sum_{j=m+1}^{N}\left(\begin{array}{c} j-1 \\ m \end{array}\right) = \left(\begin{array}{c} N \\ m+1 \end{array}\right). \quad \text{(A13)}$$

Second, I substitute into (A12) the definition of the hypergeometric function

$${}_1F_1(a,b;z) = \sum_{k=0}^{\infty}\frac{(a)_k}{(b)_k}\frac{z^k}{k!}, \quad \text{(A14)}$$

where $(a)_k = \Gamma(a+k)/\Gamma(a)$ is the Pochhammer symbol, and use the fact that $\Gamma(k+2) = (k+1)!$. After some simplifications, I obtain

$$\frac{\langle\Psi_{\rm mdd}|\hat{V}_{be}|\Psi_{\rm mdd}\rangle}{Ne^2/a_0} = -\sum_{m=0}^{N-1}\frac{(-1)^m}{m!}\left(\begin{array}{c} N \\ m+1 \end{array}\right)\sum_{k=0}^{\infty}\frac{(-N)^k}{k!(k+1)!}\Gamma\left(m+k+\frac{1}{2}\right). \quad \text{(A15)}$$

Third, I change the order of summation over k and m,

$$\frac{\langle\Psi_{\rm mdd}|\hat{V}_{be}|\Psi_{\rm mdd}\rangle}{Ne^2/a_0} = -\sum_{k=0}^{\infty}\frac{(-N)^k}{k!(k+1)!}\sum_{m=0}^{N-1}\frac{(-1)^m}{m!}\left(\begin{array}{c} N \\ m+1 \end{array}\right)\Gamma\left(m+k+\frac{1}{2}\right) \quad \text{(A16)}$$

and take the sum over m,

$$\sum_{m=0}^{N-1}\frac{(-1)^m}{m!}\left(\begin{array}{c} N \\ m+1 \end{array}\right)\Gamma\left(m+k+\frac{1}{2}\right) = \frac{\Gamma\left(k+\frac{1}{2}\right)\Gamma\left(N-k+\frac{1}{2}\right)}{\Gamma\left(\frac{3}{2}-k\right)\Gamma(N)}. \quad \text{(A17)}$$

Then, using the properties of the Γ function,

$$\Gamma(z+1) = z\Gamma(z), \;\; \Gamma\left(\frac{1}{2}+k\right)\Gamma\left(\frac{1}{2}-k\right) = \frac{\pi}{\cos\pi k} \quad \text{(A18)}$$

I obtain

$$\frac{\langle\Psi_{\rm mdd}|\hat{V}_{be}|\Psi_{\rm mdd}\rangle}{Ne^2/a_0} = \frac{2}{\pi\Gamma(N)}\sum_{k=0}^{\infty}\frac{N^k}{k!(k+1)!}\frac{\Gamma^2\left(k+\frac{1}{2}\right)\Gamma\left(N-k+\frac{1}{2}\right)}{(2k-1)}. \quad \text{(A19)}$$

The series here can be presented in the form

$$\sum_{k=0}^{\infty}\frac{N^k}{k!(k+1)!}\frac{\Gamma^2\left(k+\frac{1}{2}\right)\Gamma\left(N-k+\frac{1}{2}\right)}{(2k-1)} = -\pi\Gamma\left(N+\frac{1}{2}\right){}_2F_2\left(-\frac{1}{2},\frac{1}{2};2,\frac{1}{2}-N;-N\right), \quad \text{(A20)}$$

so that finally I obtain

$$\frac{\langle \Psi_{\mathrm{mdd}} | \hat{V}_{be} | \Psi_{\mathrm{mdd}} \rangle}{Ne^2/a_0} = -2\frac{\Gamma\left(N+\frac{1}{2}\right)}{\Gamma(N)}\,{}_2F_2\left(-\frac{1}{2},\frac{1}{2};2,\frac{1}{2}-N;-N\right). \tag{A21}$$

This formula is used in the main text, Equation (74). Calculations in this Section have been performed with the help of Wolfram Mathematica, https://www.wolfram.com/mathematica (accessed on 21 January 2024).

Appendix C. Data Files

The .dat files containing numerical data on the many-body states and expansion coefficients for different number of particles N can be found in Ref. [37]. In this reference, there are seven directories named Nx, where x denotes the number of particles $N = 2, \ldots, 8$. Each directory has five files (except the directory N8 that has four files). These files contain the following information:

1. The file Nmbs.Nx.Ltotyy.dat contains a single number, which is the number of many-body states N_{mbs} for the given N and $\mathcal{L} = 3N(N-1)/2$. yy is a two-digit number corresponding to $\mathcal{L}$. Example: the file Nmbs.N7.Ltot63.dat contains the number $N_{mbs} = 8033$.
2. The file MBstates.Nx.Ltotyy.dat contains N_{mbs} many-body states $|s\rangle$. Example: the file MBstates.N7.Ltot63.dat has 8033 lines containing the many-body states running from the state number 1, $|0,1,2,3,4,5,48\rangle$ up to the state number 8033, $|6,7,8,9,10,11,12\rangle$.
3. The file LaughlinCs.Nx.Ltotyy.dat contains the integer numbers C_s^{LS} obtained using the binomial expansion of the polynomial factors in the Laughlin function (5) with $m = 3$, see Section 6.2. Example: the first and the last lines in the file LaughlinCs.N7.Ltot63.dat contain the numbers $C_{|0,1,2,3,4,5,48\rangle} = 0$ and $C_{|6,7,8,9,10,11,12\rangle} = 135135$.
4. The file LaughlinAs.Nx.Ltotyy.dat contains the real expansion coefficients A_s^{LS}, as shown in Equation (93), of the Laughlin function over the basis many-body states, see Section 6.2.
5. The file GrStateAs.Nx.Ltotyy.dat contains the real expansion coefficients A_s^{GS} of the true ground state function over the basic many-body states, i.e., the eigenvector of the Hamiltonian corresponding to the lowest energy eigenvalue. The subdirectory N8 does not contain this file.

References

1. von Klitzing, K.; Dorda, G.; Pepper, M. New Method for High-Accuracy Determination of the Fine-Structure Constant Based on Quantized Hall Resistance. *Phys. Rev. Lett.* **1980**, *45*, 494–497. [CrossRef]
2. Prange, R.E.; Girvin, S.M. (Eds.) *The Quantum Hall Effect*; Springer: New York, NY, USA, 1990.
3. Tsui, D.C.; Stormer, H.L.; Gossard, A.C. Two-Dimensional Magnetotransport in the Extreme Quantum Limit. *Phys. Rev. Lett.* **1982**, *48*, 1559–1562. [CrossRef]
4. Willett, R.; Eisenstein, J.P.; Stormer, H.L.; Tsui, D.C.; Gossard, A.C.; English, J.H. Observation of an even-denominator quantum number in the fractional quantum Hall effect. *Phys. Rev. Lett.* **1987**, *59*, 1776–1779. [CrossRef] [PubMed]
5. Wigner, E. On the interaction of electrons in metals. *Phys. Rev.* **1934**, *46*, 1002–1011. [CrossRef]
6. Laughlin, R.B. Anomalous quantum Hall effect: An incompressible quantum liquid with fractionally charged excitations. *Phys. Rev. Lett.* **1983**, *50*, 1395–1398. [CrossRef]
7. Bychkov, Y.A.; Iordanskii, S.V.; Eliashberg, G.M. Two-dimensional electrons in a strong magnetic field. *JETP Lett.* **1981**, *33*, 143–146.
8. Yoshioka, D.; Fukuyama, H. Charge density wave state of two-dimensional electrons in strong magnetic fields. *J. Phys. Soc. Jpn.* **1979**, *47*, 394. [CrossRef]
9. Yoshioka, D.; Lee, P.A. Ground-state energy of a two-dimensional charge-density-wave state in a strong magnetic field. *Phys. Rev. B* **1983**, *27*, 4986–4996. [CrossRef]
10. Tao, R. Comment on Laughlin's wavefunction for the quantised Hall effect. *J. Phys. C Solid State Phys.* **1984**, *17*, L53–L58. [CrossRef]
11. Maki, K.; Zotos, X. Static and dynamic properties of a two-dimensional Wigner crystal in a strong magnetic field. *Phys. Rev. B* **1983**, *28*, 4349–4356. [CrossRef]

12. Yoshioka, D.; Halperin, B.I.; Lee, P.A. Ground state of two-dimensional electrons in strong magnetic fields and 1/3 quantized Hall effect. *Phys. Rev. Lett.* **1983**, *50*, 1219–1222. [CrossRef]
13. Available online: https://www.nobelprize.org/prizes/physics/1998/summary/ (accessed on 21 January 2024).
14. Girvin, S.M.; Jach, T. Interacting electrons in two-dimensional Landau levels: Results for small clusters. *Phys. Rev. B* **1983**, *28*, 4506–4509. [CrossRef]
15. Haldane, F.D.M. Fractional Quantization of the Hall Effect: A Hierarchy of Incompressible Quantum Fluid States. *Phys. Rev. Lett.* **1983**, *51*, 605–608. [CrossRef]
16. Levesque, D.; Weis, J.J.; MacDonald, A.H. Crystallization of the incompressible quantum-fluid state of a two-dimensional electron gas in a strong magnetic field. *Phys. Rev. B* **1984**, *30*, 1056–1058. [CrossRef]
17. Jain, J.K. Composite–Fermion Approach for the Fractional Quantum Hall Effect. *Phys. Rev. Lett.* **1989**, *63*, 199–202. [CrossRef]
18. Kasner, M.; Apel, W. Electrons in a strong magnetic field on a disk. *Ann. Phys.* **1994**, *3*, 433–459. [CrossRef]
19. Tsiper, E.V.; Goldman, V.J. Formation of an edge striped phase in the $\nu = 1/3$ fractional quantum Hall system. *Phys. Rev. B* **2001**, *64*, 165311. [CrossRef]
20. Morf, R.H.; d'Ambrumenil, N.; Das Sarma, S. Excitation gaps in fractional quantum Hall states: An exact diagonalization study. *Phys. Rev. B* **2002**, *66*, 075408. [CrossRef]
21. Wan, X.; Yang, K.; Rezayi, E.H. Reconstruction of fractional quantum Hall edges. *Phys. Rev. Lett.* **2002**, *88*, 56802. [CrossRef] [PubMed]
22. Wan, X.; Rezayi, E.H.; Yang, K. Edge reconstruction in the fractional quantum Hall regime. *Phys. Rev. B* **2003**, *68*, 125307. [CrossRef]
23. Ciftja, O.; Wexler, C. Monte Carlo simulation method for Laughlin-like states in a disk geometry. *Phys. Rev. B* **2003**, *67*, 75304. [CrossRef]
24. Ciftja, O.; Lapilli, C.M.; Wexler, C. Liquid crystalline states for two-dimensional electrons in strong magnetic fields. *Phys. Rev. B* **2004**, *69*, 125320. [CrossRef]
25. Ciftja, O.; Ockleberry, N.; Okolo, C. One-Particle Density of Laughlin States at Finite. *N. Mod. Phys. Lett. B* **2011**, *25*, 1983–1992. [CrossRef]
26. Eisenstein, J.P.; Stormer, H.L. The fractional quantum Hall effect. *Science* **1990**, *248*, 1510–1516. [CrossRef]
27. Girvin, S.M. Introduction to the fractional quantum Hall effect. *Séminaire Poincaré* **2004**, *2*, 53–74.
28. Jain, J. (Ed.) *Composite Fermions*; Cambridge University Press: Cambridge, UK, 2012.
29. Hansson, T.H.; Hermanns, M.; Simon, S.H.; Viefers, S.F. Quantum Hall physics: Hierarchies and conformal field theory techniques. *Rev. Mod. Phys.* **2017**, *89*, 025005. [CrossRef]
30. Murthy, G.; Shankar, R. Hamiltonian theories of the fractional quantum Hall effect. *Rev. Mod. Phys.* **2003**, *75*, 1101–1158. [CrossRef]
31. Goldman, V.J.; Su, B. Resonant Tunneling in the Quantum Hall Regime: Measurement of Fractional Charge. *Science* **1995**, *267*, 1010–1012. [CrossRef] [PubMed]
32. Saminadayar, L.; Glattli, D.C.; Jin, Y.; Etienne, B. Observation of the $e/3$ Fractionally Charged Laughlin Quasiparticle. *Phys. Rev. Lett.* **1997**, *79*, 2526–2529. [CrossRef]
33. de-Picciotto, R.; Reznikov, M.; Heiblum, M.; Umansky, V.; Bunin, G.; Mahalu, D. Direct observation of a fractional charge. *Nature* **1997**, *389*, 162–164. [CrossRef]
34. Landau, L.D.; Lifshitz, E.M. *Quantum Mechanics (Non-Relativistic Theory)*; Elsevier: Oxford, UK, 1994; problem 1 to §112.
35. Fock, V. Bemerkung zur Quantelung des harmonischen Oszillators im Magnetfeld. *Z. Phys.* **1928**, *47*, 446. [CrossRef]
36. Ciftja, O. Detailed solution of the problem of Landau states in a symmetric gauge. *Eur. J. Phys.* **2020**, *41*, 35404. [CrossRef]
37. Mikhailov, S.A. Available online: https://arxiv.org/abs/2206.05152v5, Ancillary Files. 2023. (accessed on 21 January 2024).
38. Mikhailov, S.A.; Ziegler, K. Floating Wigner molecules and possible phase transitions in quantum dots. *Eur. Phys. J. B* **2002**, *28*, 117–120. [CrossRef]
39. Yannouleas, C.; Landman, U. Two-dimensional quantum dots in high magnetic fields: Rotating-electron-molecule versus composite-fermion approach. *Phys. Rev. B* **2003**, *68*, 35326. [CrossRef]
40. Yannouleas, C.; Landman, U. Symmetry breaking and quantum correlations in finite systems: Studies of quantum dots and ultracold Bose gases and related nuclear and chemical methods. *Rep. Prog. Phys.* **2007**, *70*, 2067–2148. [CrossRef]
41. Lewin, M.; Lieb, E.H.; Seiringer, R. Statistical mechanics of the uniform electron gas. *J. L'École Polytech.-Math.* **2018**, *5*, 79–116. [CrossRef]
42. Lewin, M.; Lieb, E.H.; Seiringer, R. Floating Wigner crystal with no boundary charge fluctuations. *Phys. Rev. B* **2019**, *100*, 35127. [CrossRef]
43. Laughlin, R.B. Quantized motion of three two-dimensional electrons in a strong magnetic field. *Phys. Rev. B* **1983**, *27*, 3383–3389. [CrossRef]
44. Haldane, F.D.M.; Rezayi, E.H. Finite-Size Studies of the Incompressible State of the Fractionally Quantized Hall Effect and its Excitations. *Phys. Rev. Lett.* **1985**, *54*, 237–240. [CrossRef] [PubMed]
45. Johri, S.; Papić, Z.; Schmitteckeret, P.; Bhatt, R.N.; Haldane, F.D.M. Probing the geometry of the Laughlin state. *New J. Phys.* **2016**, *18*, 25011. [CrossRef]

46. Trugman, S.A.; Kivelson, S. Exact results for the fractional quantum Hall effect with general interactions. *Phys. Rev. B* **1985**, *31*, 5280–5284. [CrossRef] [PubMed]
47. Bedanov, V.M.; Peeters, F.M. Ordering and phase transitions of charged particles in a classical finite two-dimensional system. *Phys. Rev. B* **1994**, *49*, 2667–2676. [CrossRef] [PubMed]
48. Prudnikov, A.P.; Brychkov, Y.A.; Marichev, O.I. *Integrals and Series, Special Functions*; Nauka: Moscow, Russia, 1983; Volume 2.